

Department of Precision and Microsystems Engineering

Modal derivatives based reduced-order modelling in parametrically driven structures and frequency dividers

J.L. van den Broek

Report no : 2019.038
Coach : Dr. P.Tiso
Professor : Dr. F.Alijani
Specialisation : DMN
Type of report : MSc. thesis
Date : November 13, 2019

Modal derivatives based reduced-order modelling in parametrically driven structures and frequency dividers

by

J.L. van den Broek

to obtain the degree of Master of Science
at the Delft University of Technology,
to be defended publicly on November 27-th, 2019 at 9:30.

Report no : 2019.038
Coach : Dr.P.Tiso
Professor : Dr.F.Alijani
Specialisation : DMN
Type of report : Master thesis
Date : 13-11-2019

An electronic version of this thesis is available at <http://repository.tudelft.nl/>.

Abstract

The application of Modal Derivatives (MDs) in convention reduction methods applied in Finite Elements Models (FEMs) is an effective method to capture the geometric nonlinearity of the structures. In this work, the performances of MDs augmented Reduced Order Bases (ROBs) are investigated for steady-state responses of parametrically driven structures.

It is shown that MDs play a crucial role in the operation of simple parametrically excited cantilever structures. Furthermore, the reduced-order models of a Frequency Divider (FD) are considered. In this thesis, an FD is considered that consists of cascading mechanical components, each of which is excited by the preceding one by means of parametric resonance. The modularity of the FDs makes them excellent candidates for component mode synthesis, where each substructure of the cascade is independently reduced and connected to other members via common interface.

We show that MDs-based reduced-order models can aid in capturing properly the dynamics of FDs with much fewer degrees of freedom compared to the original finite element formulations. Furthermore, we propose novel modifications of the conventional Craig-Bampton reduction to enhance its performance in parametrically excited structures. A specific estimator is introduced that expresses the performances of the different ROMs in terms of accuracy in the steady-state responses. This accuracy is based on the amplitude and the frequency.

Acknowledgements

Developing and writing a thesis is not something I did fully on my own, without the contribution of many others the thesis would not exist in the form it is right now. Therefore I would like to give some words of thank to the people who played a role in the development of the project.

In advance, I would like to express my gratitude to my daily supervisor Paolo for hosting me at the ETH in Zürich. He was a great source of inspiration and motivation. Furthermore, he challenged me to improve my skills and knowledge during the project. I also would like to thank my home supervisor, Farbod, from Delft University of Technology. He played an essential role in the finishing part of the thesis when I came back to the Netherlands, his feedback was very helpful and always motivating.

Besides my supervisors I would like to thank the PhD student J.Marconi from Politecnico Milano for his unconditional help and effort during the project. He was always available for a talk and interesting discussion about the work. No matter what it was, he was always open and available to help. I really appreciated the hours we spent with just making some derivations and calculations on whiteboards and with discussing results and possible ways to solve problems.

Finally, I am grateful for the help and support of my family and friends in the Netherlands and Switzerland. They motivated me to keep going.

Nomenclature

In this work several symbols and abbreviations are used. It is important to note letters that bold letters refer to vectors while bold capital letters refer to matrices.

List of symbols

A	Cross-sectional area
c	Maximal normalized cross correlation coefficient
C	Damping matrix
d	Depth of a structure
E	Young's modulus
F	Force vector
$F(t)$	Time-dependent force vector
F^{ext}	External force vector
F^{NL}	Nonlinear force vector
f_i	i -th eigenfrequency
G	Flexibility matrix
G_c	Constrained flexibility matrix
g_N	External force component
h	Force amplitude
I	Moment of inertia
I	Identity matrix
J	Jacobian
K	Stiffness matrix
K_n	Constrained stiffness matrix
L	Element length
m	Number of reduced DoFs
M	Mass matrix
n	Total number of DoFs
N	Elastic property of material
P	Inertia-relief projection matrix
q	Full DoF displacement vector
Q	Tensor
R	Rotation matrix
u	Displacement in axial direction
V	Reduction basis
w	Width of the structure

Greek symbols:

α	Rayleigh coefficient related to the mass matrix
β	Rayleigh coefficient related to the stiffness matrix
Γ	Collection of constraint modal derivatives
ζ	Collection of amplitudes of modal derivatives
η_i	Reduced coordinate i
$\boldsymbol{\eta}$	Reduced DoF vector
Θ_i	Vibration mode
Θ	Collection of modal derivatives
λ	Collection of amplitudes of vibration modes
Λ	Nonlinear mapping
ρ	Density.
σ	Collection of amplitudes of constraint modal derivatives
ϕ	Vibration modes
ϕ_I	Internal vibration modes
ϕ_f	Free vibration modes
ψ_a	Attachment modes
ψ_c	Constraint modes
ω	Frequency in radians per second
ϑ	Mode component

Subscripts and superscripts:

(\bullet)	First time derivative
$(\ddot{\bullet})$	Second time derivative
$(\tilde{\bullet})$	Reduced component
$(\bullet)^e$	Component at element level
$^x(\bullet)$	Order of a tensor
$(\bullet)_I$	Internal component
$(\bullet)_B$	External component

list of abbreviations and acronyms

CMS	Component Mode Synthesis
FD	Frequency divider
FE	Finite Element
FEM	Finite element model
DoF	Degree of freedom
ROM	Reduced-order model
MOR	Model order reduction
CB-I	Craig-Bampton-I reduction basis
CB-II	Craig-Bampton-II reduction basis
SMs	Static modes
VMs	Vibration modes
MDs	Modal derivatives
RBMs	Rigid body modes
CMDs	Constraint modal derivative
Global	Global reduction basis

Contents

1	Introduction	1
1.1	Model order reduction	2
1.1.1	Component Mode Synthesis.	2
1.1.2	Guyan reduction	3
1.1.3	Craig-Bampton reduction	3
1.1.4	Rubin reduction	4
1.1.5	Global reduction	4
1.1.6	Nonlinear model order reduction	4
1.2	Parametric resonance	5
1.3	Resonance cascade frequency divider	5
1.4	Summary	7
1.5	Research question	7
1.6	Performance estimations of the reduction methods.	8
1.7	Thesis outline.	8
2	Paper	11
3	Reduced-order models of beam structures	29
3.1	Model validation	29
3.1.1	Eigenfrequency validation	30
3.1.2	Comparison of time responses	30
3.2	Transverse excited cantilever beam.	31
3.3	Transverse excited clamped-clamped beam	33
3.4	Numerical results of frequency dividers	34
3.4.1	Numerical results of a 2-stage frequency divider.	35
3.4.2	Three-stage frequency divider.	40
4	Conclusions	45
5	Recommendations	47
6	Reflection	51
6.1	Reflection on the timeline	51
6.2	Contributions.	52
6.3	Personal developments	52
A	Derivation of modes	53
A.1	Internal Vibration modes	53
A.2	Free Vibration modes	54
A.3	Constrained modes	54
A.4	Attachment modes	54
A.5	Rigid body modes	56

B	Derivation of reduction bases	57
B.1	Global reduction	57
B.2	Guyan reduction	57
B.3	Craig-Bampton method	58
B.4	Rubin reduction	59
C	Principles of parametric resonance	63
D	Derivation of modal derivatives	65
D.1	Illustration of the modal derivatives	66
E	Derivation of constraint modal derivatives	69
E.1	Illustration of constraint modal derivatives	70
F	Derivation of the tensors	73
F.1	Computing the tensors on element level	73
F.2	Rotation of the element tensor	75
F.3	Computation of the reduced-order tensors	75
F.4	Matlab implementations	76
	Bibliography	77



Introduction

The Finite Element Method (FEM) is widely used in industry and research as a numerical method for solving problems in engineering and mathematical physics. The FEM is typically used in areas of interest that include heat transfer, structural dynamics, mass transfer, fluid dynamics, and electromagnetic potentials. The basic principle of the FEM is that a model is discretized in a finite number of elements such that an accurate approximation of the response of the actual system is found. Over the years, the finite element models increased in size and complexity and as a consequence, the number of elements of the models increased. Accordingly, the number of unknowns, also called the degrees of freedoms (DoFs), that follow from the governing equations increased as well. A higher number of DoFs normally means that more computational time is required, especially in the case of dynamic time integration. It has been shown that the computational effort of a finite element analysis is proportional to the cubic of the problem size [31]. Therefore, in terms of computational efficiency, there is a huge demand for keeping the number of unknowns relatively low. However, simply taking a lower number of elements in a model does not inure the accuracy of the static and dynamic solutions. This would imply that a trade-off should be made between the number of elements and the required accuracy. However, the sometimes high number of DoFs (typically up to several millions) that are stemming from the governing equations is usually a result of the formulations of the FEM itself. Often, this high number of DoFs is not required for an accurate approximation of the solution of the problem.

Fortunately, several reduction methods were introduced and developed that allow keeping the high number of elements while reducing the number of DoFs and still retaining sufficient accuracy. Traditional reduction techniques like Guyan reduction [11], Craig-Bampton reduction [12], and Rubin reduction [14] have been introduced a couple of decades ago. In several works, it has been shown that these conventional reduction techniques are perfectly able to approximate with high accuracy the full-DoF statics and dynamics of systems [9, 10]. Depending on the type of problem and the boundary conditions, one of the reduction techniques suits best for the specific application.

At the moment that these conventional reduction methods were introduced, they were only designed for static responses and linear dynamic problems. Later, the demand for nonlinear FE models increased and over periods methods were developed that enabled nonlinear dynamic analysis. One of these methods was the application of modal derivatives (MDs) [13] in conventional reduction methods. The MDs can account for the geometric nonlinearity, and it has been shown that modal derivative enriched reduction bases in Reduced-Order Models (ROMs) are perfectly able to approximate nonlinear transient time responses with high accuracy [1, 2, 5].

However, for many applications, the focus lays rather on the steady-state response of a system than

the transient time response. The field of parametric resonance is an example where the steady-state response is the relevant part of the system response. The working principle of some types of mechanical multi-stage frequency dividers is based on parametric resonance [43]. However, more applications exist where one might be mainly interested in the steady response of the system. Therefore it is interesting to investigate the behavior of nonlinear ROMs in steady-state responses of systems.

1.1. Model order reduction

Originally, Model Order Reduction (MOR) was developed in the field of systems and control theory. The aim was to reduce the complexity of dynamical systems while preserving their input-output behavior as much as possible [32]. MOR, in general, is all about simplification of dynamical models that may contain many unknowns. These simplifications are needed to perform simulations and analysis within an acceptable amount of time or a limited storage capacity. The idea is that the information and features of an unreduced full-sized system can be described by a much smaller system with fewer unknowns, which is called the reduced system. For some MOR methods the kernel that enables this kind of decrease in the number of DoFs is the use of modes in a projection basis. In that case, the MOR is about approximating the full DoF response by a linear combination of a smaller set of modes. Once all nodes of a structure are relative to each other 'coupled' in a certain mode, the amplitude of that mode then describes how that specific mode is contributing to the response of the system. The amplitude of that mode is now a reduced DoF. The modes can be spanned in a basis which forms the reduction basis V of the system. Now the basis projects the reduced set of DoFs to a full set of DoFs. The corresponding formula is given as:

$$\mathbf{q} = V\boldsymbol{\eta}, \quad (1.1)$$

where $\mathbf{q} \in R^n$ is the full DoF displacement vector while $\boldsymbol{\eta} \in R^m$ is the generalized reduced set of DoFs. m is the number of modes that are spanned in the reduction basis while n is the number of full DoFs, such that $V \in R^{n \times m}$. By using the reduction basis, the full number of EoMs can be mapped to a reduced set of EoMs. This is known as Bubnov-Galerkin projection, or simply Galerkin projection [33]. The modes that are included in the reduction basis are characteristic for the different types of reduction.

1.1.1. Component Mode Synthesis

Normally complex structures are composed of several relatively simple components that are assembled. Examples are trusses, rotors, wind turbines, air wings, vehicles, and many more applications. In such cases, it is convenient to describe the dynamic model of the overall system by taking the features and dynamic properties of the substructures [34]. Component Mode Synthesis (CMS) is based on this idea, where the entire system is described by the dynamic behaviors of the individual substructure, and the model size reduction is carried out on a substructure level. The substructures can be reduced to super elements where the boundary DoFs of the substructures remain unaffected and intact. Afterward, the reduced substructures are easily assembled through standard FE assembly procedures to obtain the ROM of the entire system. These principles of reduction on substructure level are illustrated in Fig. 1.1. This figure also shows the reduction of the system without substructuring by a reduction basis that is related to the entire system. Several reduction methods were developed that are suitable for CMS. In the following three subsections three reduction methods that are widely used in CMS, namely Guyan reduction, Craig-Bampton reduction and Rubin reduction are discussed briefly, and the details of how to apply them to dynamical problems can be found in Appendix B.

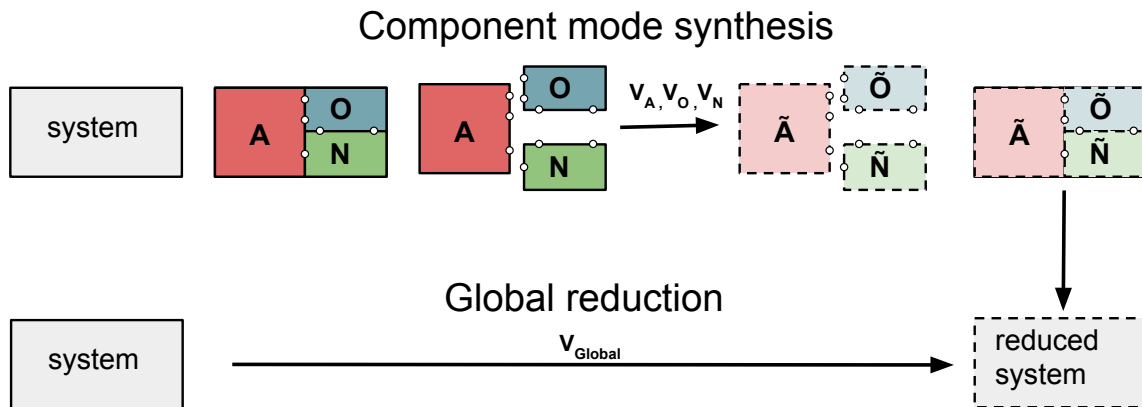


Figure 1.1: Schematic representations of component mode synthesis and global reduction. In CMS the initial system is divided into substructures, in the figure denoted as structures A, O and N. Then the substructures are reduced by the substructure reduction bases V_A, V_O and V_N individually. Finally, the reduced system is obtained by the assembly of the reduced substructures. Note that the boundary nodes of substructures indicated with the white dots remain untouched by reduction. For global reduction there exists a global reduction basis V_{Global} , such that the initial system can be reduced directly by this reduction base.

1.1.2. Guyan reduction

Guyan reduction is one of the oldest reduction techniques for FE methods. Guyan introduced the method in a half-page long paper in 1965 [11]. The same reduction technique was introduced independently by Irons a few years later. Therefore, the method is also known as the Guyan-Irons method. However, the reduction technique is in general known as Guyan reduction or static condensation. The Guyan reduction basis comprises static modes only. The method reduces the DoFs by ignoring the inertial terms of the equilibrium equations and by expressing the unloaded DoFs in terms of loaded DoFs. The unloaded DoFs are also denoted as the internal DoFs or the enslaved DoFs, while the loaded DoFs are the boundary DoFs or also called master DoFs. For linear static problems, the Guyan reduction gives an exact approximation of the full, unreduced system. But under certain conditions, Guyan reduction can also be successfully applied to linear dynamic systems. In that case, one assumes that all internal nodes respond quasi-statically to the displacements of the boundary nodes. The attractiveness of the Guyan reduction is found in its very straight forward computations and simplicity. The main drawback of the Guyan reduction is that the internal dynamics of the structure are completely ignored, however, the method is still widely used in structural dynamics.

1.1.3. Craig-Bampton reduction

The Craig-Bampton reduction can be seen as an extension of the Guyan reduction. In the Craig-Bampton reduction, information about the internal dynamics is included in the reduced component model. This is achieved by augmenting the Guyan reduction basis with internal vibration modes, thus a Craig-Bampton reduction basis comprises dynamic modes as well. The result is a more complete and versatile basis to describe the dynamic behavior of the component. The classic Craig-Bampton reduction method based on Internal Vibration Modes (IVMs) was first proposed by

Hurty in 1965 [35]. Later, the technique was simplified by Craig and Bampton in 1968 [12]. The method was even more developed by Craig [36]. The advantages of the Craig-Bampton reduction are its simplicity and the straight forward computation of the reduction base. Furthermore, highly accurate models are obtained by using a relatively low number of modes. A drawback is the fact that due to the type of ingredients used in the bases, the Craig-Bampton reduction basis can in practice not be obtained experimentally [10]. Another disadvantage is the fact that the reduction basis needs to be recomputed in case of changed boundary nodes since the IVMs then change as well.

1.1.4. Rubin reduction

After the introduction of the reduction basis composed of IVMs by Craig and Bampton, researchers were soon focusing on the application of free vibration modes in the reduction basis. The use of Free Vibration Modes (FVMs) seems more natural since these types of modes are the 'real' modes of the system. Furthermore, FVMs are more attractive in the case that the modes of the reduction basis are obtained from modal testing, or when the component modes need to be verified experimentally [10]. FVMs were first used in a reduction basis by MacNeal in 1971 [26], and later in 1975 by Rubin [14]. These methods were later analyzed and developed by Craig and Chang [36]. Besides the dynamic FVMs, the Rubin reduction basis comprises rigid body modes and static attachment modes. In general, a Rubin reduction basis is usually more accurate than a Craig Bampton reduction basis in the lower frequency domain. Especially the rigid body modes of the Rubin reduction basis have a significant influence on the accuracy in the lower frequency domain. Besides the better accuracy, another advantage over the Craig-Bampton reduction is the fact that the Rubin reduction basis does not need to be entirely recomputed in case of changed boundary nodes, since the FVMs remain then the same [10]. A disadvantage of the Rubin reduction is the less straightforward and more intricate computations of the modes and the reduction basis.

1.1.5. Global reduction

Instead of decomposing the entire system in substructures, one could also form a reduction basis at global level, i.e. for the assembled system. In that case the ingredients of the reduction basis are the global vibration modes. The effectiveness of the method for a simple structure composed of beams has been shown in the work of Sombroek et al [16]. The advantage of this method is the fact that no substructuring is required. Furthermore, the computation of the reduction basis is very simple but still convenient for dynamic analyses. The disadvantages of this reduction method are especially found in case of large and complex assembled systems. In such systems, the 'offline' computation time of the vibration modes for complex systems can increase to unacceptable amounts. Furthermore, the reduction basis related to the entire structure can be impractically large. In such cases, CMS might be a much more attractive approach.

1.1.6. Nonlinear model order reduction

The reduction methods discussed in the previous sections are perfectly applicable to linear systems, however, in reality, every system incorporates a certain amount of nonlinearity. One of the most important nonlinearities in structural dynamics is the geometric nonlinearity. Geometric nonlinearity is associated with the geometry and boundary conditions of a structure. It is defined as the internal effects of a structure caused by a change of the geometry as it deflects. In a geometric linear setting, the equations of motion are defined concerning an undeformed configuration of the system, while in a nonlinear setting the EoMs are dependent on the current state of the system. In many applications with small deformations, rotations or strains, the nonlinearities in the system may be neglected since the nonlinearities remain sufficiently small. However, in some cases, one cannot simply ignore nonlinearity, for example in the case of large deflections. However, this does not mean geometric nonlinearity automatically mean large deformations, it rather means that the

EoMs are written in terms of the deformed state of the system.

One approach to account for geometric nonlinearities is the use of Modal Derivatives (MDs), where the reduction bases of conventional reduction methods are enriched by this special type of mode. The concept of MDs was introduced by Idelsohn and Cardona in 1985 [13]. It has its merits in particular in structural mechanics and dynamics, because it preserves the nonlinear eigenfrequencies. Moreover, it has been tested successfully for several applications. For a long time, there was a lack of theoretical foundation regarding MDs. Weeger et al. [4] closed this gap by investigating their approximation properties. Furthermore, their usage as components in reduction bases has been validated analytically. Modal derivatives can be computed both analytically and numerically [13]. A numerical approach is described by the finite difference method.

Originally, MDs were computed by differentiating the nonlinear eigenvalue problem with respect to the linear vibration modes. This results in a quite complex expression since it also involves the derivatives of eigenfrequencies. However, most works that include the use of MDs are neglecting these terms, referring to the so-called definition without mass consideration. That means that MDs are in fact static corrections of two Vibration Modes (VMs) in a reduction basis, such that they describe the essential nonlinear contributions for the elastic geometric nonlinearities induced by the VMs. Physically, the modal derivative θ_{ij} corresponding to the vibration modes ϕ_i and ϕ_j represent the change in the VM ϕ_i corresponding to a displacement given in the direction of VM ϕ_j [2]. See appendix D for the derivation of the modal derivatives.

Wenneker and Tiso [2] show that MDs can be successfully implemented in CMS. Later, the ideas of an MD-enhanced Rubin substructuring method as well as an enhanced Craig-Bampton substructuring method were developed by Wu et al. [1, 5]. These works show the successful application of MD-enhanced reduction bases in transient nonlinear analyses.

1.2. Parametric resonance

One phenomenon in structural dynamics that is interesting to investigate with FE models is parametric resonance. For beam models, in case of forces acting in an axial direction of system the stiffness and damping terms of the model may become time-dependent. Such systems are known as parametric excited systems [20]. See appendix C for an example of a 2-DoF parametrically excited structure. A system may be exposed to parametric resonance if the force excitation frequency is close to a parametric resonance frequency of the system, i.e. $\mu \approx \mu_{i,s}^{pr}$ or a combination of parametric resonances [20], $\mu \approx \mu_{i\pm j,s}^{cpr}$, where the fundamental parametric resonance frequency is given as:

$$\mu_{i,s}^{pr} = 2 \frac{\omega_i}{s}. \quad (1.2)$$

The parametric combination resonance is given as:

$$\mu_{i\pm j,s}^{cpr} = \frac{|\omega_i \pm \omega_j|}{s}, \quad (1.3)$$

where ω_i and ω_j denote the i -th and j -th eigenfrequencies of the undamped system [20]. Parametric resonance is different from regular resonance since it exhibits instability phenomena. For many MEMs devices, the phenomenon of parametric resonance form the basis of their operating principle, but in more systems the occurrence of parametric resonance is crucial for the working principle of the system [6], for example the in the next section expounded mechanical frequency divider.

1.3. Resonance cascade frequency divider

Frequency dividers (FDs) are mechanical devices that allow obtaining vibrations of a given component at a fraction of some input frequency. Applications of FDs, multipliers, and converters are

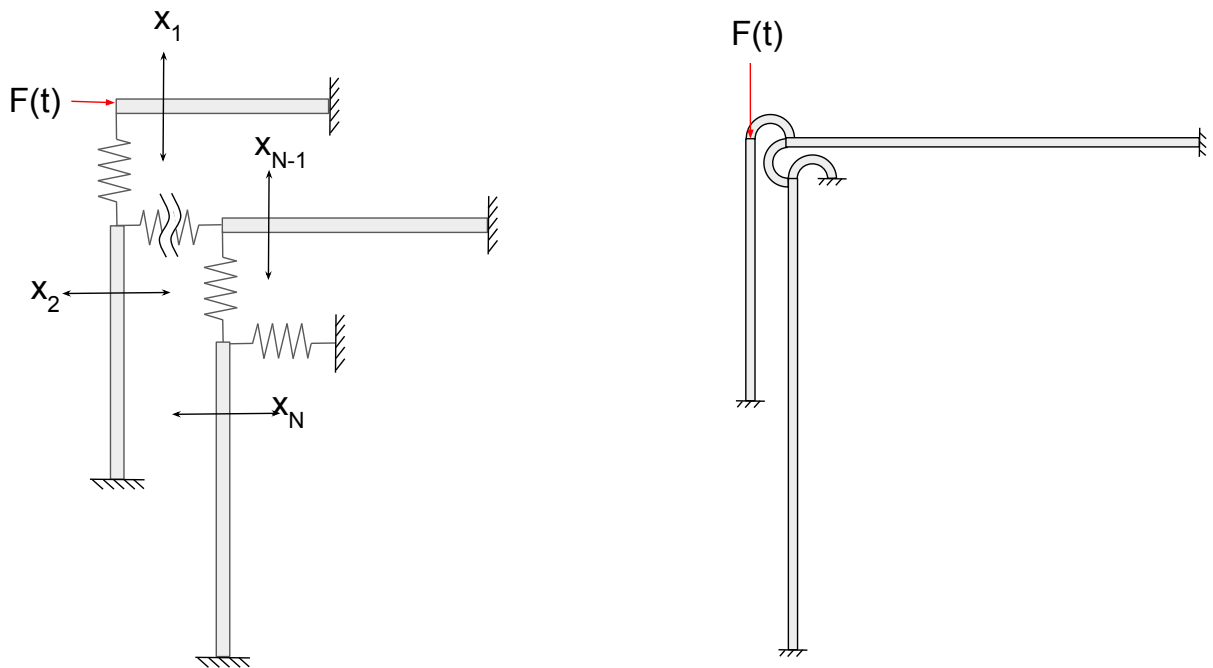


Figure 1.2: Schematic representations of the resonance cascade as investigated and developed by Qalandar et al [6]. The left figure represents a multi-stage frequency divider composed of N beams. The right figure represents the geometry of a 3 stage frequency divider based on the design developed by Qalandar, where the resonators are connected by semi-circular hooks.

found in a variety of applications, for example in vibration energy harvesters, phase-locked loops, quantum cascade lasers and RF transceivers [6]. An interesting application of frequency division is found in a MEMS resonance cascade frequency divider as investigated by Qalandar et al [6]. A micromechanical cascade demonstrates a multi-stage frequency division in an array of resonators. The frequency division is obtained in a purely mechanical manner. The resonance cascade consists of k sequentially perpendicular microbeams that are connected by semi-circular hooks that act as linear elastic couplings between the resonators. The system vibration modes are localized in the microbeams of the structure. The dimensions of the beams are carefully chosen such that the eigenfrequencies of the resonator beams have ratios close to $1 : 2 : 4 : \dots : 2^k$. A frequency division among the chain of resonators is obtained as the highest mode — let's call this the first stage — of the resonator array is excited in a parametric manner. This first stage parametrically excites the next stage in the chain that corresponds to mode number 2, whereupon mode number 2 parametrically excites mode number 3, etc. Stage after stage is activated until all modes of the cascade are activated due to the transfer of energy between the resonators. An analytical formulation of the frequency divider is formulated by Strachan [15]. A schematic representation of the resonance cascade is given in Fig. 1.2. If one now wants to make a FEM of this device, the number of unknowns stemming from the governing FE equations will increase rapidly due to discretizations of the model. An approach to circumvent a high-dimensional FEM of the FD is the application of the earlier mentioned reduction methods. In the case of FE reduction, it is expected that MDs need to be included in the reduction basis to account for the required geometric nonlinearities in the structure. The modularity of the FD makes it an excellent candidate for the application of CMS where the components of the FD are reduced individually. Therefore, the FD is an excellent benchmark to test the application of MDs-based reduction methods.

1.4. Summary

Finite element models are used in a variety of disciplines. Over decades, the complexity of the finite element models increased and accordingly the number of degrees of freedom in these models increased as well. This normally slows down computation times and requires more memory, and accordingly, the computational costs rise. Model order reduction was introduced to reduce the number of DoFs while retaining sufficient accuracy of the model. Last century, several projection-based reduction methods were developed. Examples are: Guyan reduction, Craig-Bampton reduction, and Rubin reduction. These reduction methods have been successfully applied to linear static and dynamic analyses. Later, modal derivatives were developed to capture the geometric nonlinearities in FE models. For simplicity reasons, static modal derivatives were introduced where the inertia components of the conventional modal derivatives are neglected. The conventional reduction techniques were successfully augmented with these static modal derivatives. Studies have shown that these enriched reduction methods can be used successfully in component mode synthesis, where transient responses of several systems were investigated. Research on conventional reduction methods have shown that, depending on the type of problem and boundary conditions, one of the reduction methods may give a better approximation of the full unreduced system than others. This applies to both linear as nonlinear analyses. Another possible reduction technique is in this work indicated as global reduction. This reduction method has a reduction basis that composes vibration modes and modal derivatives only, and is related to the entire assembled system. A simple overview of the general advantages and disadvantages of all considered reduction methods is given in table 1.1. Based on the literature study, a rough representation of the advantages and drawbacks of the reduction methods is given in the table.

Overview of the reduction methods					
	static modes	dynamic modes	accuracy static	accuracy dynamic	implementation
Guyan	yes	no	+	-	++
Craig-Bampton	yes	yes	+	+/-	+
Rubin	yes	yes	+	+	+/-
Global	no	yes	?	+	++

Table 1.1: A compact overview of the considered reduction methods. The overview shows the type of modes used in the reduction base, the accuracy and the implementation. The implementation indicates how easy the reduction basis is computed.

1.5. Research question

Based on the literature review, the following gap was identified: No research is found that considers MD-augmented conventional reduction methods for attaining the responses of parametrically excited structures. Moreover, no work is found that considers parametric excitation and resonance in combination with component mode synthesis. Therefore, it would be valuable to investigate a case where MDs, CMS and steady-state responses of parametrically excited structures are all of the interest. This is case is found in a mechanical frequency divider based on the model developed by Qalandar et al. [6]. The modularity of the frequency divider makes it an excellent candidate for component mode synthesis. Furthermore, the array of resonators that form the FD is activated by means of parametric resonance. This makes the FD a perfect benchmark for this project. This leads to the following main research question:

'How well can the reduced-order models based on modal derivatives approximate the responses of parametrically excited structures?'

To answer this question, a first logic and interesting step would be the analysis of some simple parametrically excited single beam structures. Such an analysis could indicate the applicability of the considered reduction methods in case of parametric resonance given some specific boundary conditions. This leads to the first subquestion:

'What is the influence of specific boundary conditions on the performance and applicability of different reduced-order models of parametrically excited structures?'

Then, the more complex frequency divider is used as a benchmark problem. As highlighted in the first part of the introduction, it is interesting to find manners to keep the number of modes in the reduction basis of the frequency divider as low as possible while retaining sufficient accuracy. This leads to the second subquestion:

'Which of the considered MDs-based ROMs of the frequency divider gives the highest performance in terms of computational efficiency and accuracy, and how can this efficiency be improved?'

In this thesis, answers are sought for these questions.

1.6. Performance estimations of the reduction methods

At this point where the relevant aspects of the project are introduced and the research questions are formulated, an indicator needs to be defined that at the end will be used to answer the research questions. Once an appropriate reduction method is chosen, in order to reproduce the full DoF nonlinear time response, one might be interested in an expression for the performance of that ROM, for example in terms of an error between the ROM and the full computation. Researches in the past have frequently used error-estimations that are based on a comparison of the displacements obtained with the ROMs and the displacements obtained with the full, unreduced computation. An option is a root mean square error estimator where the calculation of the error is based on the difference between the displacement vectors [37] obtained with the ROM and the full computation. Another option is the global relative error [38]. These error estimators are all convenient and precise for transient analyses. However, for a steady-state analysis, such error estimators are sometimes too harsh and therefore not automatically suitable. In steady-state responses, for example, a phase shift between the ROM and the full computation may be present. It is possible that a ROM is reproducing the overall behavior of the full nonlinear response very accurately and precise but with a (small) shift in time. A displacement-based estimator would immediately penalize such time shifts, therefore, one would rather tend to error estimations where 'similarity' between the shapes of the steady-state response is of more importance and the similarity of the amplitudes. Cross-correlation or coherence-based estimators are then a good alternative. This means that a higher correlation or coherence means a higher similarity and thus a higher performance of the ROM. In this work, the performances of the investigated ROMs are expressed in terms of a maximal normalized cross-correlation coefficient.

1.7. Thesis outline

In this section, a brief outline of the thesis is presented. Every subsection corresponds to a chapter in the thesis.

Paper

In chapter 2, the paper is presented that contains the main content of the thesis. An introduction to relevant topics is given. Then the reduction methods and different type of mode shapes are pre-

sented. The next part presents the numerical results and finally, a conclusion is drawn.

Reduced order models of beam structures

This chapter contains some additional numerical results that are too extensive to include in the content of the paper. First a validation of the codes is presented, then ROMs of a few transverse excited single beam models are considered and finally, ROMs of two frequency dividers are presented.

Conclusions

In this chapter, conclusions are drawn based on the results and findings that are collected during the thesis project.

Recommendations

This chapter discloses recommendations that are based on detected problems during the project. Methods are proposed in order to further improve the results that are achieved. Furthermore, this chapter discloses recommendations based on outstanding questions and issues that are identified over time. Besides, this chapter also addresses recommendations for future work related to the work done in this project.

Reflection

A brief reflection is presented regarding the master thesis project. It covers a reflection on the global timeline, a reflection on the contributions of this project, and a reflection on personal developments evolved during the master thesis.

Appendices

The appendices in this report present the derivations of the reduction bases, the derivations of the modes that form the ingredients of the reduction bases, the derivation of the tensors and the principles of parametrically excited structures are presented.

2

Paper

Modal derivative based reduced-order modeling for parametrically driven structures and frequency dividers

J.L. van den Broek
Delft University of Technology

The application of Modal Derivatives (MDs) in conventional reduction methods applied in Finite Elements Models (FEMs) is an effective method to capture the geometric nonlinearities that are present in the model. In this contribution, we assess different model order reduction techniques for geometrically nonlinear systems when applied to systems operating at parametric resonance. Specifically, we compare the Craig-Bampton reduction and Rubin methods, where the bases are augmented with modal derivatives, and we consider a reduction method for the entire system, without substructuring. We show that MDs play a crucial role in the operation of simple parametric excited cantilever structures. Furthermore, a special type of MDs is introduced to improve the performance of the Craig-Bampton reduction. A mechanical Frequency Divider (FD) is used as a benchmark problem to investigate the applicability of MDs-based reduced-order models (ROMs) of more complex parametric resonating structures. The FD consists of cascading mechanical components, each of which is excited by the preceding one utilizing parametric resonance. The modularity of the FDs makes them excellent candidates for component mode synthesis, where each substructure of the cascade is independently reduced and connected to other members via common interface. We show that the MDs play an important role in the operation of the ROMs of the FD. The performance of each considered reduction method is assessed by computing the cross-correlation of time histories of the full model and the ROMs. All considered reduction techniques can capture the parametric resonance and frequency division. Our results consistently indicate that a global reduction without substructuring is preferable to any substructuring method, as it delivers more accurate and smaller ROMs.

Keywords: Finite element method, Reduced-order models, Parametric resonance, Geometric nonlinearity, Modal derivatives, Steady-state responses.

Notations

1. Non-bold letters indicate scalars quantities, for example E, I and $F(t)$
2. Small bold letters and small Greek symbols indicate vectors, for example \mathbf{q} and ϕ
3. Bold capital letters and capital symbols indicate matrices, for example \mathbf{A} and Γ
4. Tensors are denoted with the super- and subscripts in front of symbol or letter as ${}^a_b\mathbf{Q}$, where a indicates the order of the tensor while b is just an index

1 Introduction

The Finite Element Method (FEM) is widely used in industry and research as a numerical method for solving problems in engineering and mathematical physics. The FEM is typically used in areas of interest that include heat transfer, structural dynamics, mass transfer, fluid dynamics, and electromagnetic potentials. In this paper, we consider Finite Element (FE) models that are related to the field of structural dynamics.

The constantly increasing power and storage capacities of computers enable analyses of more extensive and complex structures, which on its turn increased the demand for faster and more efficient computations. As the complexity and normally the number of elements in the structure increase, the number of unknowns, called the Degrees of Freedom (DoFs), that follow from the governing FEM equations increase as well. This normally slows down computation times and requires more memory. Fortunately, reduction methods were developed to effectively reduce the number of DoFs while retaining sufficient accuracy [9, 10], this is also known as Model-Order Reduction (MOR).

Traditional reduction techniques like Guyan's reduction [11], Craig-Bampton reduction [12], and Rubin's reduction [14] have been introduced a couple of decades ago. This class of reduction methods effectively reduce the number of DoFs by projecting the equations of motion on a suitable reduction basis. In several works, it has been shown that these traditional reduction techniques are perfectly able to approximate the full-DoF linear static and dynamic analyses of systems with high accuracy, for example in [9]. Depending on the type of problem and the boundary conditions, one of the reduction techniques may be the best choice for a specific application, as can be seen in [2].

Over the decades, the demand for nonlinear FE models increased. In 1985, to account for geometric nonlinearities in

FE models, the concept of Modal Derivatives (MDs) was introduced [4, 13]. The reduction bases of the linear reduction techniques were enriched with these MDs [1]. Several studies have shown the importance of MDs for transient nonlinear time responses of systems [2, 5, 8, 19]. Furthermore, it has been shown that some of the MDs enriched reduction methods can be effectively used in Component Mode Synthesis (CMS) [2]. CMS is a method where the dynamics of the entire system is described by the dynamics of the substructures, and the model size reduction is carried out on a substructure level. This method normally improves computational efficiency. Another advantage of this approach is the modularity of the reduced system, which is practical for design and optimization purposes [24].

In this paper, the applicability of MD enriched reduction methods in parametric resonating structures is investigated. The focus lies on the steady-state responses of the models. Parametric excitations are commonly seen in structures under axial harmonic forcing where stiffness and damping terms become time-dependent. A system may exhibit parametric resonance if the parametric excitation frequency is equal or close to a fundamental parametric resonance of the system [20]. In this research, first, ROMs of four parametric excited single cantilever beam structures with different boundary conditions are considered. The aim is to get a better understanding of the behavior of ROMs in case of parametric excitations and to get an understanding of the influence of specified boundary conditions on the applicability of the different reduction methods. A von-Karman nonlinear kinematic model is assumed, which is valid for small strains and moderate rotations. The considered type of damping in this work is the proportional Rayleigh damping.

Besides the simple parametric excited beam structures, the ROMs of a mechanical Frequency Divider (FD) are investigated as well. FDs, in general, are mechanical devices that allow obtaining vibrations of a given component at a fraction of some input frequency. A chain of such nonlinear resonators with natural frequency ratios of approximately 2:1 was investigated by Qalander et al [6]. An analytical formulation of this class of FDs is presented by Strachan et al. [15]. A similar parametrically resonating phenomenon was investigated in [17]. In this contribution we consider such an array of resonator micro beams in which the subsequent beams are connected by weak springs. See Fig.1 for a schematic representation of the FD. The FE model of the FD is due to its modularity an excellent candidate for investigating the applicability of CMS. Furthermore, the working principle of the investigated FD is based on parametric resonance and nonlinearities. The FD is, therefore, an interesting system to use as a benchmark problem to investigate the applicability of MD-based reduction techniques to resonant cascade structures in combination with CMS.

In this paper, 4 different types of model order reduction are applied to the FEM of a 3-stage FD. The Craig-Bampton reduction, Rubin reduction, and global reduction are investigated. For some of the components Guyan reduction is used as well. A full nonlinear computation is done to find the time response of the resonators in the system, this computation

is further compared with our ROMs. For both the Craig-Bampton reduction as the Rubin reduction, the resonance cascade is divided into substructures which are reduced individually. The global reduction is directly applied to the entire array of resonators without division in substructures.

In this paper, we also propose a method to enhance the performance of an MDs-enriched Craig-Bampton reduction basis utilizing Constraint Modal Derivatives (CMDs). The results show that augmenting the reduction basis with CMDs improves the accuracy.

Furthermore, we propose a tensor form of the nonlinear force vector and stiffness matrix for improving computational efficiency.

An error estimator is proposed to compare the performance of the ROMs with the full nonlinear computation in a steady-state response. The considered estimator is based on cross-correlation between the time histories obtained with the full model and the ROMs.

The paper is organized as follows. Section 2 describes the principles of model order reduction: nonlinear substructuring, different types of modes and the nonlinear reduction methods are briefly introduced. Section 3 briefly describes the model of the frequency divider. Section 4 shows the numerical results of the simple cases and the FD to assess the accuracy and applicability of the presented formulations. Finally, conclusions are drawn in section 5.

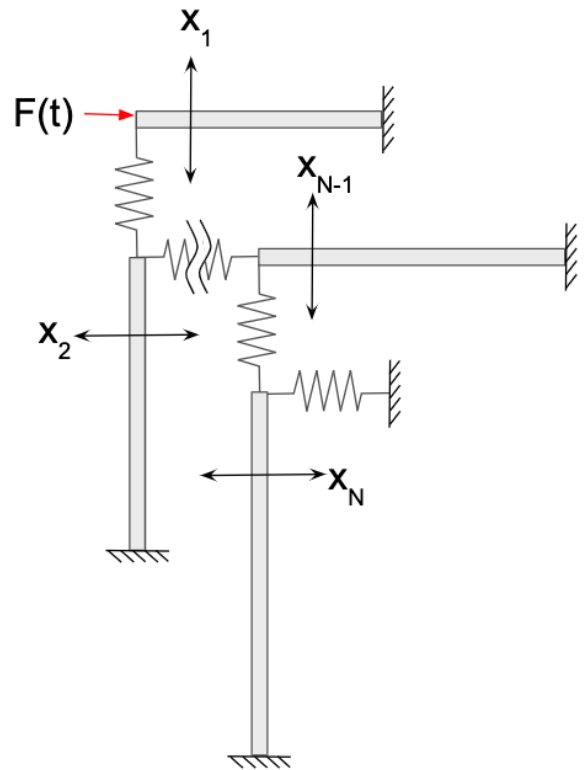


Fig. 1. Schematic representations of a frequency divider resonance cascade. The harmonic force $f(t)$ parametric excites X_1 , whereupon X_1 parametric excites X_2 etc. This kind of representation is introduced in the work of Strachan et al. [15]

2 Model order reduction

Normally, in structural dynamics, the response of a high dimensional system is (approximately) captured in a lower-dimensional subspace. The goal of some reduction methods is to find a suitable lower-dimensional reduction basis that contains enough information to describe with sufficient accuracy the high dimension response. Let's consider a n -DoF high dimensional system, and let $\mathbf{q}(t) \in \mathbf{R}^n$ be the vector of nodal generalized displacements. In presence of geometric nonlinearities, the equation of motion of the discretized system is given as:

$$\mathbf{M}\ddot{\mathbf{q}}(t) + \mathbf{C}\dot{\mathbf{q}}(t) + \mathbf{K}\mathbf{q}(t) + \mathbf{f}^{\text{NL}}(\mathbf{q}(t)) = \mathbf{f}^{\text{ext}}(t), \quad (1)$$

where $\mathbf{M} \in \mathbf{R}^{n \times n}$ is the system mass matrix, $\mathbf{C} \in \mathbf{R}^{n \times n}$ is the system damping matrix, $\mathbf{K} \in \mathbf{R}^{n \times n}$ is the linear tangent stiffness matrix, $\mathbf{f}^{\text{NL}}(\mathbf{q}(t)) \in \mathbf{R}^n$ is the nonlinear force vector, and $\mathbf{f}^{\text{ext}}(t) \in \mathbf{R}^n$ is the external force vector, which may be time dependent. The vector $\mathbf{q}(t)$ may be approximated as a linear combination of $m < n$ modes:

$$\mathbf{q}(t) \approx \sum_{i=1}^m \mathbf{v}_i h_i(t), \quad (2)$$

where $\mathbf{v}_i \in \mathbf{R}^n$ is a constant high-dimensional mode and $h_i(t)$ is the corresponding time-dependent amplitude of the mode. The modes can be collected in a reduction basis $\mathbf{V} \in \mathbf{R}^{n \times m}$ as:

$$\mathbf{V} = [\mathbf{v}_1, \mathbf{v}_2, \dots, \mathbf{v}_m], \quad (3)$$

while the corresponding amplitudes are collected in the time-dependent vector $\boldsymbol{\eta}(t) \in \mathbf{R}^m$:

$$\boldsymbol{\eta}(t) = [h_1(t), h_2(t), \dots, h_m(t)]. \quad (4)$$

The amplitudes of the modes stored in the vector $\boldsymbol{\eta}(t)$ are in fact the reduced set of DoFs. The high dimensional vector \mathbf{q} and its time derivatives can now be projected on the basis \mathbf{V} , such that we can write:

$$\mathbf{q}(t) \approx \mathbf{V}\boldsymbol{\eta}(t), \quad \dot{\mathbf{q}}(t) \approx \mathbf{V}\dot{\boldsymbol{\eta}}(t), \quad \ddot{\mathbf{q}}(t) \approx \mathbf{V}\ddot{\boldsymbol{\eta}}(t), \quad (5)$$

where $\dot{\boldsymbol{\eta}}$ and $\ddot{\boldsymbol{\eta}}$ are the first and second order time derivatives of the reduced coordinate vector $\boldsymbol{\eta}$ respectively. For the sake of simplicity, we omit the time dependency indicator $\bullet(t)$ for both $\boldsymbol{\eta}(t)$ and $\mathbf{q}(t)$ in the remaining part of this paper. Via Galerkin projection the reduced equations of motion are obtained by projection of the full equations of motion on the reduction basis \mathbf{V} :

$$\mathbf{V}^T \mathbf{M} \mathbf{V} \ddot{\boldsymbol{\eta}} + \mathbf{V}^T \mathbf{C} \mathbf{V} \dot{\boldsymbol{\eta}} + \mathbf{V}^T \mathbf{K} \mathbf{V} \boldsymbol{\eta} + \mathbf{V}^T \mathbf{f}^{\text{NL}}(\mathbf{V}\boldsymbol{\eta}) = \mathbf{V}^T \mathbf{f}^{\text{ext}}(t). \quad (6)$$

Or equivalently:

$$\tilde{\mathbf{M}}\ddot{\boldsymbol{\eta}} + \tilde{\mathbf{C}}\dot{\boldsymbol{\eta}} + \tilde{\mathbf{K}}\boldsymbol{\eta} + \tilde{\mathbf{f}}^{\text{NL}}(\boldsymbol{\eta}) = \tilde{\mathbf{f}}^{\text{ext}}(t), \quad (7)$$

where $\tilde{\mathbf{M}}, \tilde{\mathbf{C}}$ and $\tilde{\mathbf{K}} \in \mathbf{R}^{m \times m}$ are the reduced mass, reduced damping and reduced linear stiffness matrices respectively, while $\tilde{\mathbf{f}}^{\text{ext}}(t) \in \mathbf{R}^m$ is the reduced time-dependent external force vector.

If we now consider an unreduced system composed of r unreduced substructures, then the assembly of the global system mass matrix is written as:

$$\mathbf{M}_{\text{global}} = \text{assembly}(\mathbf{M}^{(1)}, \dots, \mathbf{M}^{(r)}), \quad (8)$$

in which the superscript r denotes the substructure number. The structure is assembled according to standard substructure assembly strategies using boolean matrices which ensure that a pair of boundary nodes of two connected substructures have equal displacements. Furthermore, the boolean matrices ensure that the boundary forces of two connected substructures are in equilibrium [7]. In the same manner, the matrices and vectors $\mathbf{K}_{\text{global}}, \mathbf{C}_{\text{global}}, \mathbf{f}_{\text{global}}^{\text{NL}}$ and $\mathbf{f}_{\text{global}}^{\text{ext}}$ are assembled.

Let's now consider a system composed of several substructures. Depending on the type of reduction there exist two ways to obtain the reduced model of this assembled system. The first option is that the ROM is obtained by projection of a reduction basis that corresponds to the entire assembled system. In that case eq. 6 can be applied where the matrices and vectors in the equation are replaced by matrices and vectors that correspond to the total global, assembled system. The other way is that the substructures are reduced individually and assembled afterward, this method is known as component mode synthesis. In that case, the reduced global system matrices $\tilde{\mathbf{K}}_{\text{global}}$ and $\tilde{\mathbf{C}}_{\text{global}}$ are found in the same manner as presented here for the mass matrix:

$$\tilde{\mathbf{M}}_{\text{global}} = \text{assembly}(\tilde{\mathbf{M}}^{(1)}, \dots, \tilde{\mathbf{M}}^{(r)}). \quad (9)$$

In this paper, both methods are used to find the ROM of the entire assembled system. In the remaining part of this paper the superscripts of the system matrices and vectors are omitted for simplicity. The formulations in the next sections are all with respect to the substructures unless stated otherwise.

2.1 Tensor formulation of the nonlinear force vector and stiffness matrix

The solution of eq.2. is typically obtained by time integration, for instance with a Newmark's integration scheme, which requires Newton iterations within each time step to achieve convergence. In a full, unreduced system, the internal nonlinear force vector and the nonlinear stiffness matrix are updated every iteration; this might be very computational inefficient. In this paper, the internal nonlinear forces are based on the von-Karman kinematic model, which results in

a polynomial form of the nonlinear forces up to the third order, as a function of the displacement vector \mathbf{q} :

$$\mathbf{f}^{\text{NL}}(\mathbf{q}) = {}^2\mathbf{Q} \cdot \mathbf{q} + {}^3\mathbf{Q} : (\mathbf{q} \otimes \mathbf{q}) + {}^4\mathbf{Q} : (\mathbf{q} \otimes \mathbf{q} \otimes \mathbf{q}), \quad (10)$$

where ${}^2\mathbf{Q}$, ${}^3\mathbf{Q}$ and ${}^4\mathbf{Q}$ are second, third and fourth order tensors respectively. The operator \otimes signifies the Kronecker or dyadic product. In the same manner, the nonlinear stiffness matrix can be written in a tensor form. The nonlinear stiffness matrix is found as the derivative of \mathbf{f}^{NL} with respect to the displacement vector \mathbf{q} :

$$\mathbf{K}^{\text{NL}}(\mathbf{q}) = \frac{\partial \mathbf{f}^{\text{NL}}(\mathbf{q})}{\partial \mathbf{q}} = {}^2\mathbf{Q} + 2 \cdot {}^3\mathbf{Q} \cdot \mathbf{q} + 3 \cdot {}^4\mathbf{Q} : (\mathbf{q} \otimes \mathbf{q}). \quad (11)$$

Note that eq.9. and eq.10. do not reflect the way nonlinear forces are computed. In fact, \mathbf{f}^{NL} is obtained by assembling of contributions at element level. The tensors ${}^2\mathbf{Q}$, ${}^3\mathbf{Q}$ and ${}^4\mathbf{Q}$ are therefore never available because of excessive storage requirements. Nevertheless, a useful property of the application of tensors is the fact that inside the iteration loop the updated versions of the reduced stiffness matrix $\tilde{\mathbf{K}}^{\text{NL}}$ and the reduced nonlinear force vector $\tilde{\mathbf{f}}^{\text{NL}}$ can be computed without first considering element contributions from the full displacement vector \mathbf{q} . In that case, a reduced formulation of the tensors is used where $\tilde{\mathbf{f}}^{\text{NL}}$ and $\tilde{\mathbf{K}}^{\text{NL}}$ are found as a polynomial function of the reduced coordinate vector $\boldsymbol{\eta}$. The reduced tensor formulations are given as:

$$\tilde{\mathbf{f}}^{\text{NL}}(\boldsymbol{\eta}) = {}^2\tilde{\mathbf{Q}} \cdot \boldsymbol{\eta} + {}^3\tilde{\mathbf{Q}} : (\boldsymbol{\eta} \otimes \boldsymbol{\eta}) + {}^4\tilde{\mathbf{Q}} : (\boldsymbol{\eta} \otimes \boldsymbol{\eta} \otimes \boldsymbol{\eta}), \quad (12)$$

and:

$$\tilde{\mathbf{K}}^{\text{NL}}(\boldsymbol{\eta}) = \frac{\partial \tilde{\mathbf{f}}^{\text{NL}}(\boldsymbol{\eta})}{\partial \boldsymbol{\eta}} = {}^2\tilde{\mathbf{Q}} + 2 \cdot {}^3\tilde{\mathbf{Q}} \cdot \boldsymbol{\eta} + 3 \cdot {}^4\tilde{\mathbf{Q}} : (\boldsymbol{\eta} \otimes \boldsymbol{\eta}), \quad (13)$$

with ${}^2\tilde{\mathbf{Q}} \in \mathbf{R}^{m \times m}$, ${}^3\tilde{\mathbf{Q}} \in \mathbf{R}^{m \times m \times m}$ and ${}^4\tilde{\mathbf{Q}} \in \mathbf{R}^{m \times m \times m \times m}$, where again m is the number of reduced coordinates or equivalently the number of modes in the reduction basis. By virtue of eq.12 and eq.13, it is not necessary to call elemental functions to evaluate the nonlinear forces, as the reduced tensors can be computed 'offline' and once for all, i.e. outside the loops of the Newton-Raphson iteration scheme, this results in a more efficient nonlinear time integration. The derivation of the relevant tensors can be found in Appendix A.

2.2 Computation of the reduction basis

A reduction basis \mathbf{V} should comprise a set of modes that can reproduce the full nonlinear solution with sufficient accuracy. To achieve this, different types of modes that contain relevant information on the system dynamics need to be included in the reduction basis. Each of the conventional

reduction methods uses its characteristic modes. Guyan reduction [11], Craig-Bampton reduction [12], and Rubin reduction [14] are all applicable to popular component mode synthesis methods. The reduction bases of these methods are designed such that the boundary DoFs of the system remain unreduced. This is done to facilitate straightforward system assembly after reduction on substructure level. The partition of the coordinate vector in boundary and internal components is written as:

$$\mathbf{q} = \begin{bmatrix} \mathbf{q}_B \\ \mathbf{q}_I \end{bmatrix}, \quad (14)$$

where the subscript I refers to the internal DoFs, while the subscript B refers to the boundary DoFs. The boundary nodes, in general, are the nodes that are fixed, sharing nodes with other substructures, or nodes that are imposed by external forces. Internal nodes are nodes that are neither coupled to other substructures nor fixed nor imposed by external forces. If the partition as in eq. 20 is used, the system matrices are accordingly partitioned. For a linear substructure, we can partition the equations of motion in boundary and internal components as:

$$\begin{bmatrix} \mathbf{M}_{BB} & \mathbf{M}_{BI} \\ \mathbf{M}_{IB} & \mathbf{M}_{II} \end{bmatrix} \begin{bmatrix} \ddot{\mathbf{q}}_B \\ \ddot{\mathbf{q}}_I \end{bmatrix} + \begin{bmatrix} \mathbf{K}_{BB} & \mathbf{K}_{BI} \\ \mathbf{K}_{IB} & \mathbf{K}_{II} \end{bmatrix} \begin{bmatrix} \mathbf{q}_B \\ \mathbf{q}_I \end{bmatrix} = \begin{bmatrix} \mathbf{f}^{\text{ext}}_B(t) \\ \mathbf{0} \end{bmatrix} + \begin{bmatrix} \mathbf{g} \\ \mathbf{0} \end{bmatrix}, \quad (15)$$

where \mathbf{g} is a vector that contains the boundary forces coming from connection with other parts of the system. In the following sections, we briefly recap the typical modes that could be used to form the basis \mathbf{V} .

2.2.1 Free vibration modes

The free vibration modes represent the vibration modes of an unconstrained structure, i.e. the structure is free-floating in space. The i -th free vibration mode, $\phi_{f,i}$, is obtained by solving the following eigenvalue problem:

$$(\mathbf{K} - \omega_i^2 \mathbf{M}) \phi_{f,i} = \mathbf{0}, \quad (16)$$

where \mathbf{K} and \mathbf{M} are the linear system stiffness matrix and the system mass matrix respectively. The free vibration modes are collected in the columns of the matrix Φ_f .

2.2.2 Internal vibration modes

The internal vibration modes or fixed vibration modes are the vibration modes that correspond to a structure where all boundary nodes are fixed. The i -th internal vibration mode $\phi_{I,i}$ is found by solving the following eigenvalue problem:

$$(\mathbf{K}_{II} - \omega_i^2 \mathbf{M}_{II}) \phi_{I,i} = \mathbf{0}. \quad (17)$$

The internal vibration modes are collected in the columns of the matrix Φ_I .

2.2.3 Rigid body modes

Rigid body modes describe the motion of a body in space without any deformation. Since these motions do not cause any internal elastic forces, the rigid body modes Φ_r are in fact calculated as the null space of the unconstrained system stiffness matrix [21]:

$$\Phi_r = \text{null}(\mathbf{K}). \quad (18)$$

For relatively simple and small systems this approach for finding the rigid body modes works well, but for larger system matrices this approach is rather inefficient. Therefore, for more complex structures, the rigid body modes are mostly computed geometrically [18].

2.2.4 Constraint modes

The constraint modes are modes that describe the shape of the structure in case of an imposed unit displacement of one of the boundary DoFs while keeping the other boundary DoFs fixed, i.e $\mathbf{q}_B = \mathbf{0}$. Constraint modes are static modes, in contrast with the vibration modes which are dynamic modes. The starting point is a static equilibrium described as:

$$\mathbf{K}\mathbf{q} = \mathbf{f}^{\text{ext}}, \quad (19)$$

where \mathbf{f}^{ext} is an external force vector acting on the boundary DoFs. After partition in boundary and interior DoFs, the latter equation can be written as:

$$\begin{bmatrix} \mathbf{K}_{BB} & \mathbf{K}_{BI} \\ \mathbf{K}_{IB} & \mathbf{K}_{II} \end{bmatrix} \begin{bmatrix} \mathbf{q}_B \\ \mathbf{q}_I \end{bmatrix} = \begin{bmatrix} \mathbf{f}^{\text{ext}}_B \\ \mathbf{0} \end{bmatrix}. \quad (20)$$

From the lower part of the latter equation, it follows that the interior DoFs can be written as a function of the boundary DoFs:

$$\mathbf{q}_I = -\mathbf{K}_{II}^{-1}\mathbf{K}_{IB}\mathbf{q}_B = \Psi_c\mathbf{q}_B, \quad (21)$$

where Ψ_c is called the condensation matrix. The columns of the condensation matrix form the constraint modes. The number of boundary DoFs equals the number of modes that are contained in the condensation matrix. For instance, a 2D beam structure normally contains six constraint modes associated with its 6 boundary DoFs.

2.2.5 Attachment modes

Attachment modes are modes that describe the shape of the structure in case of an imposed unit force on one of the boundary nodes while imposing a zero force on the other boundary nodes. Like constraint modes, attachment modes are static modes. The matrix that contain the attachment modes, denoted as Ψ_a , is calculated as:

$$\Psi_a = \mathbf{K}^{-1}\mathbf{F}, \quad (22)$$

where \mathbf{K} is the linear stiffness matrix. The matrix \mathbf{F} is the force matrix where the columns of the matrix impose an unit force on the boundary DoFs. The matrix \mathbf{F} is given as:

$$\mathbf{F} = [\mathbf{I}, \mathbf{0}]^T. \quad (23)$$

Where \mathbf{I} is the identity matrix acting on \mathbf{q}_B , and $\mathbf{0}$ is the null matrix acting on \mathbf{q}_I . If the relevant substructure is fully constrained, the attachment modes are easily computed according to Eq. 22. In the case of a component with rigid body modes, eq. 22 is singular and not solvable directly. In that case, the attachment modes are calculated as:

$$\Psi_a = \mathbf{P}^T\mathbf{G}\mathbf{P}\mathbf{F}, \quad (24)$$

where \mathbf{G} is a generalized or pseudo-inverse of the stiffness matrix \mathbf{K} , and \mathbf{P} is the projection matrix [12] given as:

$$\mathbf{P} = (\mathbf{I} - \mathbf{M}\Phi_r(\Phi_r^T\mathbf{M}\Phi_r)^{-1}\Phi_r^T). \quad (25)$$

2.3 Modal derivatives

For linear systems, the response of the system can be accurately approximated by a truncated set of linear vibration modes:

$$\mathbf{q} \approx \sum_{i=1}^m \phi_i h_i = \Phi\eta, \quad (26)$$

where $\Phi = [\phi_1, \phi_2, \dots, \phi_m] \in \mathbf{R}^{n \times m}$ and $\eta = [h_1, h_2, \dots, h_m]^T \in \mathbf{R}^m$. The full DoF vector \mathbf{q} is written as a function of η such that $\mathbf{q} = \mathbf{q}(\eta) = \Phi\eta$. For a nonlinear system, eq. 26 will no longer hold since the modes are in fact deformation dependent, and therefore they do not describe nonlinear second-order effects. MDs were introduced [13] to account for the second order effects and are in fact the second-order terms of a Taylor series expansion around an equilibrium position $\mathbf{q}_{eq} = \mathbf{0}$ [16]:

$$\mathbf{q}(\eta) = \left. \frac{\partial \mathbf{q}}{\partial \eta} \right|_{eq} \cdot \eta + \frac{1}{2} \frac{\partial^2 \mathbf{q}}{\partial \eta \partial \eta} : \eta \otimes \eta. \quad (27)$$

The partial derivatives are given as:

$$\frac{\partial \mathbf{q}}{\partial h_i} = \phi_i, \quad \frac{\partial^2 \mathbf{q}}{\partial h_i \partial h_j} = \frac{\partial \phi_i}{\partial h_j} = \theta_{ij}, \quad (28)$$

where $\theta_{ij} \in \mathbf{R}^n$ is the MD. Thus MDs stem from the directional derivatives of the eigenvalue problem in the direction of the vibration modes. The MDs considered in this work are known as static MDs, which in contrast to the conventional MDs ignore inertia terms [4, 25]. The static MD related to the vibration modes ϕ_i and ϕ_j of a structure is calculated as:

$$\theta_{ij} = \left. \frac{\partial \phi_i}{\partial h_j} \right|_{eq} = \mathbf{K}^{-1} \left. \frac{\partial \mathbf{K}^{\text{NL}}}{\partial h_j} \right|_{eq} \phi_i. \quad (29)$$

An FE formulation of the modal derivative for a beam element is given in Appendix B. MDs are symmetric, i.e. $\theta_{ij} = \theta_{ji}$, the proof for this symmetry is given in [4]. This means that given a set of k vibration modes, there exist $d = k(k+1)/2$ unique MDs. The MDs are collected in the columns of the matrix Θ .

2.4 Constraint modal derivatives

A special type of modal derivatives is the Constraint Modal Derivative (CMD). The formulation of the CMD is quite similar to the formulation of the static modal derivative in eq. 29. The static CMD γ_{ij} associated to the constraint modes ψ_i and ψ_j is calculated as:

$$\gamma_{ij} = -\mathbf{K} \left. \frac{\partial \mathbf{K}}{\partial \mathbf{q}_{B,j}} \right|_{eq} \psi_{c,i}, \quad (30)$$

where the boundary DoF $\mathbf{q}_{B,j}$ is in fact the i -th amplitude of the constraint mode $\psi_{c,i}$. The CMDs are collected in the matrix Γ . For the computation of a CMDs, we only consider the out of plane constraint modes and the rotational constraint modes, thus 4 constraint modes for a beam structure with its boundary nodes at the ends. This means that $4(4+1)/2 = 10$ CMDs can be computed for such structures. However, 5 linear independent modes can be subtracted out of these 10 modes, therefore, there exist 5 unique constraint modal derivatives for a beam structure. An FE formulation of the CMD is given in Appendix C.

2.5 Guyan reduction

One of the simplest and oldest reduction methods is the Guyan reduction [11], which is applicable for static reduction and slow dynamic systems where the eigenfrequency of the structure is much higher than the excitation frequency, i.e. $\omega_{exc} \ll \omega_1$. The relation between the full, high-dimensional set of DoFs and the reduced set of DoFs for Guyan reduction is given as:

$$\mathbf{q} \approx \begin{bmatrix} \mathbf{I} \\ \Psi_c \end{bmatrix} \mathbf{q}_B = \mathbf{V}_{Gyn} \mathbf{q}_B. \quad (31)$$

This means that in case of Guyan reduction, the boundary DoFs are the reduced coordinates. This means that the interior DoFs of the structure are 'enslaved' by the boundary DoFs.

2.6 Craig-Bampton reduction

Craig-Bampton reduction can be seen as an extension of the Guyan reduction with internal vibration modes. This means that the Craig-Bampton reduction basis comprises both static and dynamic modes, and therefore, the Craig-Bampton reduction basis also contains dynamic information about the system. The Craig-Bampton reduction bases can contain additional information about the nonlinear behavior of the system by augmenting the reduction basis with MDs

and CMDs. In this paper, we make a distinction between Craig-Bampton bases augmented with MDs only, denoted as \mathbf{V}^I_{CB} , and Craig-Bampton reduction bases augmented with both MDs and CMDs: \mathbf{V}^{II}_{CB} . The relation between the full set of DoFs and the Craig-Bampton reduction basis augmented with MDs is given as:

$$\begin{bmatrix} \mathbf{q}_B \\ \mathbf{q}_I \end{bmatrix} \approx \begin{bmatrix} \mathbf{I} & \mathbf{0} & \mathbf{0} \\ \Psi_c & \Phi_I & \Theta_I \end{bmatrix} \begin{bmatrix} \mathbf{q}_B \\ \lambda \\ \zeta \end{bmatrix} = \mathbf{V}^I_{CB} \eta^I_{CB}. \quad (32)$$

From the latter equation it follows that the reduced coordinate vector η^I_{CB} is given as:

$$\eta^I_{CB}{}^T = [\mathbf{q}_B^T, \lambda^T, \zeta^T], \quad (33)$$

where the vector λ contains the amplitudes of the internal vibration modes while the vector ζ contains the amplitudes of the modal derivatives.

If we now consider the Craig-Bampton reduction basis \mathbf{V}^{II}_{CB} , the mapping between the full set of DoFs and the reduced coordinate vector is written as:

$$\begin{bmatrix} \mathbf{q}_B \\ \mathbf{q}_I \end{bmatrix} \approx \begin{bmatrix} \mathbf{I} & \mathbf{0} & \mathbf{0} & \mathbf{0} \\ \Psi_c & \Phi_I & \Theta_I & \Gamma_I \end{bmatrix} \begin{bmatrix} \mathbf{q}_B \\ \lambda \\ \zeta \\ \chi \end{bmatrix} = \mathbf{V}^{II}_{CB} \eta^{II}_{CB}. \quad (34)$$

This yields that the reduced coordinate vector η^{II}_{CB} is given as:

$$\eta^{II}_{CB}{}^T = [\mathbf{q}_B^T, \lambda^T, \zeta^T, \chi^T], \quad (35)$$

where the vector χ contains the amplitudes of the CMDs.

2.7 Rubin reduction

Rubin reduction is a reduction method where free vibration modes and rigid body modes are used as dynamic ingredients of the reduction basis. Furthermore, attachment modes account for the static part of the reduction basis. The relation between the full set of DoFs and the Rubin reduction basis augmented with MDs is given as:

$$\begin{bmatrix} \mathbf{q}_B \\ \mathbf{q}_I \end{bmatrix} \approx \begin{bmatrix} \mathbf{I} & \mathbf{0} & \mathbf{0} & \mathbf{0} \\ \mathbf{A} & \mathbf{B} & \mathbf{C} & \mathbf{D} \end{bmatrix} \begin{bmatrix} \mathbf{q}_B \\ \xi \\ \iota \\ \mu \end{bmatrix} = \mathbf{V}_R \eta_R. \quad (36)$$

From the latter equation, it follows that the reduced coordinate vector η_R is given as:

$$\eta_R{}^T = [\mathbf{q}_B^T, \xi^T, \iota^T, \mu^T], \quad (37)$$

where ξ, ι and μ are the vectors that contain the amplitudes of the modes in \mathbf{B}, \mathbf{C} and \mathbf{D} respectively. The components of the Rubin reduction basis \mathbf{V}_R are calculated as:

$$\mathbf{A} = \Psi_{a,B} \Psi_{a,B}^{-1}, \quad (38)$$

$$\mathbf{B} = \Phi_{r,I} - \Psi_{a,B} \Psi_{a,B}^{-1} \Phi_{r,B}, \quad (39)$$

$$\mathbf{C} = \Phi_{f,I} - \Psi_{a,B} \Psi_{a,B}^{-1} \Phi_{f,B}, \quad (40)$$

and

$$\mathbf{D} = \Theta_I - \Psi_{a,B} \Psi_{a,B}^{-1} \Theta_B. \quad (41)$$

Again, the subscripts B and I refer to the boundary and interior parts of the modes.

2.8 Global reduction

In global reduction, the reduced model of the entire system is found without first reducing the substructures separately. This means that the modes in the global reduction basis correspond to the entire assembled structure. The system vibration modes, Φ_G , and their corresponding MDs, Θ_G , are the only ingredients that are comprised in the reduction basis. The i -th global vibration mode, $\phi_{G,i}$ is found by solving the following eigenvalue problem:

$$(\mathbf{K}_{\text{global}} - \omega_i^2 \mathbf{M}_{\text{global}}) \phi_{G,i} = \mathbf{0} \quad (42)$$

This kind of reduction basis, also called a linear reduction base, was effectively used and discussed in [3, 16, 22]. The formulation of the global reduction basis that contains k vibration modes and all their corresponding MDs is given as:

$$\mathbf{V}_G \approx [\Phi_G, \Theta_G] = [\phi_{G,1}, \phi_{G,2}, \dots, \phi_k, \theta_{G,11}, \theta_{G,12}, \dots, \theta_{G,kk}]. \quad (43)$$

The relation between the full set of DoFs and the reduced set is thus given as:

$$\mathbf{q} \approx \mathbf{V}_G \eta_G, \quad (44)$$

where η_G is the reduced set of coordinates that contains the amplitudes of Φ_G and Θ_G .

In this work, the vibration modes in the global reduction basis are sequentially ordered according to their corresponding eigenfrequency, this means that the vibration mode $\phi_{G,1}$ corresponds to the lowest eigenfrequency while $\phi_{G,k}$ is the k -th vibration mode that corresponds to the k -th eigenfrequency of the system. For example: if the reduction basis composes 4 vibration modes, it means that the first 4 vibration modes of the system are considered in the reduction basis.

3 Description of a mechanical frequency divider resonance cascade

Benchmark in this work is an FD that consists of a chain of 3 resonators with natural frequency ratios of approximately 2:1. The operation of the resonance cascade is based on nonlinear dynamics and its robustness is found in parametric resonances. The in this paper considered FD is based on the device presented by Qalandar et al. [6]. The FD consists of resonance beams that are sequentially perpendicularly oriented. A schematic representation of the resonator array is given in Fig.1. The resonator beams are interconnected by semi-circular hooks that act as relatively weak springs. The dimensions of the beams should be chosen properly such that the natural frequency f_N of resonator number N in the chain equals:

$$f_N = \frac{1}{2^N} f_1, \quad (45)$$

where f_1 is the natural frequency of the first beam in the array.

The FD is activated by a harmonic point force that is axially imposed on the first beam in the array. The excitation frequency equals twice f_1 . As a consequence, the beam starts to resonate in a parametric manner what leads to a beam displacement denoted as X_1 . Now the harmonic displacement X_1 on its turn, due to geometric nonlinearity, parametrically excites the next beam in the chain, this results in a transverse displacement, denoted by X_2 , whereupon the motion X_2 parametrically excites X_3 , and so on. Finally, the entire array of resonators is activated. The energy from one resonator beam is transferred to the next beam and vice versa via the semi-circular connecting components f . This means that there exists a complex back and forward coupling between the resonator beams in the structure. To activate the whole chain, proper boundary conditions and parameter settings should be chosen. The amplitudes of the beams are dependent on the amplitude of the harmonic excitation and the excitation frequency. The amplitudes of the beam need to be sufficiently large to overcome damping and mistuning [6]. The force amplitude should be sufficiently large and the excitation frequency needs to be sufficiently close to twice the eigenfrequency of the first beam in the chain. A sweep of both parameters results in an instability map of the structure for the different modes. To activate the entire cascade, both parameters should be chosen carefully such that they both lie inside all instability regions of the resonators in array. [6]

4 Numerical results

In this section, first, ROMs of 4 simple single beam structures that are parametric excited are considered. In the next part of this section the ROMs of a three-stage resonance cascade are presented. In this section, the following reduction bases are used:

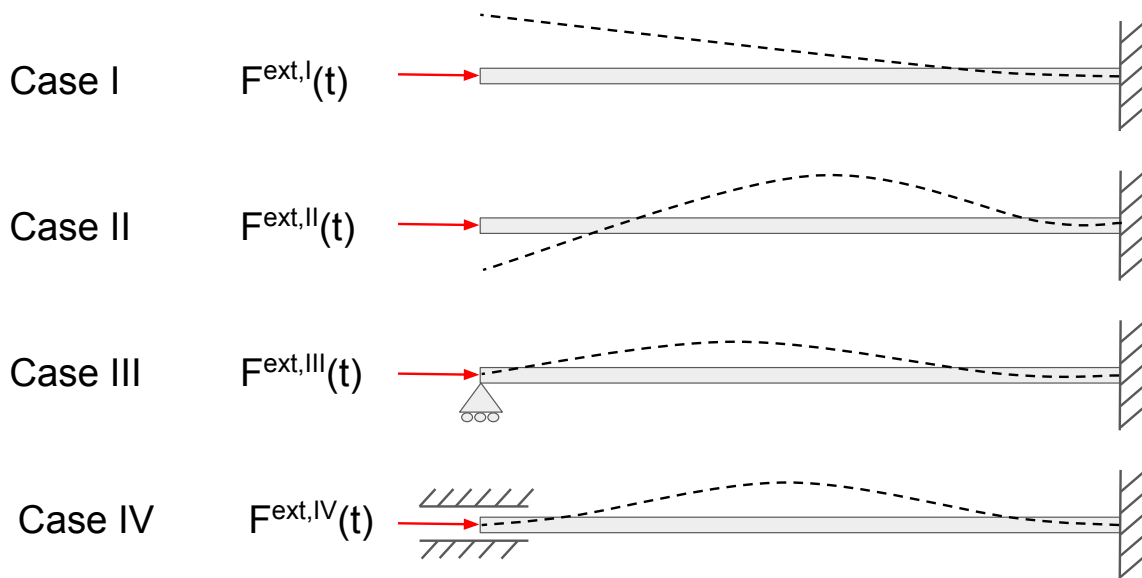


Fig. 2. Schematic representation of the different considered cases, the dashed lines represent the mode shapes of the structure in case of parametric resonance.

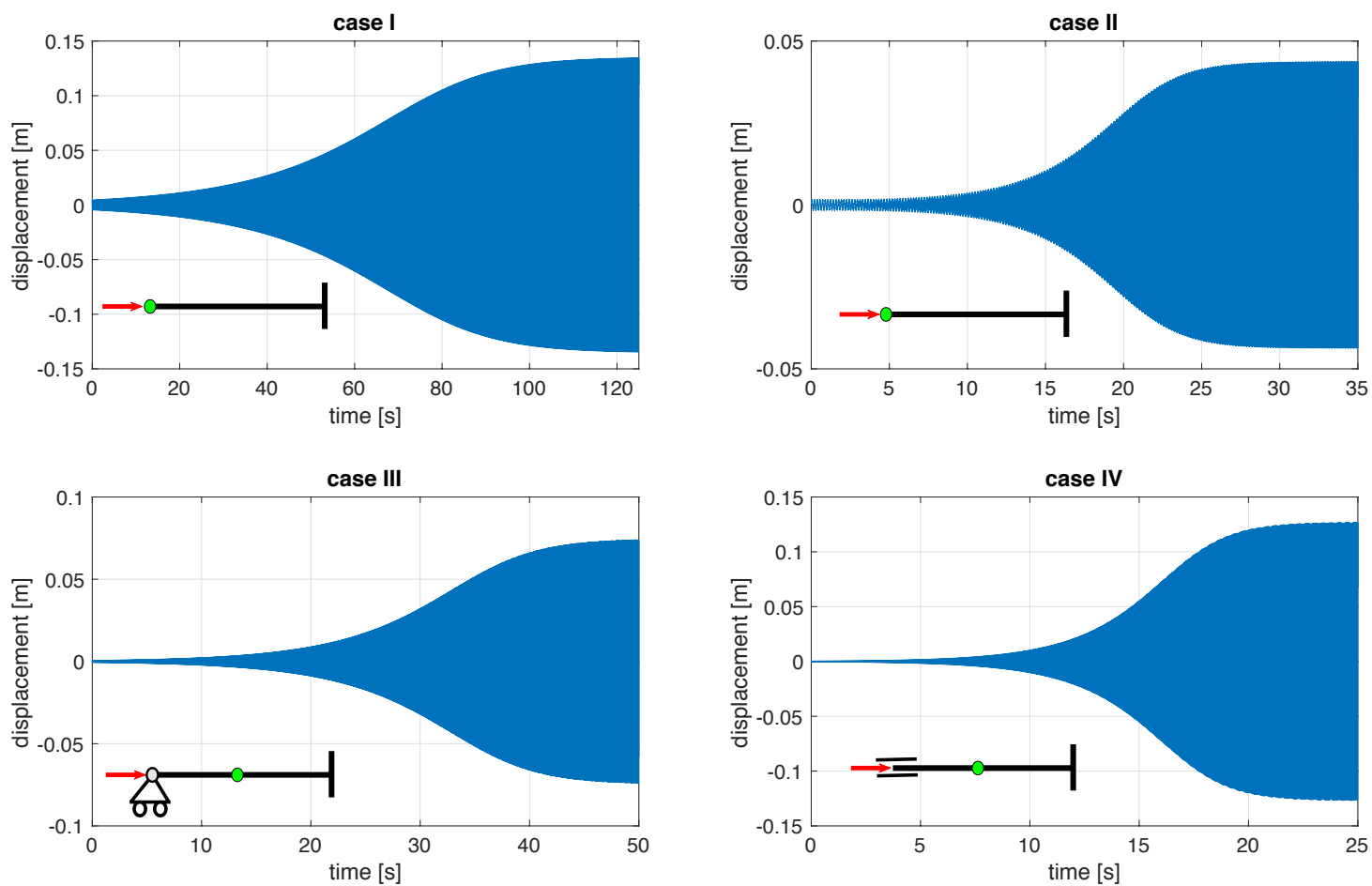


Fig. 3. Full nonlinear time responses of the four considered cases. The green dot in the small structures below the time responses indicates the location where the transverse displacement in the specific case is measured.

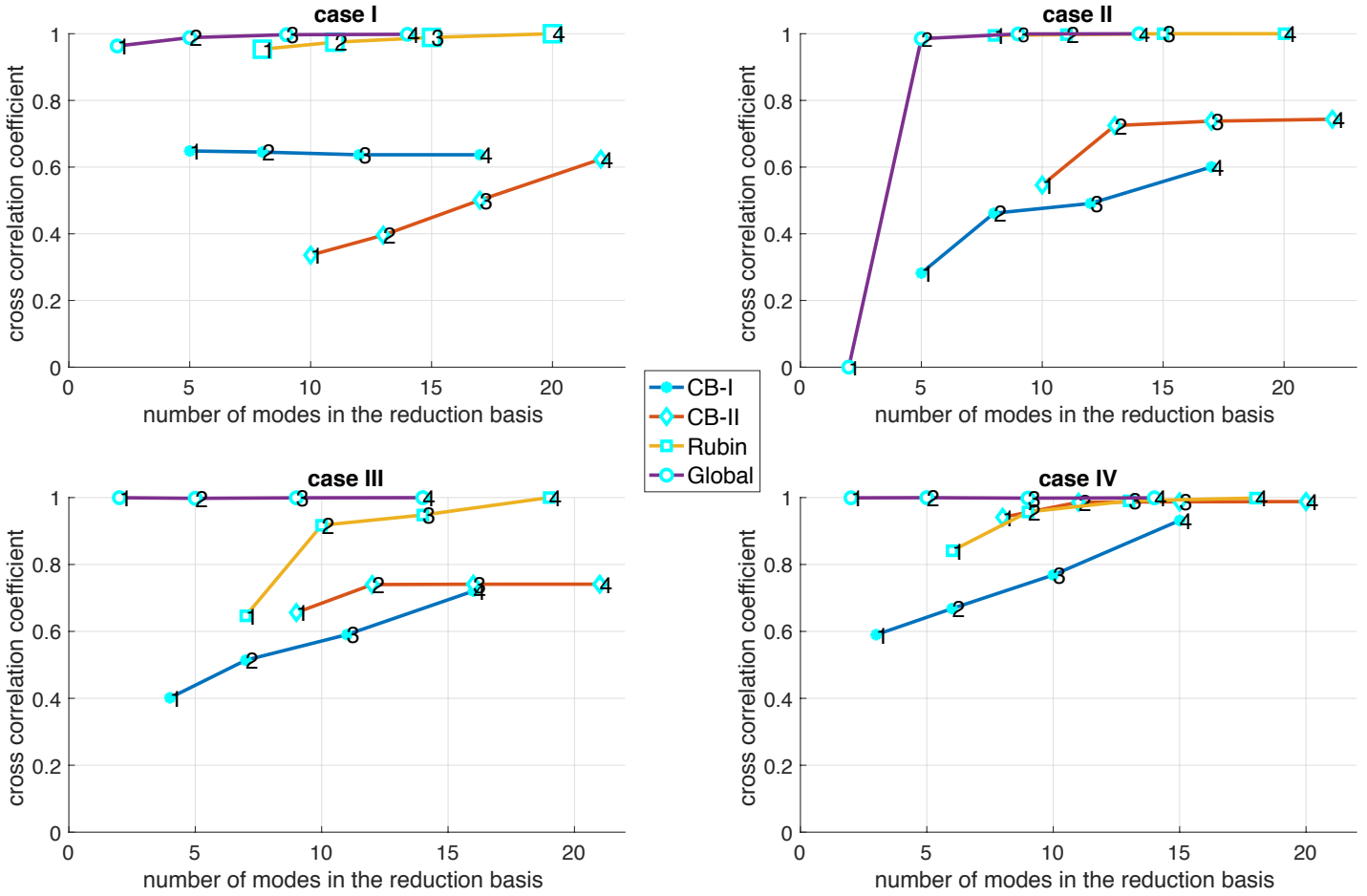


Fig. 4. Maximal normalized cross-correlations of the ROMs of the parametrically excited cases. The black numbers in the markers indicate the number of vibration modes in the reduction base: free, fixed or global vibration modes, depending on the type of reduction. All corresponding MDs are included in the bases as well.

1. CB-I: Craig-Bampton reduction augmented with MDs only
2. CB-II: Craig-Bampton reduction augmented with both MDs and CMDs
3. Rubin: Rubin reduction augmented with MDs
4. Global: Global reduction basis composed of system vibration modes and the corresponding MDs

4.1 ROMs of parametric excited single beam structures

In order to understand the effect and performance of the different reduction techniques applied to the FEM of multi-stage resonance cascade, we first consider 4 simple cantilever beam structures that are excited axially to achieve parametric resonance. A schematic representation of the four cases is shown in Fig.2. Each beam structure consists of 20 von-Karman kinematic nonlinear beam elements. The length of the beams is for all cases 2.5 m. The Young's modulus is 190 GPa, while the width and the thickness of the beams are both 0.025 m. In the first case, the beam is fixed at one end and free at the other end, the excitation frequency is twice the natural frequency of the beam. For the second case, the boundary conditions are the same as for the first case, but now the

excitation frequency is twice the second eigenfrequency of the structure. In the third case, again the beam is fixed at one side while the other side is constrained in the transverse direction, as represented in Fig.2. The excitation is twice the first eigenfrequency. In the fourth case, both the transverse displacement and the rotation of the free end of the structure are constrained, represented in Fig.2. by a slider constraint. All models are excited by a simple harmonic force, denoted as:

$$F^{ext}(t) = H \cdot \sin(\omega t), \quad (46)$$

where H is the force amplitude which is 790 N, 750 N, 750 N and 2250 N for the four cases respectively. ω is the excitation frequency which is twice the eigenfrequency of interest of the beam structures. See Tab.1 for the eigenfrequencies.

In order to activate the resonance, a relatively small transverse force component is imposed on the structures at the initial time step.

For all cases, a stable steady-state response is reached. See Fig.3 for the full nonlinear time responses of the four cases. The figure clearly shows that a steady-state response is reached for all cases. Now for each of the four cases, the

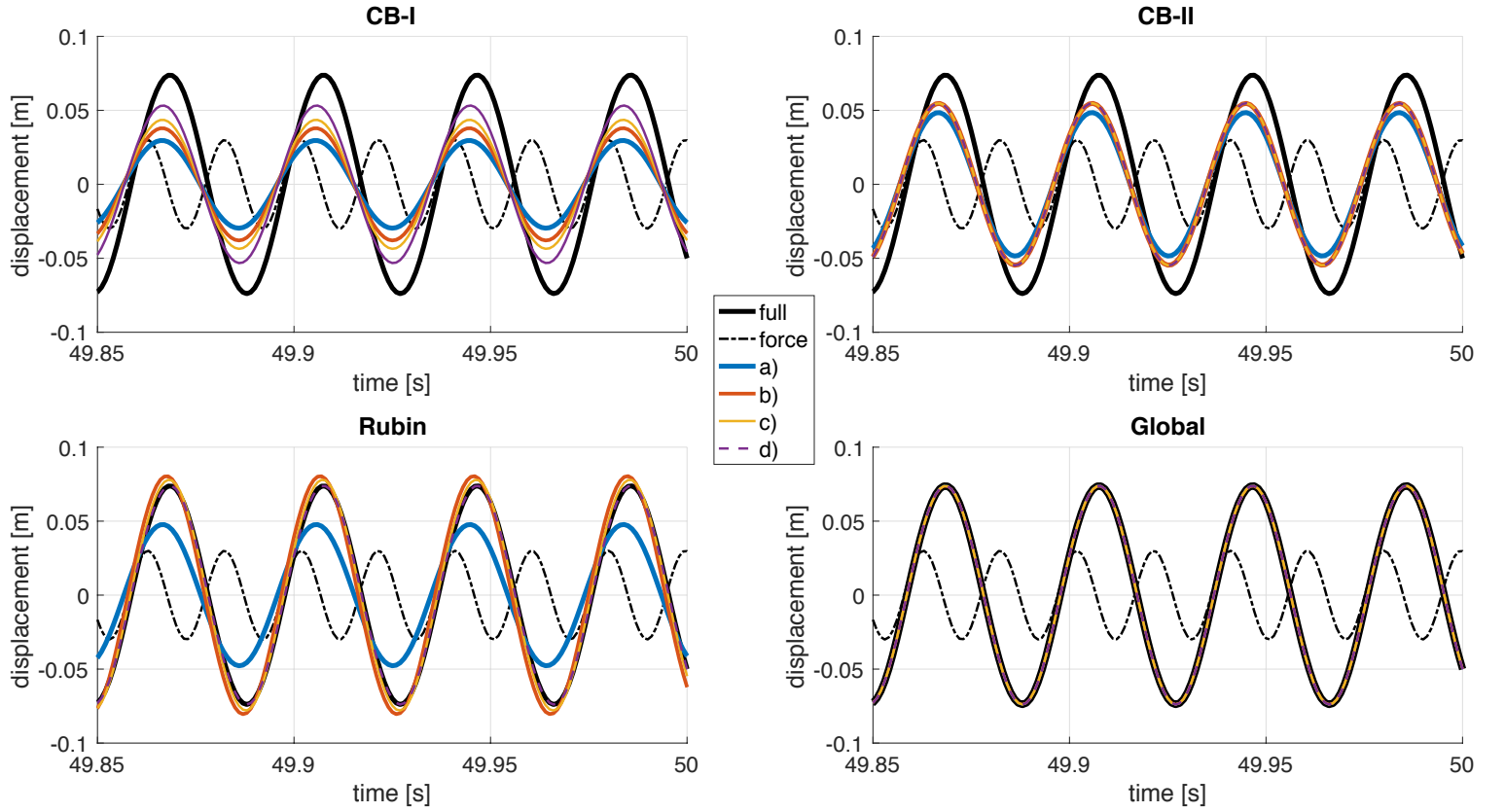


Fig. 5. Steady-state responses of the different ROMs of case III. The lines a-d correspond to the number of vibration modes + corresponding MDs considered in the reduction bases for each reduction method: a) 4 vibration modes + 10 MDs; b) 3 vibration modes + 6 MDs; c) 2 vibration modes + 3 MDs, and d) 1 vibration mode + 1 MD.

case	I	II	III	IV
eigenfrequency [Hz]	5.84	36.6	25.6	37.1

Table 1. Relevant eigenfrequencies of the different cases. Note that for case II the second eigenfrequency is represented. The eigenfrequencies of case I and II are the same.

4 different reduction bases (CB-I, CB-II, Rubin and global) are used to obtain the different ROMs.

In this research, the performance of the ROMs is expressed by a cross-correlation coefficient, which is a measure of similarity between signals. The cross-correlation is based on a convolution between two signals for different relative displacements, known as lags, and denoted as τ . A certain response of the full solution may appear at time t while it appears in the ROM at $t + \tau$. This method is convenient for this purpose since it does not penalize eventual phase shifts between the ROM and the full solution. Furthermore, the method accounts for amplitude differences. The discrete formulation of the cross-correlation function is given as:

$$Z_{xy}[\tau] = (\mathbf{x} \star \mathbf{y})[\tau] = \sum_{m=-\infty}^{\infty} \overline{\mathbf{x}[m]} \mathbf{y}[m + \tau], \quad (47)$$

where \mathbf{x} is a vector that contains the displacements in time

of at a specific point in the full model, and \mathbf{y} is a vector that contains the displacements in time at the same location but obtained with the ROM.

Let's denote the value of τ for which the maximum convolution of \mathbf{x} and \mathbf{y} is obtained as τ_{max} , furthermore let's denote the maximum auto correlation of the full nonlinear solution as $Z_{xx,max}$. Now the maximal normalized correlation coefficient is calculated as:

$$\begin{cases} c = \frac{Z_{xy}(\tau_{max})}{Z_{xx,max}} & \text{if } Z_{xy}(\tau_{max}) < Z_{xx,max} \\ c = \left(\frac{Z_{xy}(\tau_{max})}{Z_{xx,max}} \right)^{-1} & \text{if } Z_{xy}(\tau_{max}) > Z_{xx,max} \end{cases} \quad (48)$$

Due to the normalization, the correlation coefficients have values between 0 and 1, where 0 indicates zero correlation and thus a bad performance of the ROM, while a coefficient of 1 indicates a high correlation and therefore a good performance of the ROM.

Fig.4 represents the maximal normalized correlation coefficients for the different reduction techniques applied on the 4 cases in relation to the number of modes that are comprised in the reduction bases. The numbers in the markers indicate the number of vibration modes that are included in the reduction basis. All corresponding MDs are included in the reduction base, i.e. if d vibration modes are included in the basis, then $d(d + 1)/2$ corresponding MDs are in-

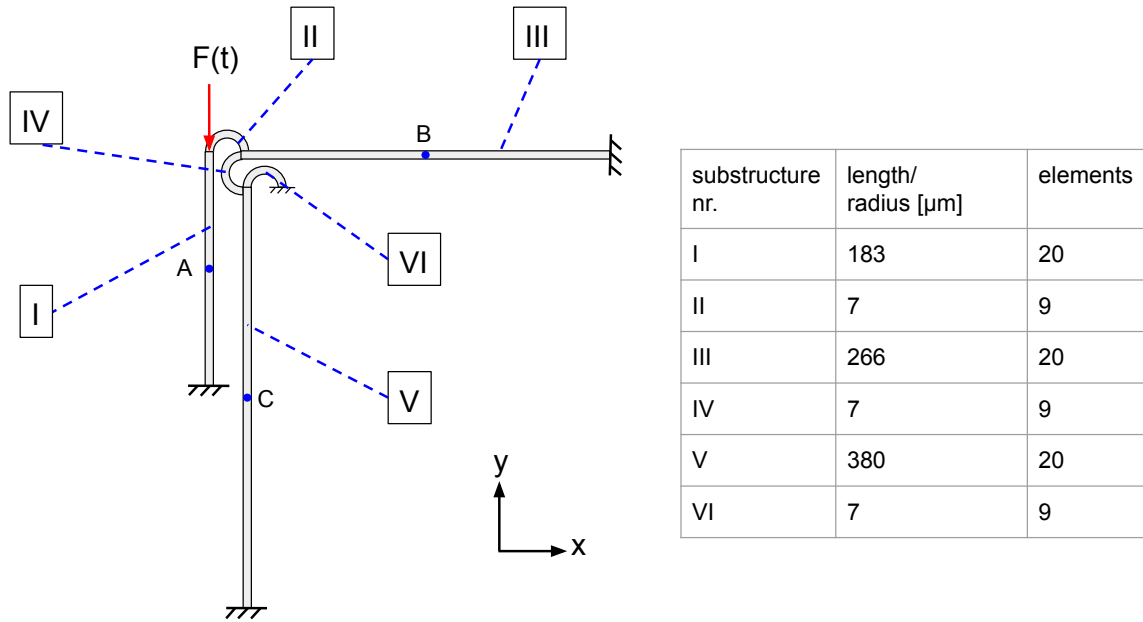


Fig. 6. Schematic representation of the investigated resonance cascade. The numbers I-VI label the substructures. The blue dots A-C indicate the locations where the transverse responses of the beams are measured. The table at the right side represents the lengths and radii of the components as well as the number of elements that are considered in the finite element model.

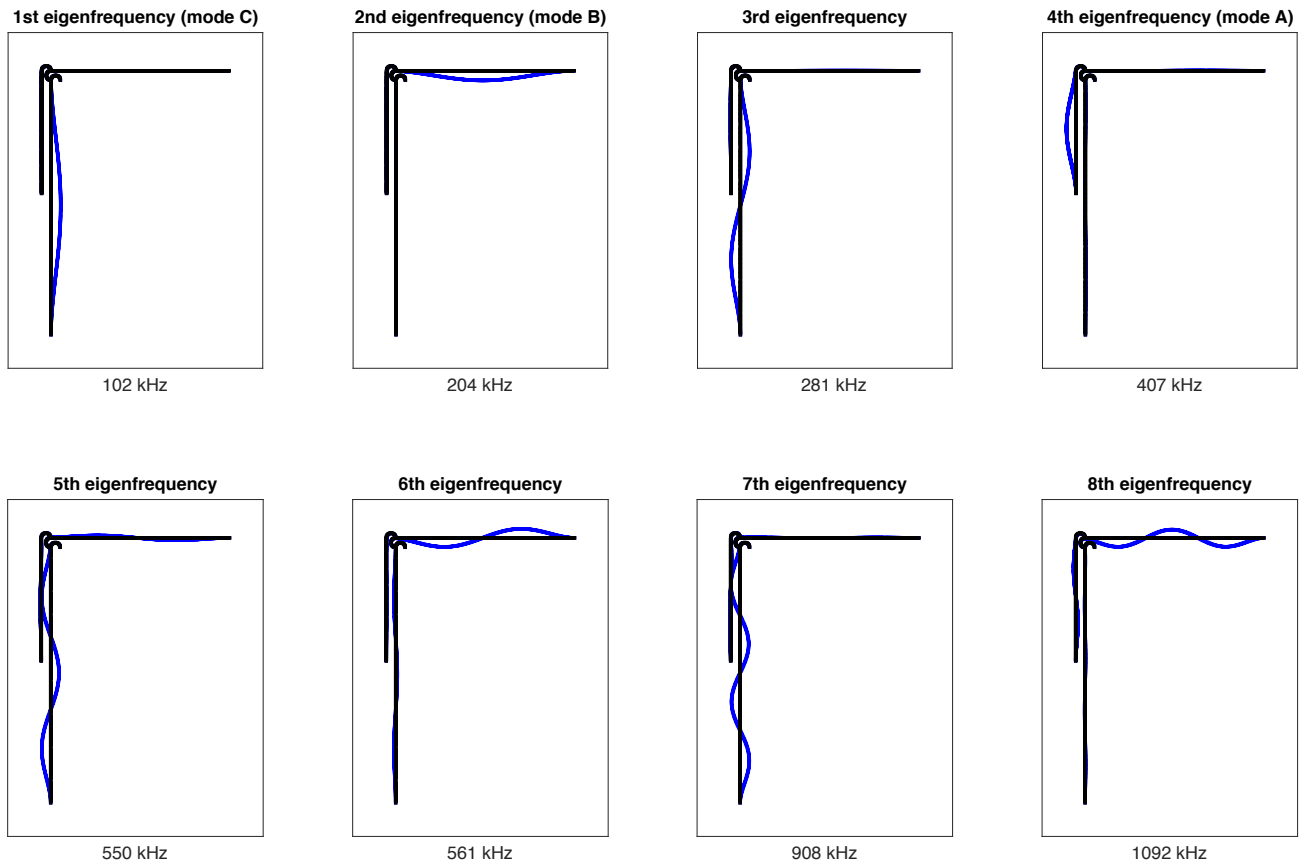


Fig. 7. The first 8 eigenfrequencies of the 3-stage FD. As a matter of fact, the eigenfrequencies 1,2 and 4 are closely related to the resonance modes that are describing the frequency division in the resonance cascade. The modes are labeled as mode A, mode B, and mode C.

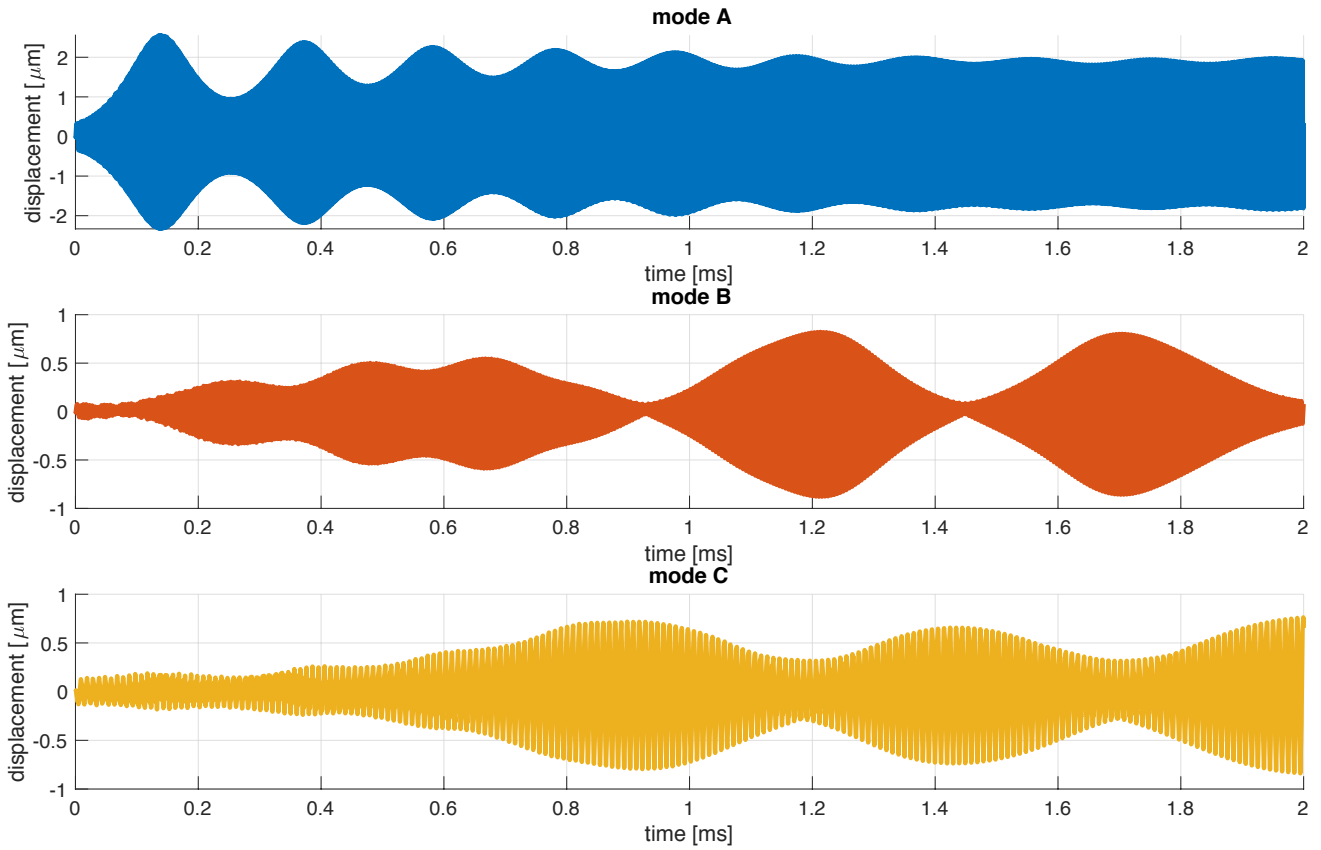


Fig. 8. Full nonlinear transient time responses of the modes A, B and C in the frequency divider. The transverse displacements are measured in the midpoints of the resonator beams.

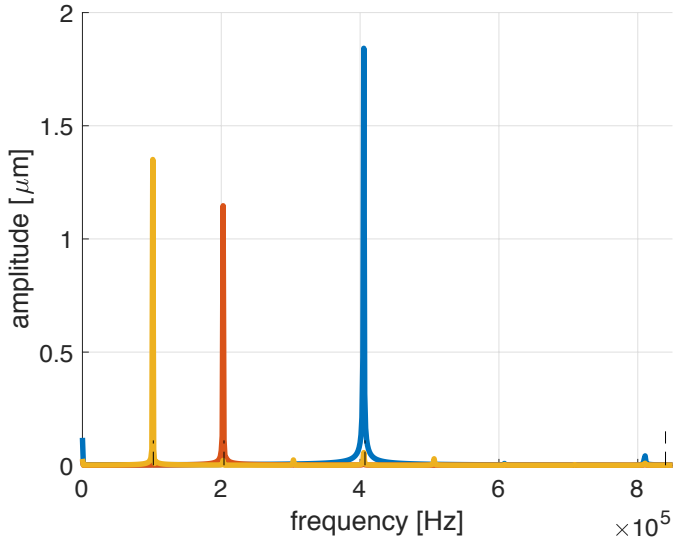


Fig. 9. Fast fourier transform of the steady-state transverse displacements measured in the locations A, B and C as indicated in Fig.6.

cluded as well. Besides the vibration modes and the MDs, the Craig-Bampton and Rubin reduction bases contain their additional specific static and dynamic modes. For the computation of the cross-correlation coefficient, the steady-state

responses of the systems are used. A sufficient number of cycles need to be used for the computation of the coefficient. In this work, more than 10 cycles in the steady-state responses are considered. Fig.4 clearly shows that in general considering more vibration modes with the corresponding MDs in the reduction bases results in a higher correlation coefficients and thus in a better approximation of the full nonlinear solution. The global reduction seems to be the best option in terms of low-dimensionality of the reduction basis. Besides that, the global reduction seems to be the most accurate one. Furthermore, Fig.4 shows that the CB-I reduction bases result in the worst approximation of the full nonlinear steady-state response. However, augmenting the reduction basis with CMDs seems to substantially improve the performance of the MDs-based Craig-Bampton reduction method. Fig.5 represents the steady-state responses of case III for the four different types of reduction basis. Fig.5 shows that for both Craig-Bampton and Rubin reduction there is a small phase difference present between the full nonlinear response and response obtained with the ROMs.

4.2 ROM of the frequency divider cascade

Now the ROMs of a 3-stage frequency divider resonance cascade are considered. The relevant FD is represented in

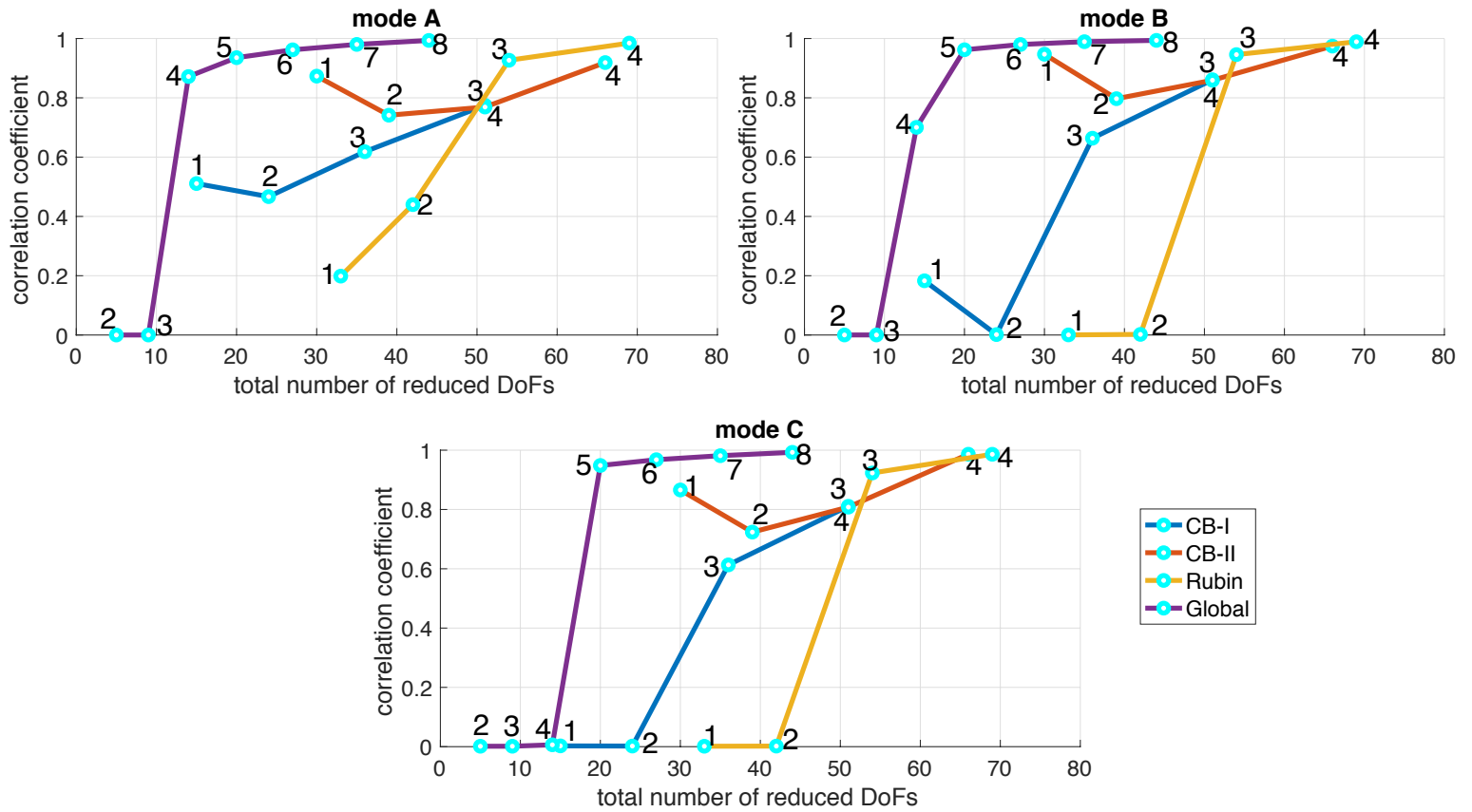


Fig. 10. Maximal normalized cross-correlation for the ROMs of the 3-stage FD. For each resonance mode localized in the stages of the FD, the correlation coefficient is computed. The black numbers in the figure indicate the number of vibration modes included in the reduction bases. All corresponding MDs are included as well. On the x-axis is the total number of DoFs in the entire reduced system indicated.

Fig.6. The device is composed of 6 substructures labeled with the letters *I – VI* as indicated in the figure. The lengths and radii of the beams and hooks are presented in the table on the right side in Fig.6. The thickness of all parts is $1.85\mu m$ while the device depth of all parts is $10\mu m$.

The three-stage FD comprises three resonance modes that are a fraction of the input frequency. These resonance modes are localized in the straight beam substructures labeled with the numbers *I, III* and *V* respectively. From this point on, the resonance modes are indicated with the letters *A – C*. As a matter of fact, the resonance modes are closely related to the first, second and fourth eigenfrequencies of the entire FD. See Fig.7 for the vibration modes and the corresponding eigenfrequencies of the system.

The structure is activated by axially exciting structure *I*, see Fig.6 for the location and direction of the force. The excitation frequency is 810 kHz, which is a bit below twice the eigenfrequency of mode A. This frequency is consciously chosen since it results in a better frequency division in the full nonlinear computation. This is in line with the findings in the work of Qalandar [6]. The excitation amplitude is set to $20\mu N$. Proportional Rayleigh damping is assumed with values $\alpha = 2.9429e - 10$ and $\beta = 1142.2$.

In the case of Craig-Bampton reductions, the hooks that connect the beams are Guyan reduced. This choice is made since the hooks are relatively stiff due to their curved geometry,

therefore the condition described in section 2.5 is satisfied. This effectively reduces the total number of DoFs. In the case of Rubin reduction, the reduction bases of the hooks comprise attachment modes and rigid body modes only. The transverse displacements of the beams are used to monitor the system responses. The transverse displacements of interest are located in the middle of the beams as indicated with the blue dots in Fig.6. The dots are labeled with the letters *A-C*, consistent to the labeling of the resonance modes. The full transient time responses of beams are represented in Fig.8. Finally, a Fast Fourier Transform (FFT) of the steady-state responses in the measurement points reveals the frequency division. The FFT of the full non-linear computation is given in Fig.9. A very clear and clean frequency division is visible in the figure. The maximal normalized cross-correlations of the different ROMs are presented in Fig.10. The results show that a global reduction basis comprising at least the first 5 vibration modes plus the corresponding MDs gives the best and computationally cheapest approximation of the full nonlinear solution. It is interesting to note that the CB-II reduction basis augmented with CMDs properly approximates the full nonlinear model, much better than the CB-I reduction basis without CMDs.

From the computations it follows that the FFTs of the ROMs with high cross-correlation coefficients give similar responses in the frequency domain, but with amplitude dif-

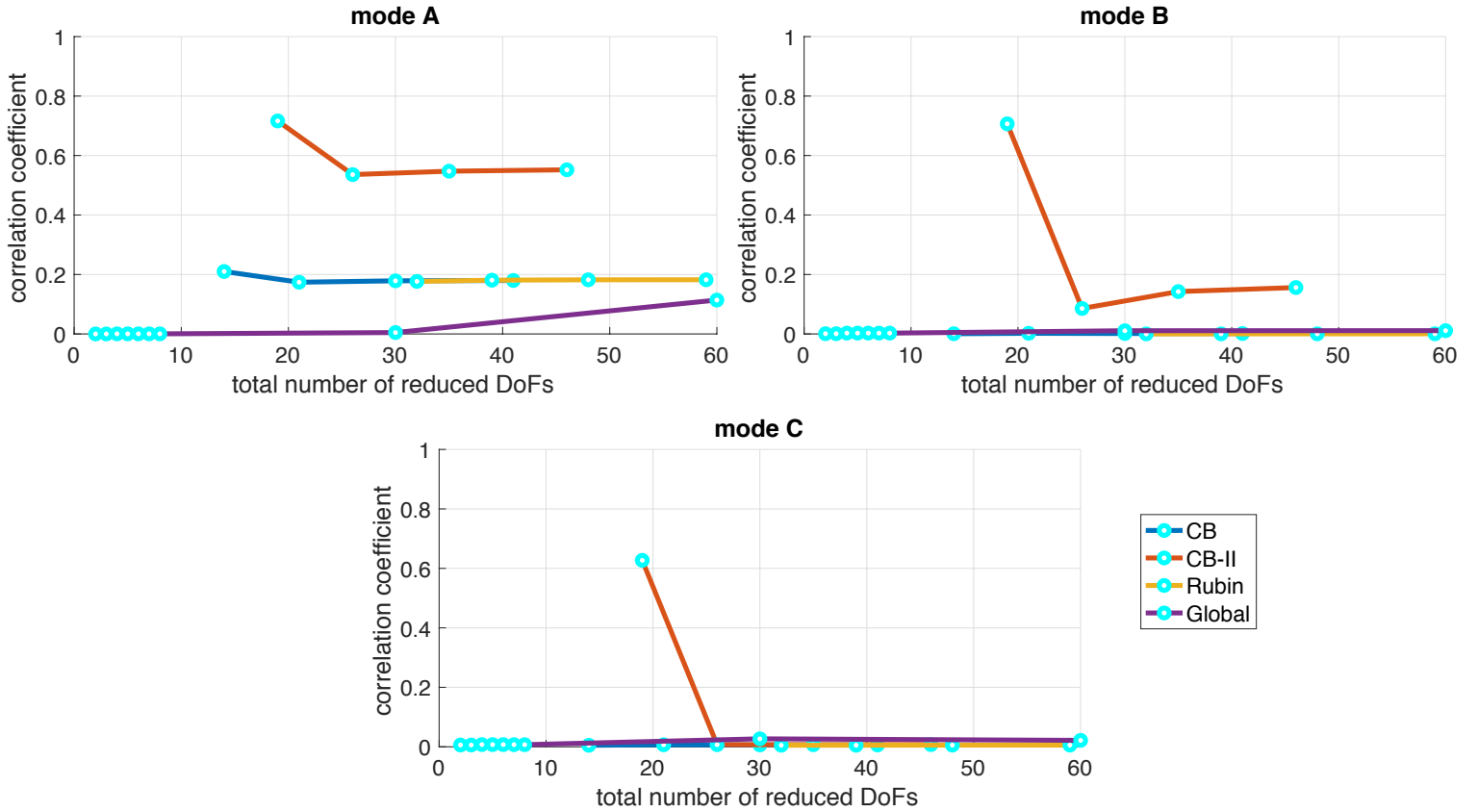


Fig. 11. Maximal normalized cross-correlation for the ROMs of the FD in case of a reduction bases without MDs. For the sake of completeness, also global ROMs are considered with reduction bases composed of 30 vibration modes and 60 vibration modes.

ferences. Finally, to represent the importance of MDs in all reduction bases, Fig.11 represents the normalized cross-correlations of the nonlinear time responses of the ROMs without MDs. It is clearly visible that in this case, all ROMs are not accurate. The amplitudes of the resonance modes are in this case very low. The only ROM that approximates the full nonlinear response a bit is the Craig-Bampton reduction augmented with CMDs, this indicates the contribution of CMDs in capturing geometric nonlinearity.

5 Conclusions

The computation of high dimensional nonlinear finite element models can be very time-consuming. To cope with this issue reduction methods were introduced to lower the number of DoFs while retaining sufficient accuracy. In this paper we considered reduction methods based on the projection of a reduced set of DoFs on a reduction basis to find the full set of DoFs. The reduction bases of conventional reduction techniques as Craig-Bampton reduction and Rubin reduction can be augmented with MDs to capture geometric nonlinearity in the Finite element models. Such Reduced-order models were successfully investigated for transient analyses of transverse excited structures. In this paper, we investigated the use of reduced-order models in the steady-state response of parametrically excited structures. Four different reduction bases are investigated: A Craig-Bampton reduction basis augmented with MDs only, A Craig-Bampton reduction ba-

sis augmented with both MDs and the in this paper proposed constrained modal derivatives, furthermore, an MD-enriched Rubin reduction basis is considered, and a global reduction basis that consists of system vibration modes plus corresponding MDs only. First, the dynamic response of 4 parametric excited beam structures with von-Karman kinematic models have been investigated. The performance of the ROMs in the steady-state responses are expressed in terms of a maximal normalized cross-correlation coefficient between the ROMs and the full nonlinear response. The steady-state responses show that the ROMs are perfectly able to capture the parametric resonance generated in the structures. The results show that for all cases the global reduction is the best reduction technique in terms of low-dimensionality and accuracy. Furthermore, the results show that enriched Rubin reduction is better approximating the full nonlinear response than the two types of Craig-Bampton reduction bases. The performance of the conventional Craig-Bampton reduction basis augmented with MDs only is quite poor, whereas augmenting the reduction basis with CMDs enhances the performance of Craig-Bampton reduction method. After considering the simple beam constructions, the reduction bases were used for obtaining ROMs of a 3-stage mechanical frequency divider. This frequency divider was a benchmark problem in this work. The Fast Fourier Transform of the steady-state time response of the full nonlinear FEM confirms that the model works as described in the pa-

per of Qalander et al [6]. From the time responses obtained with the ROMs it follows that all of the considered reduction techniques can capture the phenomenon of frequency division in the resonator array, but with different accuracy in amplitude. In this contribution, it is clearly shown that in general there exists a clear relationship between the number of modes composed in the reduction basis and the accuracy of the corresponding ROM in a steady-state response. However, in some cases the accuracy decreases in case of an increased size of the reduction basis. This is probably caused by various artificial stiffnesses in the model, stemming from the reduction in DoFs. With the FD as a benchmark, it is shown that component mode synthesis in combination with Craig-Bampton reduction and Rubin reduction can be used to approximate the responses of the system. However, the results indicate that global reduction without substructuring is preferable to any substructuring method as it delivers more accurate and smaller ROMs. Nonetheless, especially for larger and more complex systems, CMS might be a better and more practical approach than global reduction, therefore more research in nonlinear steady-state CMS methods is recommended.

The results in this paper have shown that MDs play a crucial role in ROMs of parametrically excited structures.

Appendix A: Derivation of the tensors on element level

In this appendix we will use subscripts behind a symbol for Einstein notation, while the sub- and superscripts before the symbols refer to tensors. We first need to define the vectors related to the non-linear formulations of a beam element:

$$\Gamma = \frac{1}{l} \begin{bmatrix} 1 \\ 0 \\ 0 \\ -1 \\ 0 \\ 0 \end{bmatrix}, \quad \Omega = \frac{1}{4l} \begin{bmatrix} 0 \\ 6(\zeta^2 - 1) \\ l(3\zeta^2 - 2\zeta - 1) \\ 0 \\ 6(1 - \zeta^2) \\ l(3\zeta^2 + 2\zeta - 1) \end{bmatrix} \quad (49)$$

$$\Pi = \frac{l}{l^2} \begin{bmatrix} 0 \\ 6\zeta \\ l(3\zeta - 1) \\ 0 \\ -6\zeta \\ l(3\zeta + 1) \end{bmatrix},$$

where ζ is integration variable integrated from -1 to 1 over the element length l . Now the element tensors of the nonlinear force vector denoted as ${}^2\mathbf{Q}^e \in \mathbf{R}^{6 \times 6}$, ${}^3\mathbf{Q}^e \in \mathbf{R}^{6 \times 6 \times 6}$ and ${}^4\mathbf{Q}^e \in \mathbf{R}^{6 \times 6 \times 6 \times 6}$ are calculated as

$$\begin{aligned} {}^2\mathbf{Q}^e &= JEA \int_{-1}^1 {}^2_1 \Lambda d\zeta + JEI \int_{-1}^1 {}^2_3 \Lambda d\zeta \\ {}^3\mathbf{Q}^e &= \frac{1}{2} JEA \int_{-1}^1 {}^3_2 \Lambda d\zeta + JEA \int_{-1}^1 {}^3_3 \Lambda d\zeta \\ {}^4\mathbf{Q}^e &= \frac{1}{2} JEA \int_{-1}^1 {}^4_4 \Lambda d\zeta, \end{aligned} \quad (50)$$

where J is the jacobian, E is the Young's modulus, I is the moment of inertia and A is the cross sectional area of the element. The tensors ${}^2_1\Lambda$, ${}^3_2\Lambda$, ${}^3_3\Lambda$, ${}^4_4\Lambda$ and ${}^2_3\Lambda$ are calculated as

$$\begin{aligned} {}^2_1\Lambda_{ij} &= \Gamma_i \Gamma_j, \quad {}^3_2\Lambda_{ijk} = \Gamma_i \Omega_j \Omega_k, \quad {}^3_3\Lambda_{ijk} = \Omega_i \Gamma_j \Omega_k, \\ {}^4_4\Lambda_{ijkl} &= \Omega_i \Omega_j \Omega_k \Omega_l, \quad {}^2_3\Lambda_{ij} = \Pi_i \Pi_j. \end{aligned} \quad (51)$$

Now for the nonlinear stiffness matrix, the elemental tensors ${}^2\mathbf{G}^e$, ${}^3\mathbf{G}^e$ and ${}^4\mathbf{G}^e$ are simply found as

$${}^2\mathbf{G}^e = {}^2\mathbf{Q}^e, \quad {}^3\mathbf{G}^e = 2 \cdot {}^3\mathbf{Q}^e, \quad {}^4\mathbf{G}^e = 3 \cdot {}^4\mathbf{Q}^e. \quad (52)$$

Once the elemental tensors are computed, the substructure tensors ${}^2\mathbf{Q} \in \mathbf{R}^{n \times n}$, ${}^3\mathbf{Q} \in \mathbf{R}^{n \times n \times n}$, and ${}^4\mathbf{Q} \in \mathbf{R}^{n \times n \times n \times n}$ are formed through standard finite element assembly. The reduced tensors are found as:

$${}^2\tilde{Q}_{IJ} = V_{iI} {}^2Q_{ij} V_{jJ}, \quad (53)$$

$${}^3\tilde{Q}_{IJK} = V_{iI} {}^3Q_{ijk} V_{jJ} V_{kK}, \quad (54)$$

and

$${}^4\tilde{Q}_{IJKL} = V_{iI} {}^4Q_{ijkl} V_{jJ} V_{kK} V_{lL}. \quad (55)$$

Where $\mathbf{V} \in \mathbf{R}^{n \times m}$ is the substructure reduction basis.

Appendix B: FE formulation of a modal derivative on element level

Let us assume that an element displacement vector originated from a certain vibration mode and its amplitude, $\mathbf{q}^e = \phi^e \eta$, is split into its axial components $\mathbf{q}_u^e = \phi^{e,u} \eta$ and its transverse and rotational components $\mathbf{q}_w^e = \phi^{e,w} \eta$. Now the elemental contribution of a modal derivative obtained from two vibration modes i and j is given as:

$$\theta_{ij}^e = D \int_{-1}^1 \begin{bmatrix} \mathbf{0} & (\mathbf{w}^T \phi_i^{e,w}) \mathbf{u} \mathbf{w}^T d\zeta \\ (\mathbf{w}^T \phi_i^{e,w}) \mathbf{u} \mathbf{w}^T d\zeta & (\mathbf{u}^T \phi_i^{e,u}) \mathbf{w} \mathbf{w}^T d\zeta \end{bmatrix} \begin{bmatrix} \phi_j^{e,u} \\ \phi_j^{e,w} \end{bmatrix} \quad (56)$$

, where \mathbf{u} and \mathbf{w} are given as:

$$\mathbf{u} = \frac{1}{l} \begin{bmatrix} 1 \\ -1 \end{bmatrix}, \quad \mathbf{w} = \frac{1}{4l} \begin{bmatrix} 6(\zeta^2 - 1) \\ l(3\zeta^2 - 2\zeta - 1) \\ 6(1 - \zeta^2) \\ l(3\zeta^2 + 2\zeta - 1) \end{bmatrix}. \quad (57)$$

See appendix A for the meanings of the symbols. Once the elemental contributions for a modal derivative are known, the modal derivative of the (sub)structure is assembled through standard FE assembly. Denoted as:

$$\theta_{ij} = \text{assembly}(\theta_{ij}^e). \quad (58)$$

Appendix C: FE formulation of a CMD on element level

Let us assume that $\bar{\Psi}^e = \psi_c^e \mathbf{q}_B$ is an element contribution of the static displacement $\bar{\Psi}$. We can divide this element contribution in an axial contribution $\bar{\Psi}_u^e \in \mathbf{R}^{2 \times 1} = \psi_c^{e,u} \mathbf{q}_B$ and transverse and rotational contribution $\bar{\Psi}_w^e \in \mathbf{R}^{4 \times 1} = \psi_c^{e,w} \mathbf{q}_B$. Now the elemental contribution of a CMD obtained from the constraint modes i and j is given as

$$\gamma_{ij}^e = D \int_{-1}^1 \begin{bmatrix} \mathbf{0} & (\mathbf{w}^T \psi_{c,i}^{e,w}) \mathbf{u} \mathbf{w}^T d\zeta \\ (\mathbf{w}^T \psi_{c,i}^{e,w}) \mathbf{u} \mathbf{w}^T d\zeta & (\mathbf{u}^T \psi_{c,i}^{e,u}) \mathbf{w} \mathbf{w}^T d\zeta \end{bmatrix} \begin{bmatrix} \psi_{c,j}^{e,u} \\ \psi_{c,j}^{e,w} \end{bmatrix}. \quad (59)$$

With $D = JEA$, see appendix A for the meaning. Once all elemental contribution are known one can compute the system CMD through standard FE assembly. Denoted as:

$$\gamma_{ij} = \text{assembly}(\gamma_{ij}^e). \quad (60)$$

References

- [1] Wu, L., Tiso, P., Tatsis, K., Chatzi, E., van Keulen, F. (2019). A MDs enhanced Rubin substructuring method for geometrically nonlinear multibody systems. *Multibody System Dynamics*, 45(1), 57-85. <https://doi.org/10.1007/s11044-018-09644-2>
- [2] Wenneker, F., Tiso, P.: A substructuring method for geometrically nonlinear structures. In: *Dynamics of Coupled Structures*, vol. 1, pp. 157–165. Springer, Berlin (2014)
- [3] Rutzmoser, J.B., Rixen, D.J., Tiso, P., Jain, S.: Generalization of quadratic manifolds for reduced order modeling of nonlinear structural dynamics. *Comput. Struct.* 192(Supplement C), 196–209 (2017)
- [4] Weeger, O., Wever, U., Simeon, B.: On the use of MDs for nonlinear model order reduction. *Int. J. Numer. Methods Eng.* (2016)
- [5] Wu, L., Tiso, P.: Nonlinear model order reduction for exible multibody dynamics: a MDs approach. *Multibody Syst. Dyn.* 36(4), 405–425 (2016)
- [6] Qalandar, R.K., Strachan, B.S., Gibson, B., Sharma, M., Ma, A., Shaw, W.S., Turner, L.K.: Frequency division using a micromechanical resonance cascade. *Appl. Phys. Lett.* 105, 244103 (2014)
- [7] D. de Klerk, D. J. Rixen, and S. N. Voormeeren. “General framework for dynamic substructuring: history, review and classification of techniques”. In: *AIAA journal* 46.5 (2008), pp. 1169–1181.
- [8] P. Tiso. “Optimal second order reduction basis selection for nonlinear transient analysis”. In: *Modal Analysis Topics*, Volume 3. Springer, 2011, pp. 27–39.
- [9] P. Van Der Valk. “Model Reduction Interface Modeling in Dynamic Substructuring”. MA thesis. Delft University of Technology, 2010.
- [10] S. Voormeeren. “Dynamic Substructuring Methodologies for Integrated Dynamic Analysis of Wind Turbines”. PhD thesis. Delft University of Technology, 2012.
- [11] R. Guyan. “Reduction of stiness and mass matrices”. In: *AIAA journal* 3.2 (1965), p. 380.
- [12] R. R. Craig and M. C. C. Bampton. “Coupling of substructures for dynamic analysis”. In: *AIAA journal* 6.7 (1968), pp. 1313–1319.
- [13] S. R. Idelsohn and A. Cardona. “A reduction method for nonlinear structural dynamic analysis”. In: *Computer Methods in Applied Mechanics and Engineering* 49.3 (June 1985), pp. 253–279.
- [14] S. Rubin. “Improved component-mode representation for structural dynamic analysis”. In: *AIAA journal* 13.8 (1974).
- [15] Strachan BS, Shaw SW, Kogan O. “Subharmonic resonance cascades in a class of coupled resonators”. In: *Journal of Computational and Nonlinear Dynamics* v8 n4 (2013 12 02).
- [16] C.S.M. Sombroek, P. Tiso, L. Renson, G. Kerschen, Numerical computation of nonlinear normal modes in a modal derivative subspace, *Comput. Struct.* 195 (2018) 34-46,
- [17] Lifshitz, R., Cross, M.: Response of parametrically driven nonlinear coupled oscillators with application to micromechanical and nanomechanical resonator arrays. *Phys. Rev. B* 67(13), 134302 (2003)
- [18] C. Farhat and M. Géradin. “On the general solution by a direct method of a large-scale singular system of linear equations: application to the analysis of oating structures”. In: *International Journal for Numerical Methods in Engineering* 41.4 (1998), pp. 675–696. issn: 1097-0207.
- [19] Tiso P, Rixen DJ. Reduction methods for MEMS nonlinear dynamic analysis. New York, NY: Springer New York; 2011. <https://doi.org/10.1007/978-1-4419-9719-7-6>.
- [20] Dohnal F., Ecker H. and Springer H. Enhanced damping of a cantilever beam by axial parametric excitation. *Archives of Applied Mechanics*, 2008, 78, No. 12, 935–947
- [21] Shklarski, Gil, and Sivan Toledo. “Computing the Null Space of Finite Element Problems.” *Computer Methods in Applied Mechanics and Engineering* 198, no. 37-40 (2009): 3084–3095.
- [22] Jain, Shobhit, Paolo Tiso, Johannes B Rutzmoser, and Daniel J Rixen. “A Quadratic Manifold for Model Order Reduction of Nonlinear Structural Dynamics.” *Computers and Structures* 188 (2017): 80–94.
- [23] Jain, S., Breunung, T. Haller, G. *Nonlinear Dyn* (2019) 97: 313. <https://doi.org/tudelft.idm.oclc.org/10.1007/s11071-019-04971-1>
- [24] Seshu, P. (1997). Substructuring and Component Mode Synthesis. *Shock and Vibration*. 4. 199-210. 10.1155/1997/147513.
- [25] Slaats, P. M. A., Jongh, de, J., Sauren, A. A. H. J. (1995). Model reduction tools for nonlinear structural dynamics. *Computers and Structures*, 54(6), 1155-1171 .

3

Reduced-order models of beam structures

Although beam models belong to the simplest FE models, they still play an important role in research. Over the decades, many engineering problems are solved with simple beam models. The results and proposed improvements in the reduction methods presented in chapter 2 partly arise from simpler numerical computations that are done first. In this chapter, some of the numerical results of beam models are presented. The aim of this chapter is to get a better understanding of the performance and applicability of MDs-based reduction methods in specific beam models, furthermore, the chapter presents more figures and results of the in the paper described FD. In the models considered in this chapter, the MDs play an essential role since the models are exposed to geometric nonlinear conditions. In the first section, two validations of the written codes for beam models are presented. In the subsequent sections, different ROMs of the beam models are investigated. First 2 transverse excited beam structures are considered, thereafter 2 different FDs are investigated. In accordance with the paper, 4 Different reduction bases are applied in the ROMs. Tab. 3.1 shows an overview of the concerned type of reduction bases with their ingredients, basically the mode components. See Appendix A for the formulations and derivations of the various modes. See Appendix B for the derivations of the relevant reduction bases.

Basis	SMs	VMs	MDs	RBMs	CMDs
CB-I	6-c	s	$s(s+1)/2$	-	5
CB-II	6-c	s	$s(s+1)/2$	-	-
Rubin	6-c	s	$s(s+1)/2$	3	-
Global	-	s	$s(s+1)/2$	-	-

Table 3.1: An overview of the used reduction bases and their components; SMs: static modes; VMs: vibration modes; MDs: modal derivatives; RBMs: rigid body modes; CMDs: constraint modal derivatives. s indicates the number of vibration modes included in the reduction basis. In the table, c is the number of constrained boundary DoFs of the beam structure, thus the number of static modes in the reduction basis is dependent on the boundary conditions.

3.1. Model validation

To validate the codes that are written in Matlab, first a simple cantilever model is built and compared with analytical formulations. Furthermore, a numerical time integration in Matlab is compared with a numerical integration computed with the FE software Comsol. The model considered is an undamped microcantilever beam model as represented in Fig.3.1. The length of the considered beam is $40\mu m$, the young's modulus is $190GPa$. The width w and depth d of the beam are both $1\mu m$. The density of the beam is $2329 kg/m^3$. The FE model is discretized with 25 elements. For

	Analytic	Comsol	Matlab
f_1	0.912	0.912	0.912
f_2	5.716	5.715	5.715
f_3	6.005	6.002	6.002
f_4	31.153	31.359	31.357
f_5	50.550	51.846	51.835

Table 3.2: The first 5 eigenfrequencies in MHz, calculated analytically and computed with Comsol and Matlab.

the elements, a von-Karman nonlinear model is used which is valid for small strains and moderate rotations.

3.1.1. Eigenfrequency validation

It is well known that an analytic approximation of the first five eigenfrequencies of cantilever beams can be found by using the following Euler formulas [23]:

$$f_1 = \frac{22.3733}{2\pi} \sqrt{\frac{EI}{\rho AL^4}}, \quad (3.1)$$

$$f_2 = \frac{61.6728}{2\pi} \sqrt{\frac{EI}{\rho AL^4}}, \quad (3.2)$$

$$f_3 = \frac{120.9034}{2\pi} \sqrt{\frac{EI}{\rho AL^4}}, \quad (3.3)$$

$$f_4 = \frac{199.8594}{2\pi} \sqrt{\frac{EI}{\rho AL^4}}, \quad (3.4)$$

$$f_5 = \frac{298.5555}{2\pi} \sqrt{\frac{EI}{\rho AL^4}}, \quad (3.5)$$

where A is the cross-sectional area of the beam, L is the length of the beam, E is the young's modulus, and I is the moment of inertia, which is in this case calculated as:

$$I = \frac{d \times w^3}{12}, \quad (3.6)$$

where d is the earlier mentioned depth of the beam while w is the width. Now the eigenfrequencies of the models in Matlab and Comsol are compared with the analytical calculations of the eigenfrequencies. The results are presented in Tab. 3.2.

From Tab.3.2 it follows that the differences between the calculations increase with increasing the eigenfrequency number. The differences are probably caused by FE discretizations. However, the differences between the analytic calculated eigenfrequencies and the eigenfrequencies computed with Comsol and Matlab are small enough to conclude that the computation of the eigenfrequencies stemming from the mass and stiffness matrix is correct. Besides, it is interesting to note that the frequencies obtained with both Comsol and Matlab are nearly the same.

3.1.2. Comparison of time responses

Now the time response computed with Matlab is compared and validated with the time response obtained with the model in Comsol. The simple cantilever beam as introduced in section 3.1 is

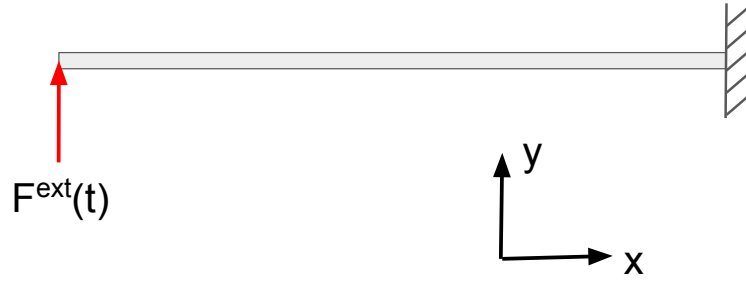
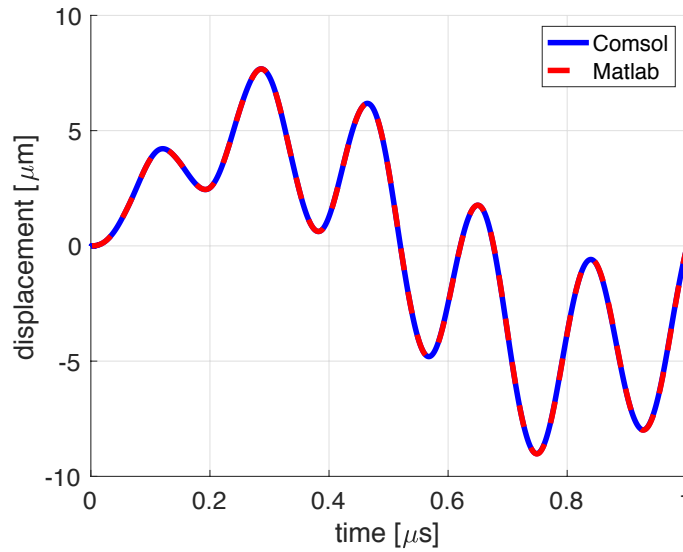


Figure 3.1: Schematic model of the transverse excited cantilever beam.



(h)

Figure 3.2: Linear time responses computed with both Comsol and Matlab. The responses are perfectly overlapping.

exposed to a harmonic transverse force acting on the free end of the cantilever beam. The external point force is described as:

$$F^{ext}(t) = H \cdot \sin(\omega t), \quad (3.7)$$

where H is the force amplitude, which is set to $20\mu N$. The excitation frequency is 5 MHz which lies between the first and the second eigenfrequency of the cantilever beam. Fig. 3.2 shows the transient linear time responses of both models. The plot clearly shows that the time responses are exactly overlapping, this is another indication that the codes in Matlab are implemented correctly.

3.2. Transverse excited cantilever beam

Let's again consider the model as presented in Fig.3.1. Both the full linear and the full nonlinear time responses of the model are represented in Fig. 3.3. It is assumed that the von-Karman kinematic model is valid for the investigated case since the displacement of the tip is in the order of the thickness of the beam. The transient responses of the considered ROMs are given in Fig. 3.4. The ROMs are obtained by reduction bases that comprise s VMs and the corresponding $s(s+1)/2$ MDs. Besides these modes, the Craig-Bampton and Rubin reduction bases also compound their typical static modes. Besides, the Rubin reduction bases also incorporate rigid body modes. Generally speaking, from the results it follows that the accuracy of the ROMs is low except in some cases. The Craig-Bampton reduction bases poorly approximate the full nonlinear solution. After the first forcing cycle, all Craig-Bampton ROMs start to deviate from the full nonlinear solution. The CB-II

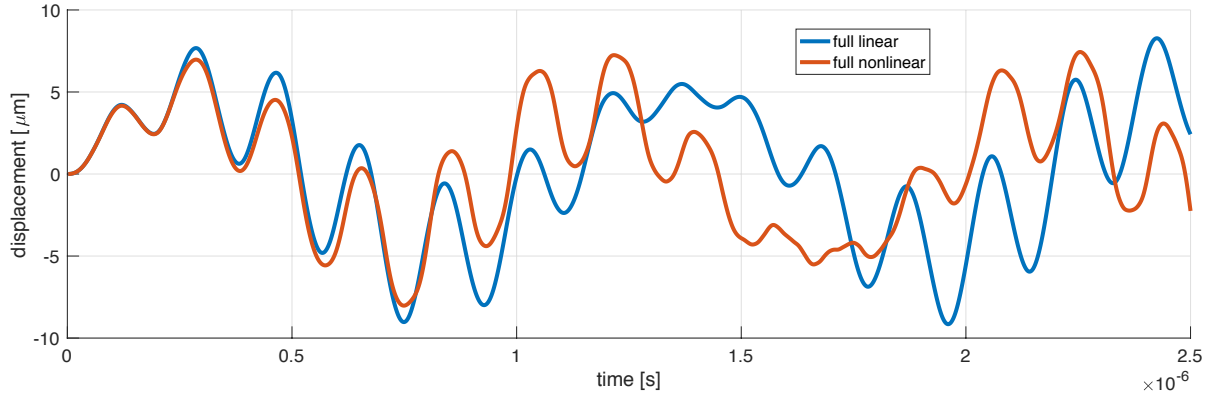


Figure 3.3: transient linear and nonlinear responses of the cantilever beam. The displacement of the free end in y -direction is plotted.

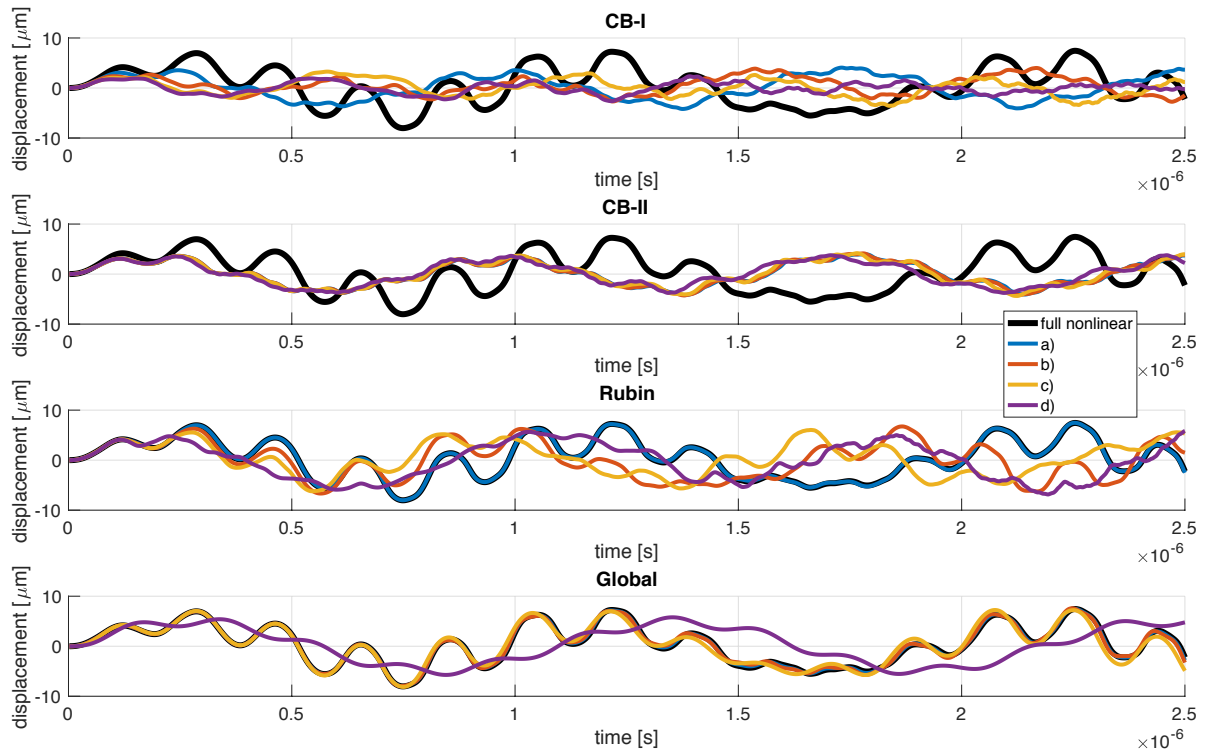


Figure 3.4: Transient nonlinear responses of the different ROMs of the cantilever beam. The reduction bases compose different numbers of vibration modes: a) 4 VMs; b) 3 VMs; c) 2 VMs; d) 1 VM. All corresponding modal derivatives are included in the reduction bases.

reduction bases which are augmented with 5 CMDs are not significantly more accurate than the CB-I reduction bases, however, the plot shows that the CB-II ROMs give responses that are more aligned. In general, the Rubin reduction bases are poorly approximating the full nonlinear solution. The only Rubin reduction basis that follows the response of the full nonlinear solution is the reduction basis that is augmented with 4 VMs and the 10 corresponding MDs. The lower-dimensional Rubin ROMs show similar responses as the Craig-Bampton ROMs.

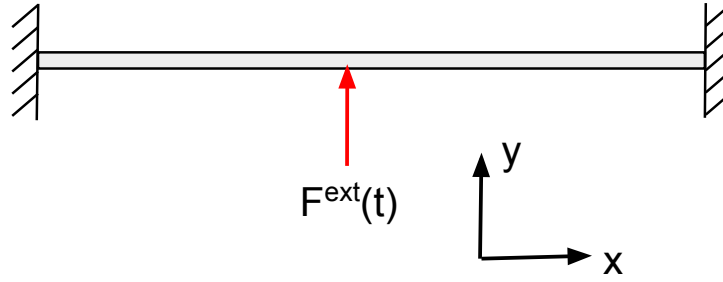


Figure 3.5: Schematic model of the transverse excited clamped-clamped beam.

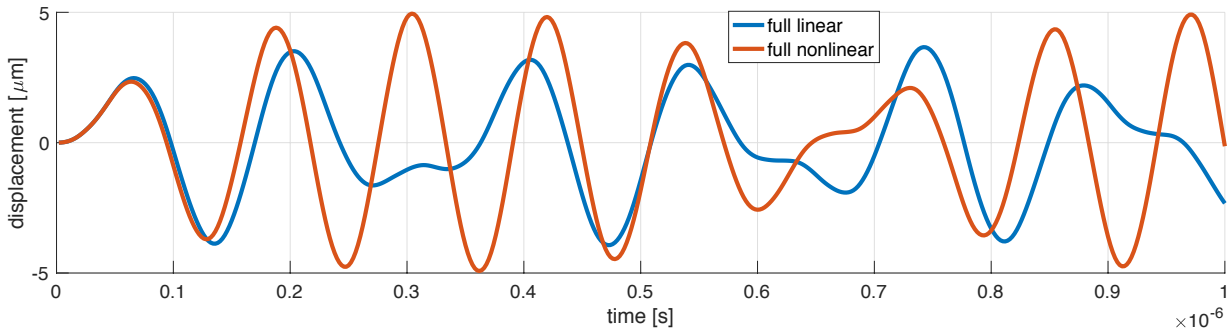


Figure 3.6: Transient linear and nonlinear responses of the clamped-clamped beam. The displacement of the middle of the beamstructure in y -direction is plotted.

The ROMs obtained with global reduction seem to approximate the full nonlinear solution much better than the ROMs obtained with Craig-Bampton and Rubin reduction. The ROMs obtained with global reduction bases composed of 2 or more vibration modes plus corresponding modal derivatives seem to perform best.

3.3. Transverse excited clamped-clamped beam

The next investigated transverse excited model is schematically represented in Fig. 3.5. In this model, both ends of the beam are clamped. The structure is divided into 2 beam model substructures such that an additional boundary node in the middle of the structure is created where the external transverse force is imposed. The lengths of the considered beams are both $40\mu m$, the young's modulus is $190GPa$. The depths and thicknesses of the beams are $4\mu m$. The density of the beam is $2328 kg/m^3$. The force amplitude is $3500\mu N$ while the force excitation frequency is $9MHz$, which lies between the first and the second eigenfrequency of the structure. These frequencies are $5.80 MHz$ and $16.0 MHz$ respectively. The substructures are both discretized with 25 elements, such that the entire structure contains 50 elements. The linear and nonlinear transient responses are given in Fig. 3.6, the displacement in the midpoint of the structure in the transverse y -direction is plotted over time. The transient responses of the ROMs are shown in figure 3.7. The results clearly show that for this model the ROMs give much better approximations of the full nonlinear solution than for the cantilever beam model in the previous section. Also the Craig-Bampton reduction now performs much better. However, it is evident that the CB-I ROM is still performing worse than the ROMs obtained with the other types of reduction bases. Remarkably, the CMDs in the CB-II reduction basis seem to greatly enhance the accuracy of the method, even for the case where the reduction basis comprises only 1 VM + corresponding MD. The reduction bases of both Rubin reduction and global reduction result in quite accurate ROMs, except for the reduction basis where only 1 VM + corre-

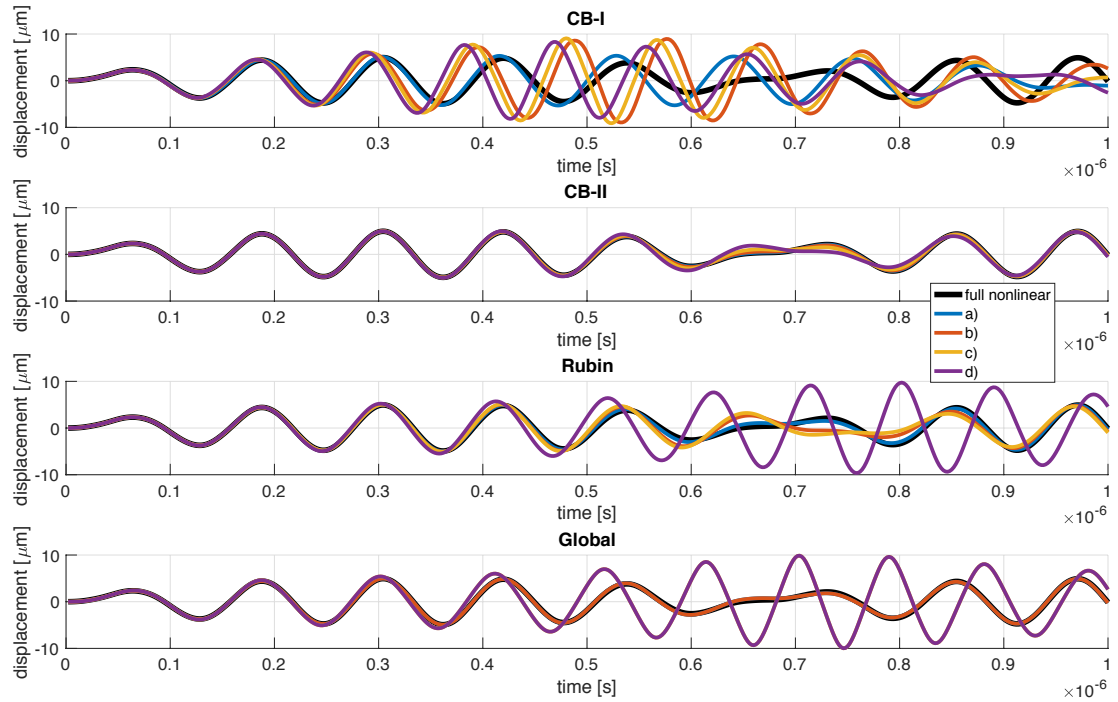


Figure 3.7: Transient nonlinear responses of the different ROMs of the clamped-clamped beam. The reduction bases compose different numbers of vibration modes: a) 4 VMs; b) 3 VMs; c) 2 VMs; d) 1 VM. All corresponding modal derivatives are included in the reduction bases.

sponding MD are incorporated. It is remarkable to note that the CB-II reduction bases seem to have the best performances of all considered reduction bases. A possible explanation for the high performance of the CB-II reduction bases is found in the fact that during excitation, the shape of both substructures is mainly described by the constraint modes, where the CMDs now account for the geometric nonlinearities in the model.

	length/radius [μm]	elements
I	183	20
II	7	9
III	266	20
IV	7	9
V	380	20
VI	7	9

Table 3.3: Dimensions of the substructures in the frequency dividers

3.4. Numerical results of frequency dividers

The numerical results of two FDs are presented in this section. The models are based on the mechanical FD as introduced by Qalander et al. [6]. The investigated models are a two-stage frequency divider and a three-stage frequency divider. Schematic representations of the two FDs are represented in Fig. 3.8. The dimensions of the substructures are given in Tab. 3.3. These dimensions are mainly based on the dimensions used for the FD in the paper of Qalander. The dimensions of the

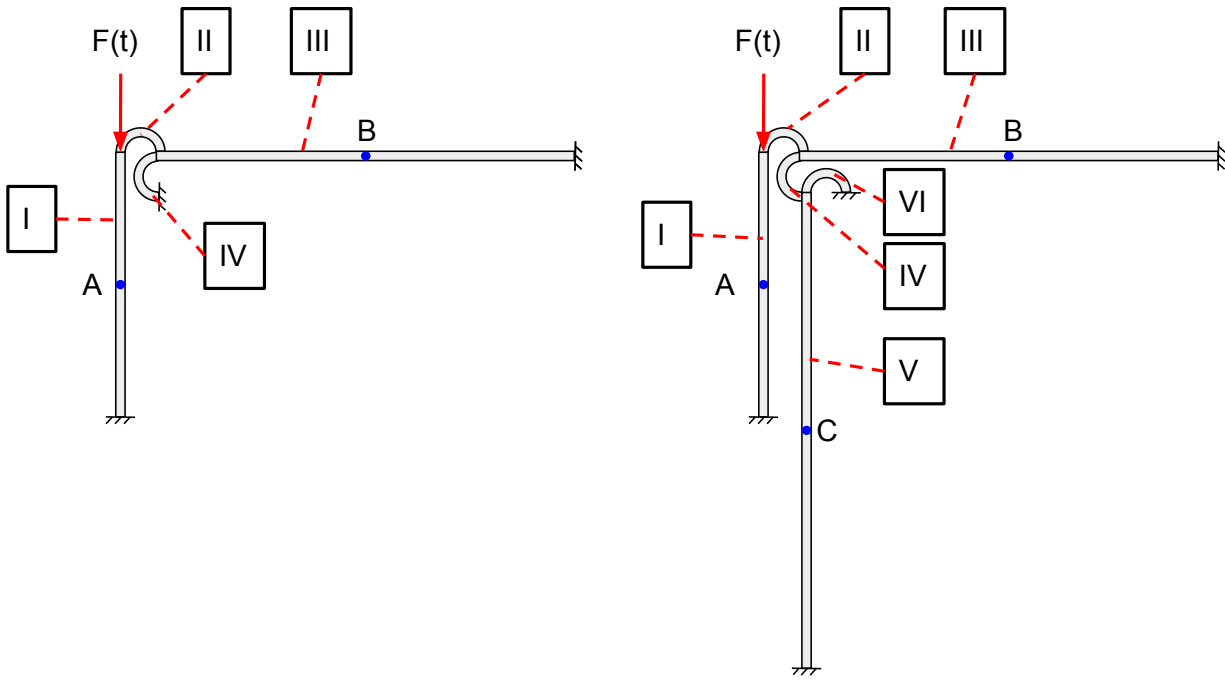


Figure 3.8: The investigated frequency dividers. On the left side the 2-stage frequency divider, on the right side the 3-stage frequency divider. The blue dots indicate the measurement points. The Roman numerals indicate the partition in substructures.

Young's modulus [GPa]	Density [kg/m^3]	Width [μm]	Thickness [μm]
148	2329	1.85	10

Table 3.4: Material and geometric properties of the FDs.

connecting hooks indicated with the labels *II*, *IV*, and *VI* are defined after some tests. As stated in the paper of Qalander [6], the stiffness of the connecting hooks need to be relatively low to spatially localize the resonance modes of the system in the beams. yet, the stiffness of the hooks needs to be sufficiently large in order to provide parametric pumping from one stage to the next. The specified dimensions of the hooks in this work are designed as such that these requirements are satisfied. The general material and geometric properties of the considered FDs are listed in Tab. 3.4.

3.4.1. Numerical results of a 2-stage frequency divider

Let's first consider a 2-stage frequency divider as represented on the left side in Fig. 3.8. The system is excited by a harmonic force that is imposed on the node that connects substructure *I* with substructure *II*. the direction of the force is indicated by the direction of the red arrow in the figure. The amplitude of the force is $30\mu N$ and the excitation frequency is $810kHz$. Small proportional Rayleigh damping is assumed with the following coefficients $\alpha = 1.96e - 10$ and $\beta = 761$. These values are roughly based on quality factors given in the paper of Qalander et al. [6], and later slightly adjusted in order to enable sufficient amplitudes of the resonance modes that are localized in the beams. Let's denote the resonance modes localized in the resonator beams *I* and *III* as the resonance modes *A* and *B* respectively.

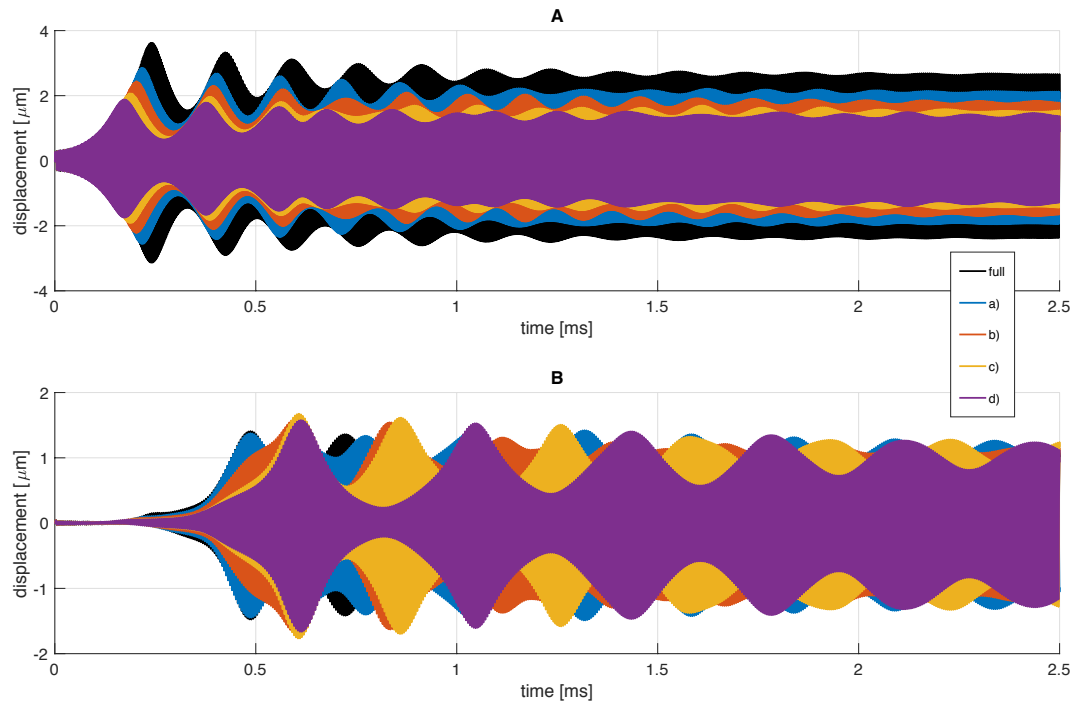


Figure 3.9: Time responses of CB-I ROMs of the 2-stage frequency divider. The displacements are evaluated in points *A* and *B* as indicated in Fig. 3.8. Different number of VMs are considered: a) 4 VMs; b) 3 VMs; c) 2 VMs; d) 1 VM. All corresponding MDs are included in the reduction basis.

Craig-Bampton-I reduction bases

If we now consider ROMs that are obtained by the earlier mentioned CB-I reduction bases, the approximated time responses of the 2-stage FD presented in Fig. 3.9 are obtained. The transient time responses up to 2.5 *ms* are plotted. The time responses beyond 2.5 *ms* show that the waves flatten out and that the responses converge towards steady-state responses. For all of the CB-I reduction bases, a frequency division of approximately $\frac{1}{2}$ and $\frac{1}{4}$ with respect to the excitation frequency is accomplished. Remarkably, even the cheapest reduction basis composed of the relevant constraint modes, plus 1 VM and the corresponding MD results in a ROM that roughly describes the full nonlinear responses. There is only a small difference in amplitude.

Obviously, including more VMs in the CB-I reduction basis results in a better approximation of mode A. The magnitude differences between the ROMs are probably caused by differences in stiffness between the models, because the reduction of the number of DoFs in a FEM normally introduces additional artificial stiffness.

Craig-Bampton-II reduction bases

Fig. 3.10 represents the time responses up to 2.5 *ms* of the ROMs obtained with CB-II reduction bases. The results clearly show that most of the CB-II ROMs show better agreement with the full nonlinear response than the CB-I reduction bases, this seems especially the case for the approximation of resonance mode A. It is remarkable that the ROMs obtained with the CB-II reduction bases show different wave patterns in the approximation of mode B, it seems there is faster convergence towards a steady-state response. There is no substantial difference in performance observable between the best CB-II reduction basis and the best performing CB-I reduction basis.

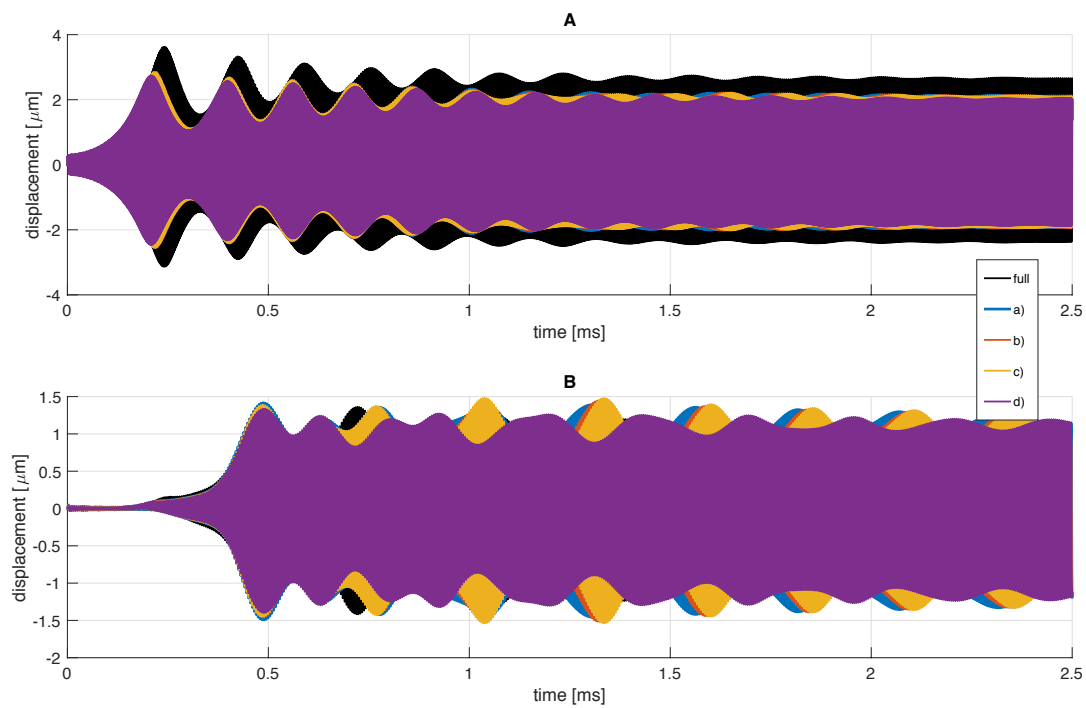


Figure 3.10: Time responses of CB-II ROMs of the 2-stage frequency divider. The displacements are evaluated in the points *A* and *B* as indicated in Fig. 3.8. a) 4 VMs; b) 3 VMs; c) 2 VMs; d) 1 VM. All corresponding MDs are included in the reduction basis.

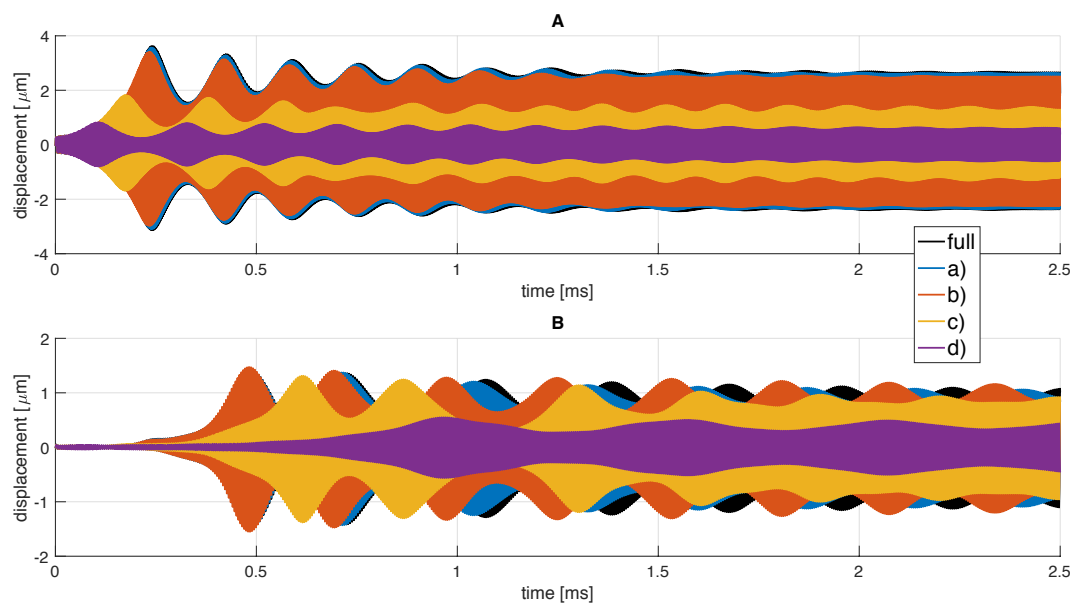


Figure 3.11: Time responses of Rubin ROMs of the 2-stage frequency divider. The displacements are evaluated in the points *A* and *B* as indicated in Fig. 3.8. a) 4 VMs; b) 3 VMs; c) 2 VMs; d) 1 VM. All corresponding MDs are included in the reduction basis.

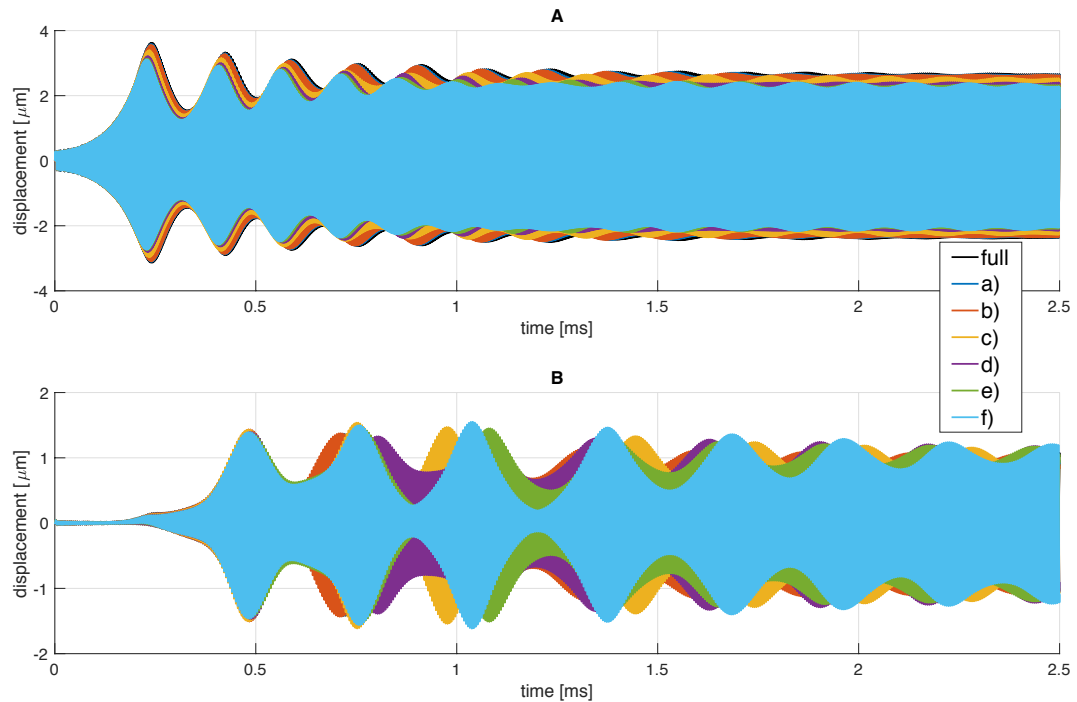


Figure 3.12: Time responses of Global ROMs of the 2-stage frequency divider. The displacements are evaluated in the points *A* and *B* as indicated in Fig. 3.8. a) 7 VMs; b) 6 VMs; c) 5 VMs; d) 4 VMs; e) 3 VMs; f) 2 VMs. All corresponding MDs are included in the reduction basis.

Rubin reduction bases

Fig. 3.11 represents the time responses of the ROMs attained with Rubin reduction bases. It is remarkable that the low dimensional Rubin reduction bases quite poorly reproduce the full nonlinear responses in the resonance modes *A* and *B*. A reasonable explanation is the fact that in contrast with the reduction bases of other reduction methods, the Rubin reduction basis does not explicitly contain modes that have similar shapes as the sought resonance modes of the structure. The free vibration modes are substantially different from the resonance modes, which are more similar to internal vibration modes and the global vibration modes of the structure. However, the Rubin reduction basis composing 4VMs + 10 MDs Rubin reduction bases show a quite good approximation of the nonlinear response, much better than the CB-I and CB-II reduction bases.

Global reduction

Fig. 3.12. shows the time responses generated with global reduction bases. It is obvious that this reduction method is the most efficient method of all considered types of ROMs of the 2-stage FD. A global reduction basis comprising 2 VMs plus 3 corresponding MDs is already roughly representing the overall responses of the system. Up to 0.5 milliseconds, the responses of the global ROMs and the full nonlinear solutions are pretty good-aligned.

Comparison of the ROMs

Fig. 3.13 presents the responses of the ROMs in the frequency domain. It is apparent that all investigated ROMs are capable to reproduce the frequency division with sufficient amplitude. Generally speaking, differences between the responses of the ROMs are found in amplitude and the overall shape of the responses. The maximal normalized cross-correlation coefficients of the ROMs of the 2-stage FD is shown in Fig. 3.14. The numbers in the markers indicate the number of VMs included

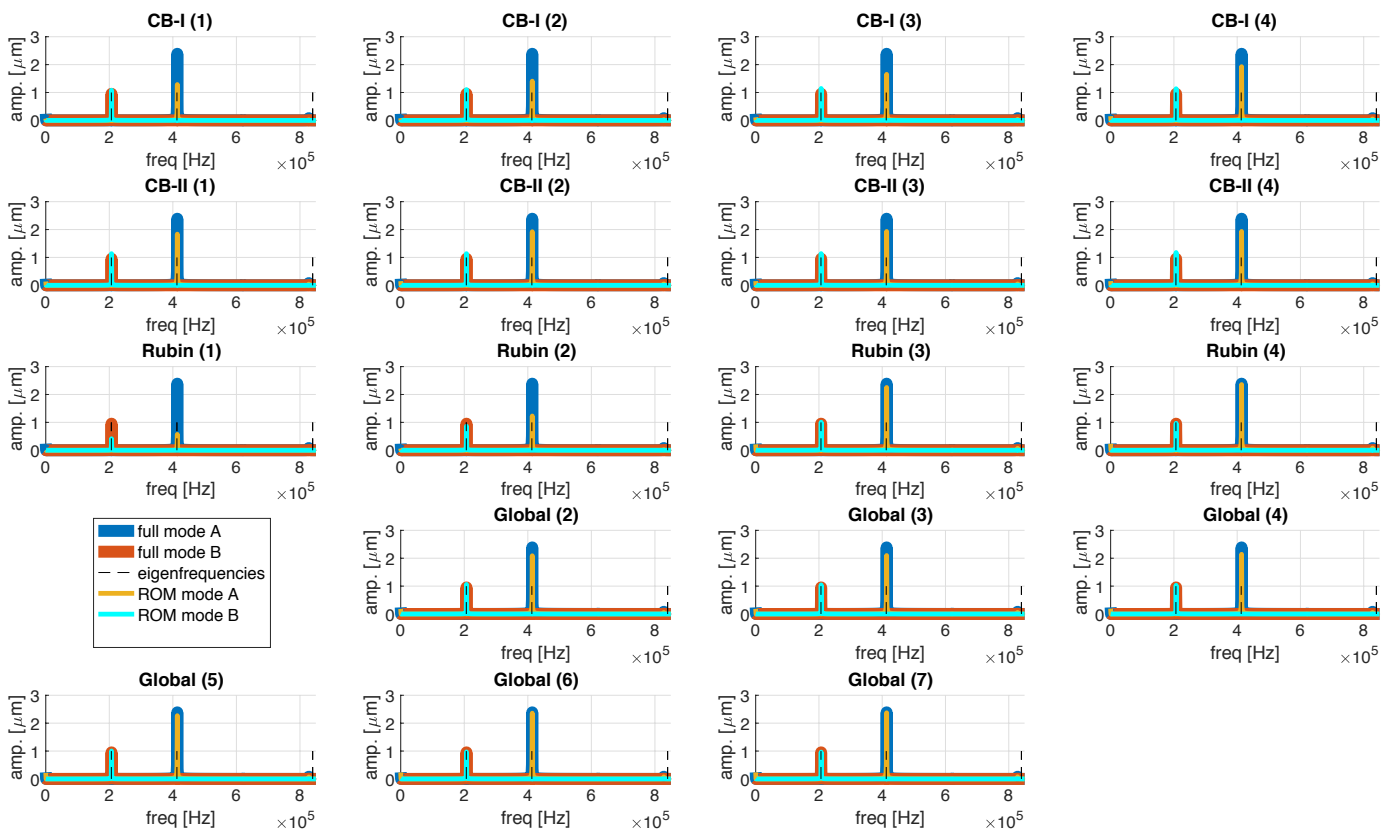


Figure 3.13: Frequency responses obtained by the ROMs of the two-stage frequency divider. The blue graphs indicate the frequency responses measured in location *A*. The red graphs represent the frequency responses measured in location *B*.

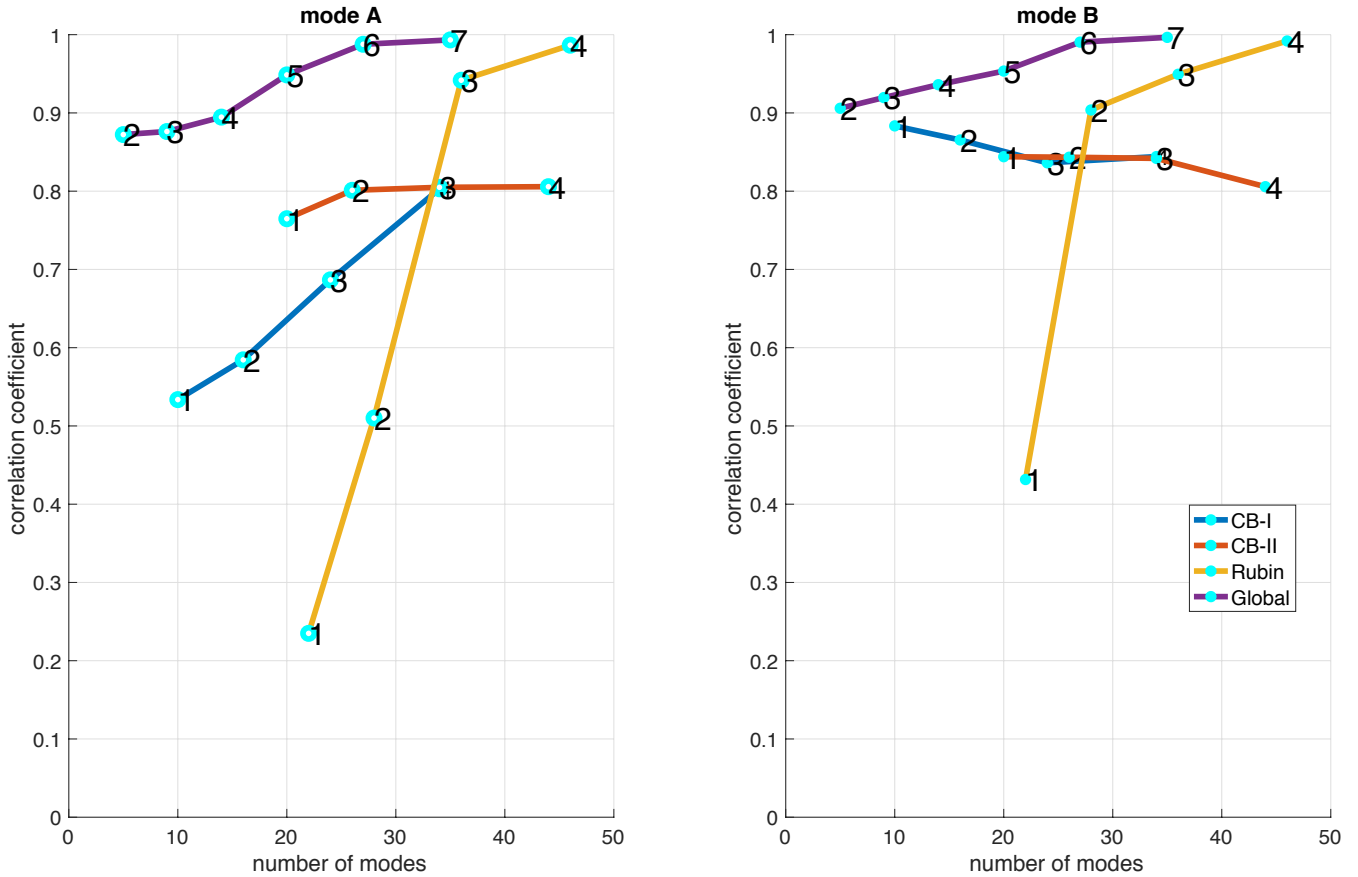


Figure 3.14: Maximal normalized cross correlation between ROMs and the full nonlinear solution of the two-stage FD. The black numbers in the markers indicate the number of vibration modes included in the reduction bases of the resonators. All corresponding MDs are included as well.

in the relevant reduction basis. The numbers on the x-axis indicate the total number of reduced DoFs in the entire system. The figure clearly shows the correlation between the maximal normalized cross-correlation and the number of reduced DoFs of the system. According to the figure, the use of RubIn reduction and Global reduction results in the most accurate ROMs. Global reduction achieves the highest accuracy with the lowest number of reduced DoFs.

3.4.2. Three-stage frequency divider

Let's now consider the 3-stage frequency divider as schematically represented on the right side in Fig. 3.8. In this case, 3 resonance modes are localized in the substructures *I*, *III* and *IV*. These resonance modes are labeled as the modes *A*, *B* and *C*. From numerical time integration it follows that even after long-time integration (6000+ forcing cycles), still no absolute, but a nearly steady-state response is achieved. This is a consequence of the relatively low damping in the system, but also because of the complex interactions between the resonance modes of the FD, as can be seen in the transient time responses. This is a drawback of time integration to find steady-state responses.

Craig-Bampton-I reduction basis

Fig. 3.15 represents the time responses of the beams in the first 2 milliseconds for the different CB-I reduction bases. It is clearly visible that in general the first stage of the frequency divider is activated first, then the second stage and the third one is activated last. This is in line with the analytical description of this class of FDs as in [15]. Furthermore, Fig. 3.15 clearly shows that the

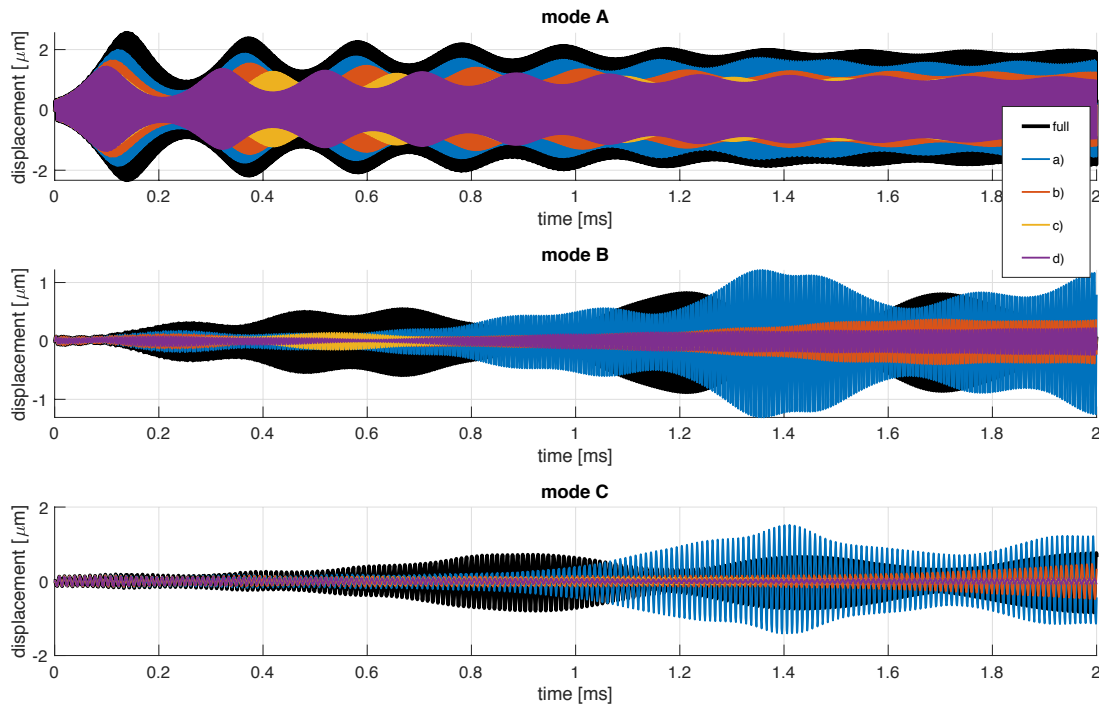


Figure 3.15: Responses of the CB-I ROMs in the beams of the frequency divider. The lines correspond to the number of vibration modes included in the reduction bases. a) 4 VMs; b) 3 VMs; c) 2 VMs; d) 1 VM

low dimensional Craig-Bampton reduction bases approximate the responses in beam B and C quite poor with too low amplitudes. Interesting are the wave patterns in the responses of the beams. The alternately varying amplitudes of the modes B and C are probably caused by interaction and the exchange of energy.

Craig-Bampton-II reduction basis

The responses of ROMs using the CB-II reduction bases are shown in Fig. 3.16. The responses clearly show that, compared to the CB-I reduction, the response in stage A is much better approximated, even for the ROM where the reduction basis comprises only 1 VM with the corresponding modal derivative. It seems that augmenting the CB-I reduction basis with CMDs greatly enhances the performance of Craig-Bampton reduction.

Rubin reduction basis

The responses of the Rubin reduction bases are shown in Fig. 3.17. The results clearly show that considering just 1 or 2 VMs plus corresponding MDs in the reduction bases poorly approximates the full nonlinear responses of all resonators, as also observed in section 3.4.1. Furthermore, it is visible that at least 3 free vibration modes plus modal derivatives need to be included in the reduction basis before the modes B and C are considerably activated. In the cases that 3 or 4 VMs are included in the reduction basis, the amplitudes in mode B and C are overestimating the full nonlinear response.

Global reduction basis

The responses of the global reduction basis are presented in Fig. 3.18. Up to 3 VMs, the system is not activated. Only if 4 VMs or more are included in the system reduction basis, the resonance modes are present. This is very intuitive since the first 3 eigenmodes are localized in the two longest resonators of the FD, the fourth eigenmode is the first mode that is localized in the shortest resonator

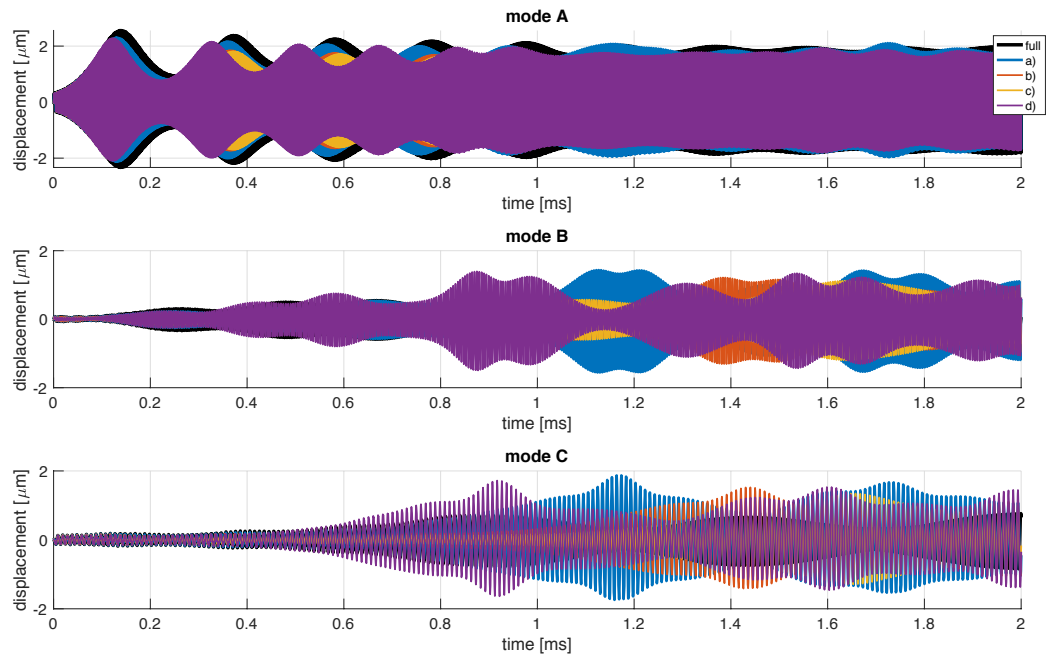


Figure 3.16: Responses of the CB-II ROMs in the beams of the frequency divider. The lines correspond to the number of vibration modes included in the reduction bases. a) 4 VMs; b) 3 VMs; c) 2 VMs; d) 1 VM

beam that is imposed directly by the external force. See Appendix G for the eigenmodes with corresponding eigenfrequencies. The system can be activated only if a vibration mode is included that corresponds to substructure I .

Comparison of the ROMs

The responses in frequency domain are presented in Fig. 3.19. From the responses, it clearly follows that all reduction methods can capture the frequency division in the resonance cascade. The responses are 'clean' in the sense that the responses in the beam are mainly described by one resonance mode with the corresponding eigenfrequency. Even after very long-time integration (6000+ forcing cycles), no absolute, but a nearly steady-state response of the structure was achieved.

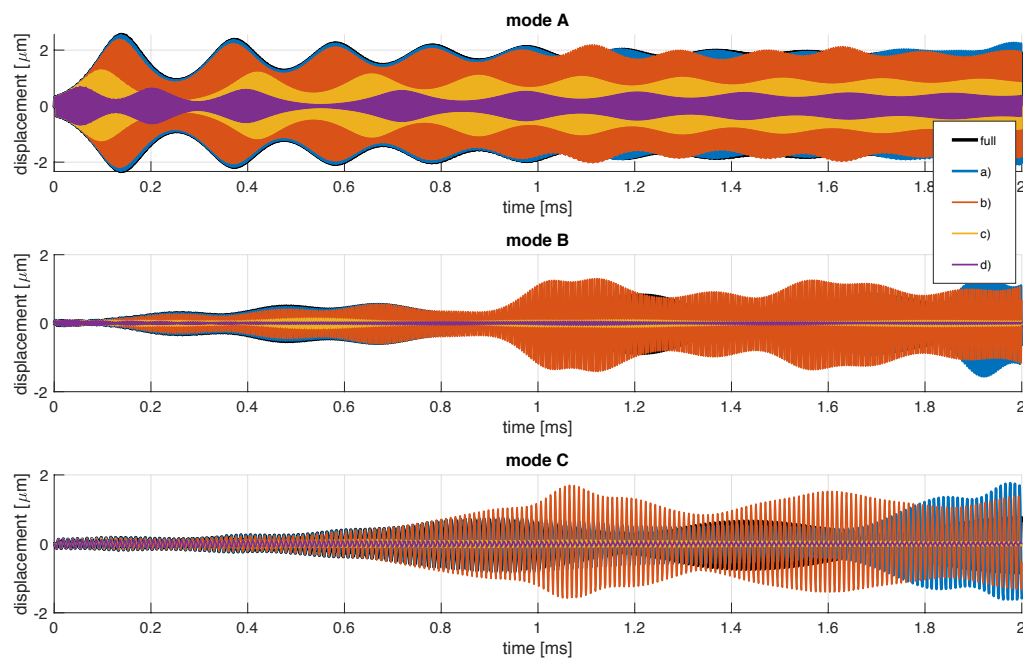


Figure 3.17: Responses of the Rubin ROMs in the beams of the frequency divider. The lines correspond to the number of vibration modes included in the reduction bases. a) 4 VMs; b) 3 VMs; c) 2 VMs; 1 VM

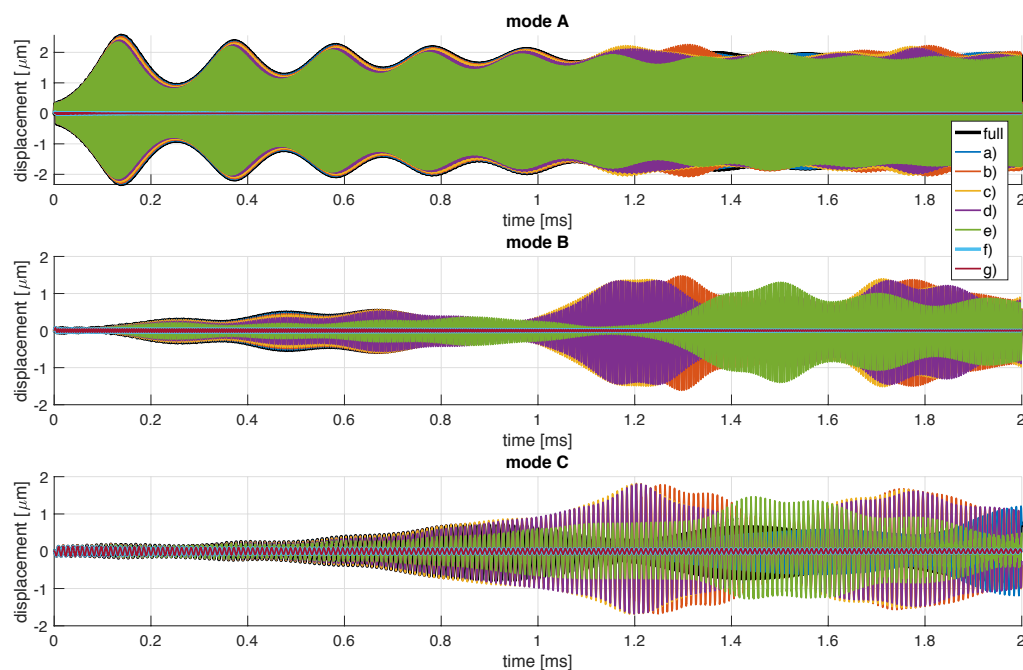


Figure 3.18: Responses of the global ROMs in the beams of the frequency divider. The different lines correspond to number of vibration modes included in the reduction bases. a) 8 VMs; b) 7 VMs; 6 VMs; c) 5 VMs; d) 4 VMs; e) 3 VMs; f) 2 VMs; g) 1 VM. All corresponding modal derivatives are included in the reduction bases.

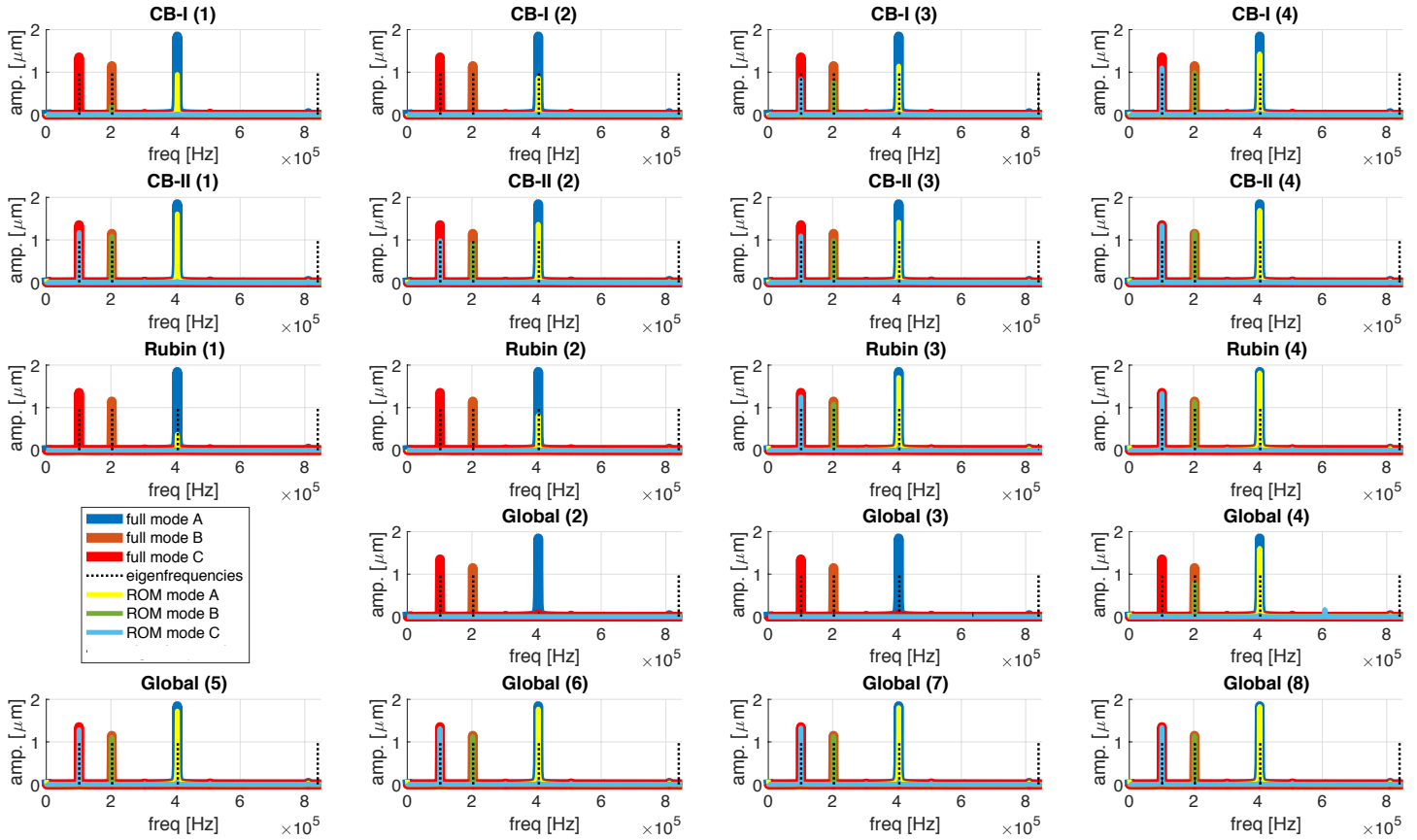


Figure 3.19: Frequency responses of ROMs of the 3-stage FD. Titles refer to the used reduction bases in the resonator beams. The number between parentheses indicate the number of VMs considered in the ROM. All corresponding MDs are included as well.

4

Conclusions

Model order reduction plays an important role in the reduction of Finite Element Models to increase computational efficiency. In this work, the emphasis was laid on the nonlinear steady-state responses of parametric excited reduced-order models. The reduced-order models considered are based on modal derivatives-based reduction bases that project the full number of unknowns originating from Finite Element equations onto a smaller set of unknowns. 3 different reduction methods with 4 different types of reduction basis were investigated. The benchmark problem was a mechanical frequency divider composed of an array of resonators that exhibits a frequency division along the chain of resonators. The input frequency is divided over the stages of the frequency divider, producing frequency ratios of approximately $\frac{1}{2}$, $\frac{1}{4}$ and $\frac{1}{8}$.

Based on the results attained during the project, the following conclusions are drawn:

1. The results in this work clearly show that modal derivative-based reduced-order models can approximate steady-state responses of simple parametrically excited structures with sufficient accuracy.
The results show that the full nonlinear steady-state responses of parametric excited single beam structures can be approximated with all reduction methods considered in this work. The performance of the reduced-order models is estimated with a maximal normalized cross-correlation coefficient.
2. The nearly steady-state responses of mechanical frequency dividers can be approximated with MDs-based ROMs. For both the 2-stage FD and the 3-stage FD, even after very long computation times, no absolute steady-state response was achieved due to the presence of very low damping in the systems. However, the overall responses in the beams after a considerable number of cycles are used to determine how well the frequency divisions in the FD are obtained with the ROMs and the average amplitudes indicate how well the ROMs are describing the overall full nonlinear time response. A normalized cross-correlation coefficient is used to estimate the performances of the ROMs.
3. Component mode synthesis can be effectively used in ROMs of complex parametric resonating structures. An array of resonators was used to test the applicability of this method. The resonators were reduced individually using Guyan reduction, Craig-Bampton reduction, and Rubin reduction. The reduced substructures were assembled after to obtain the reduced-order model of the entire frequency divider. The results show that the frequency division in the resonator array can be captured with component mode synthesis
4. The four investigated types of reduction bases perform with different accuracy in the different investigated models and cases. The steady-state time responses of the parametric excited sin-

gle beam structures show that the specified boundary conditions influence the applicability of a certain reduction base. It turns out that the more the modes in the reduction base have similar shapes as the resonance modes, the better is the reduction base sufficiently describing the response of the system. It may be concluded that the global reduction base is best approximating steady-state responses, while the CB-I reduction base, in general, performs worst.

5. A novel modification for the Craig-Bampton reduction base has been introduced. It is shown that augmenting the modal derivatives-based Craig-Bampton reduction base with constraint modal derivatives in general substantially improves the performance of the ROM in terms of accuracy and low-dimensionality. In both transient and steady-state analyses it is shown that the constraint modal derivatives are an adequate method to account for geometric nonlinearity in the model.

5

Recommendations

During this project, it became apparent that some parts of the work can be improved or investigated deeper. Furthermore, some additions are proposed for future work. The following recommendations are done:

1. The first proposed improvement is to increase the number of elements. For the sake of computation time and memory restrictions, the number of elements was kept relatively low. Despite this low number of elements, some of the computations took up to several hours. The chosen number of elements is justified with convergence checks. A higher number of elements would enable the possibility to investigate the contribution of higher frequency modes in the reduction basis. A too low number of elements makes modes coarse and spiky that normally does not inure the accuracy and applicability of the mode. Furthermore, a higher number of modes enables an extension of the reduction base with more modes. If too many modes are included in the reduction base, such that it introduces too many unknowns compared to the unreduced unknowns, the system becomes ill-conditioned and unsolvable. During this project this sometimes happened, especially in the case where all possible modal derivatives were included in the reduction base. One of the remedies was to increase the number of elements, however, there exist more elegant ways to circumvent this problem.
2. Another proposal is to use an improved error estimator. In this work, an error estimator is introduced that is based on cross-correlation between the time histories obtained with the full solution and the time histories obtained with the ROM. The advantages of this estimator are its simplicity and versatility: it accounts for both magnitude differences and frequency differences between the responses and does not penalize eventual phase shifts. Furthermore, the lag variable τ gives information about a phase difference between the two investigated signals. However, there are some limitations and weaknesses in the use of the cross correlation-based estimator. First of all, the estimator is only reliable in the case that the overall shapes of the responses are pretty identical. Large beat phenomena, for example, may deteriorate the reliability of the outcomes of the estimator. An alternative that overcomes this problem is the application of a coherence based estimator. For example the FRAC estimator [24]:

$$c_{FRAC} = \frac{\left| \sum_{j=1}^{N_f} (\mathbf{H}_f(\omega_j))^* \cdot \mathbf{H}_g(\omega_j) \right|^2}{\left[\sum_{j=1}^{N_f} (\mathbf{H}_f(\omega_j))^* \cdot \mathbf{H}_f(\omega_j) \right] \left[\sum_{j=1}^{N_f} (\mathbf{H}_g(\omega_j))^* \cdot \mathbf{H}_g(\omega_j) \right]}, \quad (5.1)$$

where $\mathbf{H}_f(\omega)$ and $\mathbf{H}_g(\omega)$ are the responses in frequency domain of the full model and the reduced model respectively. N_f is the number of frequencies. This estimator is simple and

popular [40],[24]. The coefficient c_{FRAC} is normalized, such that its value is between 0 and 1. Furthermore, the coefficient is insensitive for phase shifts between the time responses of the ROM and the full model. However, the method is insensitive to magnitude shifting, which is undesired for comparing the performance of ROMs. Therefore an extension of the FRAC is proposed to account for magnitude differences:

$$c_{FRACM} = \sqrt{\frac{\min(P_f, P_g)}{\max(P_f, P_g)}} \cdot c_{FRAC}, \quad (5.2)$$

where P is the overall power over the frequency band of concern, it is calculated as:

$$P = \sum_{j=1}^{N_f} |\mathbf{H}(\omega_j)|^2. \quad (5.3)$$

The square root in Eq. 5.2 is introduced to compensate for the square in the formulation of P , this results in a linear scaled magnitude estimator. e.g. two signals with the same frequency but with amplitudes of 3 and 6 give a c_{FRACM} value of 0.5.

3. Another alternative to determine the performance of the ROMs is the by Shin [42] proposed way to define shape similarity and magnitude similarity as two different estimators. This method has its advantages over the FRAC estimator since it is more convenient for largely deterministic signals, which is, in fact, more or less the case in a resonance steady-state response.
4. Another proposal is the use of a fast algorithm to compute steady-state responses of the ROMs. Since this work considers lightly damped systems, it takes much time before a steady-state response is achieved in the system. For the considered 3-stage frequency divider, even after many excitation cycles, there was not an absolute steady-state response achieved. Therefore, it is recommended to find the steady-state responses of the parametric excited models and frequency dividers with an algorithm that quickly computes the steady-state responses. One interesting option would be the integral equation approach proposed by Jain et al. [29]. This method can be used to quickly find the steady-state responses of a multi-DoF system. The kernel of this integral approach is a Green's function. The integral is solved with either the very fast converging Picard iteration or a Newton-Raphson iteration. It is known that excitation near resonance may cause problems for Picard convergence, therefore for the models considered in this work, Newton-Raphson iterations for the convergence of the integral approach is proposed.
For this recommendation the applicability of the integral approach for parametric excited systems is checked for the 2-DoF example in Appendix C. It turns out that the integral approach can capture the steady-state period-doubling, furthermore it is shown that indeed the Picard iterations were not able to converge. Therefore the application of the integral approach with Newton-Raphson iterations seems very interesting to use in future work, for finding steady-state responses of the parametrically excited models.
5. Another proposal is to use an improved type of damping. In this work, the damping of the system is assumed to be proportional to the mass- and stiffness matrix. The formulation of the damping matrix \mathbf{C} is simply given as:

$$\mathbf{C} = \alpha \mathbf{K} + \beta \mathbf{M}. \quad (5.4)$$

The coefficients of both α and β are based on quality factors given for the frequency divider introduced in the paper of Qalander et al. [6]. The coefficients were based on a least square

approximation of the quality factors. However, in this work the coefficients were slightly changed to increase the performance of the frequency divider. Without this change, not all of the modes in the frequency divider were activated properly i.e. amplitudes of the modes were low. More research is recommended to include a better and more realistic formulation of the damping in the system. Furthermore, it is recommended to further elaborate on the role of damping in the responses of the resonance modes in the system. It is expected that non-linear damping could lead to quickly reaching the steady-state responses in numerical time integration.

6. To reduce the number of unknowns, the investigation of a quadratic manifold is proposed. In this work, the model order reduction is based on a linear manifold, i.e. the system response is given as a linear combination of modes:

$$\mathbf{q}(t) = \sum_{i=1}^m \phi_i \eta_i(t), \quad (5.5)$$

or equivalently:

$$\mathbf{q}(t) = \mathbf{V}\boldsymbol{\eta}(t). \quad (5.6)$$

In many works, it is shown that this reduction method is accurate for linear dynamic systems. However, as soon as the reduction base is extended with modal derivatives, the size of the reduction base increases in a quadratic relationship with the vibration modes. This is undesirable since it defeats the purpose of reduction. An interesting way to keep the number of unknowns low is the application of a quadratic manifold. In this manifold a nonlinear quadratic mapping is introduced to capture the second-order components, which are described with modal derivatives in a linear manifold. This nonlinear mapping is given as:

$$\mathbf{q}(t) \approx \boldsymbol{\Lambda}(\mathbf{q}(t)) := \boldsymbol{\Theta} \cdot \mathbf{q}(t) + \frac{1}{2}(\boldsymbol{\Omega} \cdot \mathbf{q}(t)) \cdot \mathbf{q}(t). \quad (5.7)$$

In this mapping $\mathbf{q}(t) \in R^m$, m are the reduced unknowns, $\boldsymbol{\Theta} \in R^{n \times m}$ and $\boldsymbol{\Omega} \in R^{n \times m \times m}$. As a matter of fact, the modal derivatives are now hidden in $\boldsymbol{\Omega}$. This means that the amplitudes of the second-order terms are now enslaved by the amplitudes of the vibration modes. This effectively keeps the number of unknowns restricted to the amplitudes of the vibration modes. It would be interesting to test this quadratic manifold for the reduction of the investigated models in this work.

7. It is shown that reduction methods can capture the frequency division in a resonance cascade up to three stages. It would be interesting to explore ROMs of frequency dividers that comprise more stages in the resonance cascade. The expectation is that the responses of the system will become more complex and unpredictable since more back- and forward couplings will be present that influence the overall behavior of the FD. For higher-order FDs, the global reduction can probably not be used anymore because of excessive storage requirements. Component mode synthesis could then be a good approach to obtain the reduced-order model of the FD. Therefore, to validate the applicability of component mode synthesis in more complex parametric resonating structures, it would be very interesting to investigate higher multistage-stage frequency dividers.
8. Another proposal is the use of a mode selection criterion for the modal derivatives of the ROMs of the FDs to keep the number of reduced unknowns relatively low. The number of modal derivatives increases quadratically with the number of vibration modes. However, it is known that in most the cases a respectable amount of modal derivatives is redundant and not contributing to the response of the system.

Tiso [8] proposed a method to select modes for a second-order reduction basis in case of a nonlinear transient analysis. This selection criterion is based on the amplitudes of the vibration modes in linear time integration. Only the MDs related to the VMs with the highest amplitudes need to be incorporated in the reduction base.

The recommendation is to use the principles of this selection method for a nonlinear FD. Linear time integration for finding the dominant vibration modes does not make sense in this case, since nonlinearity forms the basis of the working principle of the FD. However, it is a priori known which vibration modes will probably have the highest amplitudes in the steady-state response since we know on forehand that we are looking for a steady-state response that consists of the fundamental resonance modes only. Therefore we know that modes that describe these fundamental resonance modes will have the highest amplitudes in the steady-state response. Now a selection of MDs can be made where only the MDs related to these dominant modes are considered. It should be noted that this approach probably only works for Craig-Bampton reduction and especially global reduction since these reduction bases of these methods include vibration modes that are nearly identical to the resonance modes of the FDs, in contrast with the free vibration modes in the Rubin reduction base. It would be interesting to investigate and validate this.

9. The last recommendation is to use a better tensor toolbox for the tensor approach. In this work a tensor approach is proposed for the nonlinear stiffness matrix and force vector. The derivation of the relevant tensors are presented in Appendix F. The main advantage of the approach is that the updated versions of the stiffness matrix and force vector within an iteration step are made with respect to the reduced set of coordinates instead of assembling elemental contributions of the full set of coordinates, this makes the computation more efficient and the computation time becomes independent of the number of elements in the model. In this work, the tensor approach was tried with the Sandia tensor toolbox [30]. However, the contractions of the fourth-order tensors took so much time that the computations with the tensors were even slower than without. Only in case of very fine-meshed models (1000+ elements), the tensor approach was more advantageous. Therefore, it is recommended to find a more efficient way to compute the contractions of the tensors, such that the tensor approach becomes more efficient.

6

Reflection

In this brief chapter, a reflection on the work done during this thesis project is outlined. This is done to give the reader a better idea of the content of the master thesis itself. The chapter is organized as follows: first, a brief reflection on the timeline is given, then the contributions of this work in the field of reduced-order models are given. In the third section, a reflection on personal developments is outlined.

6.1. Reflection on the timeline

The project started on the 15th of September 2018. The first months of the project were filled with extensive literature research to identify the gaps in the literature. But above all, the literature study was needed to gain knowledge in the field of finite element coding and model-order reduction. In the same period, a start was made with writing codes for finite element modeling. Since I never had done something before with coding finite element formulations myself, this took some months to fully get the hang of it. In this time, codes were written and developed for linear and nonlinear static analyses of simple structures. Later the codes were extended and enhanced with reduction methods.

In the second part that forms the core of the project, the codes were further developed and applied for more complex resonating structures. The first used reduction method, the Craig-Bampton reduction, seemed to fail in some analyses and therefore Rubin reduction and later the global reduction was implemented in the codes to look for better performing reduced-order models. The outcomes from the analyses were critically assessed and compared with results in the literature, small coding and formulation faults were detected and corrected. Model parameters were adjusted and tested to get better and reliable results.

For some analyses, the computation time increased up to several hours and as a consequence, the demand increased for making the codes more efficient. This means that the Matlab codes were further developed and optimized. The implementation of some computational tricks made the computation time up to several times faster than the originally written codes. Other aspects that were investigated but not further elaborated in this thesis are the tensor formulations and the principles of mode selection.

The last part of the thesis roughly spanned 2 months. In this part results were wrapped up and some final computations were done. First, a paper was written, later the chapters of the thesis were written down.

6.2. Contributions

Generally speaking, this work has filled some gaps that were identified in the literature. Based on the obtained results during this project, it is now known that modal derivative-based methods can approximate the responses of parametric excited structures. This could serve as a starting point for further research and other projects.

Furthermore, this work has shown that the overall behavior of a frequency divider can be approximated with a simple finite element beam structure. This opens the door for further research in the finite element modeling of mechanical frequency dividers, it could play a pivotal role in the design processes of parametric resonating structures.

This work has shown that CMS in combination with MD-based reduction methods applies to parametric resonating structures. This knowledge could serve other projects where compounded structures are exposed to parametric excitation or resonances.

This work introduced some concepts of a new type of modal derivatives, called the constraint modal derivatives. This work has shown that the constraint modal derivatives are greatly enhancing the computational efficiency and accuracy of some considered models. The concept of constraint modal derivatives might be used in future projects.

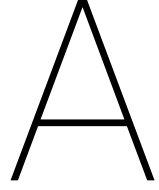
6.3. Personal developments

The guidance of my supervisor formed one of the keystones in my personal developments during the project. The almost weekly meetings motivated me to organize and plan my work and to make sufficient progress. Sometimes, my supervisor spent up to several hours during our meetings for help and discussions. Sometimes it was not possible to meet weekly, which were the more challenging moments where I had to find approaches myself to make progress and to reach the aims of the thesis. It was sometimes difficult, but on the other hand, it was also motivating and good for personal development.

I clearly remember that my supervisor drew a graph on the whiteboard in his office that would predict my progress during the research. The idea was that during the major part of the project, you are struggling and have ups and downs until you reach a point where things are coming together and you suddenly make lots of progress. This is what also happened to me during this project. For a long period, it felt like experiencing ups and downs in progress without really getting closer to a decisive solution to the problem or answers on specific open questions. However, at a certain moment things are coming together and you recognize certain patterns or earlier encountered problems that help you to more effectively and efficiently tackle problems. It is hard to end the project at a moment that it feels like you got the hang of it, however, it is also a good feeling. The most challenging part was the last months of the project. A lot of things were done and there were many subjects investigated over time. It was hard for me to make a selection of the things I would put in the thesis. Therefore, this thesis does not contain all aspects that have been touched during the research. However, as one of my supervisors said: it is a thesis, not a report.

Another point that I have learned is how to present results. My supervisor advised me to prepare slides to discuss during the meetings. It improved the overall efficiency of the meetings.

Overall, it was a good and enriching experience researching for one year. I learned to research an independent and professional level. The thesis has broadened my knowledge and it offered me various useful tools that I can use in future work. It was not always easy to tackle the problems that emerge during the project on your own. Fortunately, I have got precious help from my supervisors and a Ph.D. student that contributed to my personal developments.



Derivation of modes

A reduction basis is composed of modes. Different types of modes contain different types of information regarding the dynamic and static behavior of a system. The total time-dependent high-dimensional displacement vector $\mathbf{q}(t)$ of a system can be presented as a superposition of modes and the corresponding amplitudes:

$$\mathbf{q}(t) = \sum_{i=1}^m \vartheta_i \eta_i(t) \quad (\text{A.1})$$

Where ϑ_i can be certain mode type as will be described in the next subsections, $\eta(t)_i$ is the corresponding time-dependent amplitudes of the mode ϑ_i . For sake of simplicity, we omit the time dependency, such that we can simply write:

$$\mathbf{q} = \mathbf{V}\boldsymbol{\eta} \quad (\text{A.2})$$

The reduction basis $\mathbf{V}R^{(n \times m)}$ should comprise a set of modes such that a linear combination of these modes results in a sufficient approximation of the full nonlinear response. In order to achieve this, different types of modes are embedded in the reduction basis. Each reduction method uses its type of characteristic modes. The various types of modes will be discussed briefly in the following subsections. For some of the mode types a distinction between the so-called boundary and interior nodes is required. For a linear system, we can partition the system equations of motion in boundary- and internal components as:

$$\begin{bmatrix} \mathbf{M}_{BB} & \mathbf{M}_{BI} \\ \mathbf{M}_{IB} & \mathbf{M}_{II} \end{bmatrix} \begin{bmatrix} \ddot{\mathbf{q}}_B \\ \ddot{\mathbf{q}}_I \end{bmatrix} + \begin{bmatrix} \mathbf{K}_{BB} & \mathbf{K}_{BI} \\ \mathbf{K}_{IB} & \mathbf{K}_{II} \end{bmatrix} \begin{bmatrix} \mathbf{q}_B \\ \mathbf{q}_I \end{bmatrix} = \begin{bmatrix} \mathbf{F}^{\text{ext}}_B(t) \\ \mathbf{0} \end{bmatrix}. \quad (\text{A.3})$$

Nonlinear systems can be partitioned in the same manner.

A.1. Internal Vibration modes

Internal vibration modes are the vibration modes obtained by clamping the structure at its boundary nodes. The internal vibration modes are found by solving the following eigenvalue problem:

$$(\mathbf{K}_{II} - \omega_{I,k}^2 \mathbf{M}_{II})\boldsymbol{\phi}_{I,k} = \mathbf{0} \quad (\text{A.4})$$

Where \mathbf{K}_{II} is the internal stiffness matrix and \mathbf{M}_{II} is the internal mass matrix as obtained with the partition in eq. A.3. $\boldsymbol{\phi}_{I,k}$ is the k -th internal vibration mode and $\omega_{I,k}$ is the corresponding k -th internal eigenfrequency. The computed internal vibration modes may be collected in the matrix $\boldsymbol{\phi}_i$. The internal vibration modes only act on the internal nodes.

A.2. Free Vibration modes

Free vibration modes are obtained by solving the following eigenvalue problem:

$$(\mathbf{K} - \omega_{f,k}^2 \mathbf{M})\phi_{f,k} = \mathbf{0} \quad (\text{A.5})$$

Where \mathbf{K} is the unconstrained stiffness matrix while \mathbf{M} is the unconstrained mass matrix. $\omega_{f,k}$ is the k -th eigenfrequency corresponding to the k -th free vibration mode $\phi_{f,k}$. The free vibration modes are collected in the matrix ϕ_f . Free vibration modes act both on internal nodes and boundary nodes.

A.3. Constrained modes

The constraint modes are modes that describe the shape of the structure in case of a unit displacement on one of the boundary nodes while remaining the other boundary nodes fixed. Constraint modes are static modes, in contrast with the vibration modes which are dynamic modes. The number of constraint modes of a structure equals the number boundary DoFs. This means that a 2-dimensional beam system normally contains six constraint modes. The constraint modes ψ_c are calculated as:

$$\psi_c = -\mathbf{K}_{II}^{-1} \mathbf{K}_{IB}. \quad (\text{A.6})$$

Note that the constraint modes, in this case, are only related to the interior nodes of the structure.

A.4. Attachment modes

Another type of mode that describes how boundary nodes of a body are compatible with the boundary nodes of its neighbor bodies is the attachment mode. Attachment modes are physically describing the static response of the body by imposing a unit force on one of the boundary nodes while imposing zero forces at the remaining boundary DoFs. In case of a fully constrained structure, the attachment modes are easily computed as:

$$\psi_a = \mathbf{K}^{-1} \mathbf{F}. \quad (\text{A.7})$$

The columns of the matrix ψ_a contain the individual attachment modes, \mathbf{K} is the system stiffness matrix corresponding to the constraint structure. The columns of the matrix \mathbf{F} are unit force vectors corresponding to one of the boundary DoFs, denoted as:

$$\mathbf{F} = [\mathbf{I}, \mathbf{0}]^T, \quad (\text{A.8})$$

where \mathbf{I} is the identity matrix associated with the boundary DoFs, $\mathbf{0}$ is a null matrix associated with the internal DoFs. Since normally a structure is composed of substructures that are not fully constrained, imposing a unit force on the structure for finding the attachment modes, results in a body that will accelerate infinitely and will undergo undetermined deformations. The remedy is the application of temporary equilibrating forces which prevent these infinite accelerations. By using the equilibrating forces, the attachment modes are found by using a pseudo-inverse of the stiffness matrix:

$$\psi_a = \mathbf{K}^+ \mathbf{F} = \mathbf{G} \mathbf{F}, \quad (\text{A.9})$$

where \mathbf{K}^+ is a generalized inverse of the singular stiffness matrix \mathbf{K} . This generalized inverse is by definition the flexibility matrix \mathbf{G} . Four steps are required in order to find the attachment modes of a non-fully constrained system [9],[10]:

1. Compute the rigid body modes
2. Compute a generalized inverse of \mathbf{K}

3. Determine a self-equilibrated force vector \mathbf{F}_{eq}
4. Mass-orthogonalize the attachment modes

Every step will be considered in this section.

The first step in finding the attachment modes is to compute the rigid body modes of the structure. As a result of the non-fully constrained structure, the structure obviously has rigid body modes. In a 2D model, the motion of the body can be described by 2 translations and one rotation. See the previous appendix for the derivation of the rigid body modes.

The second step is to compute a generalized inverse of the stiffness matrix \mathbf{K} . In the case of a free-floating system, the inverse of \mathbf{K} is not unique. One way to circumvent this problem is the application of temporary imaginary links or also called isostatic constraints. This means that some DoFs are constrained during the computation of the generalized inverse. In that case we use the following equation:

$$\begin{bmatrix} \mathbf{K}_{00} & \mathbf{K}_{0B} & \mathbf{K}_{0I} \\ \mathbf{K}_{B0} & \mathbf{K}_{BB} & \mathbf{K}_{BI} \\ \mathbf{K}_{I0} & \mathbf{K}_{IB} & \mathbf{K}_{II} \end{bmatrix} \begin{bmatrix} \mathbf{0} \\ \mathbf{q}_B \\ \mathbf{q}_I \end{bmatrix} = \begin{bmatrix} \mathbf{F}_c \\ \mathbf{I} \\ \mathbf{0} \end{bmatrix}. \quad (\text{A.10})$$

Where \mathbf{F}_c are the constraint forces associated to the fixed set of DoFs. Since the structure is constrained by the isostatic constraints, the inverse of the lower part of the stiffness matrix in Eq. A.10 is not singular. Therefore the so-called constraint flexibility matrix \mathbf{G}_c is now found as:

$$\mathbf{K}^+ = \mathbf{G}_c = \begin{bmatrix} \mathbf{0} & \mathbf{0} \\ \mathbf{0} & \mathbf{K}_c^{-1} \end{bmatrix}, \quad (\text{A.11})$$

where \mathbf{K}_c^{-1} is described as:

$$\mathbf{K}_c^{-1} = \begin{bmatrix} \mathbf{K}_{BB} & \mathbf{K}_{BI} \\ \mathbf{K}_{IB} & \mathbf{K}_{II} \end{bmatrix}^{-1}. \quad (\text{A.12})$$

It is important that the constraint forces remain as small as possible for finding an as good as possible estimation of the displacements of the structure by imposing a unit force vector.

The next step in the process of obtaining the attachment modes is finding an equilibrated force vector \mathbf{F}_{eq} , such that

$$\mathbf{F}_{eq} = \mathbf{F} + \mathbf{F}_{balance}. \quad (\text{A.13})$$

This equilibrated force vector is required in order to avoid the structure from undergoing infinite rotations and undetermined deformations. The counterbalancing forces $\mathbf{F}_{balance}$ are required in order to keep the structure in static equilibrium. This obviously means that the sum of the applied forces and the sum of the moments are zero. This principle is called inertia relief [44]. The balancing forces are described by:

$$\mathbf{F}_{balance} = -\mathbf{M}\ddot{\boldsymbol{\phi}}_r. \quad (\text{A.14})$$

In order to find the second-order derivative of $\boldsymbol{\phi}_r$, we first need to separate the displacement vector \mathbf{q} into a rigid body displacement part called \mathbf{q}_r and a flexible body displacement contribution \mathbf{q}_f . If we now recall the principle of modal superposition, one can write:

$$\mathbf{q} = \mathbf{q}_r + \mathbf{q}_f = \boldsymbol{\phi}_r \boldsymbol{\eta}_r + \boldsymbol{\phi}_f \boldsymbol{\eta}_f, \quad (\text{A.15})$$

where $\boldsymbol{\eta}_r$ and $\boldsymbol{\eta}_f$ are the modal amplitudes of $\boldsymbol{\phi}_r$ and $\boldsymbol{\phi}_f$ respectively. Substitution of the latter equation in the equation of motion gives:

$$\mathbf{M}\boldsymbol{\phi}_r \ddot{\boldsymbol{\eta}}_r + \mathbf{M}\boldsymbol{\phi}_f \ddot{\boldsymbol{\eta}}_f + \mathbf{K}\boldsymbol{\phi}_r \boldsymbol{\eta}_r + \mathbf{K}\boldsymbol{\phi}_f \boldsymbol{\eta}_f = \mathbf{F}. \quad (\text{A.16})$$

Since the rigid body motions do not introduce any deformation, the term $\mathbf{K}\boldsymbol{\phi}_r\boldsymbol{\eta}_r$ can be left out of the equation ($\mathbf{K}\boldsymbol{\phi}_r = \mathbf{0}$). Pre-multiplication by $\boldsymbol{\phi}_r$ now results in the following equation:

$$\boldsymbol{\phi}_r^T \mathbf{M}\boldsymbol{\phi}_r \ddot{\boldsymbol{\eta}}_r + \boldsymbol{\phi}_r^T \mathbf{M}\boldsymbol{\phi}_f \ddot{\boldsymbol{\eta}}_f + \boldsymbol{\phi}_r^T \mathbf{K}\boldsymbol{\phi}_r \boldsymbol{\eta}_r + \boldsymbol{\phi}_r^T \mathbf{K}\boldsymbol{\phi}_f \boldsymbol{\eta}_f = \boldsymbol{\phi}_r^T \mathbf{F}. \quad (\text{A.17})$$

From the mode orthogonality principle it follows that:

$$\begin{cases} \boldsymbol{\phi}_r^T \mathbf{M}\boldsymbol{\phi}_f = \mathbf{0} \\ \boldsymbol{\phi}_r^T \mathbf{K}\boldsymbol{\phi}_f = \mathbf{0}. \end{cases} \quad (\text{A.18})$$

Thus we now can write:

$$\boldsymbol{\phi}_r^T \mathbf{M}\boldsymbol{\phi}_r \ddot{\boldsymbol{\eta}}_r = \boldsymbol{\phi}_r^T \mathbf{F}. \quad (\text{A.19})$$

Now the required formulation of $\ddot{\boldsymbol{\eta}}_r$ is found as:

$$\ddot{\boldsymbol{\eta}}_r = (\boldsymbol{\phi}_r^T \mathbf{M}\boldsymbol{\phi}_r)^{-1} \boldsymbol{\phi}_r^T \mathbf{F}. \quad (\text{A.20})$$

Substituting the formulation of $\ddot{\boldsymbol{\eta}}_r$ in Eq. A.17 yields:

$$\mathbf{F}_{eq} = (\mathbf{I} - \mathbf{M}\boldsymbol{\phi}_r (\boldsymbol{\phi}_r^T \mathbf{M}\boldsymbol{\phi}_r)^{-1} \boldsymbol{\phi}_r^T) \mathbf{F} = \mathbf{P}\mathbf{F} \quad (\text{A.21})$$

The matrix \mathbf{P} is known as the inertia-relief projection matrix. This means that the multiplication of a force vector by this matrix \mathbf{P} results in a self-equilibrated force vector [10]. This means that the matrix projects the original force vector onto a space outside the space of the rigid body modes, such that these modes are not excited by the obtained force \mathbf{F}_{eq} . By replacing the force vector in Eq. A.7, the following relation for the attachment modes can be found:

$$\tilde{\boldsymbol{\psi}}_a = \mathbf{K}^+ = \mathbf{G}_c \mathbf{F}_{eq}. \quad (\text{A.22})$$

In the last step, the attachment modes $\tilde{\boldsymbol{\psi}}_a$ need to be mass-orthogonalized with respect to the rigid body modes. The principle behind this is that the orthogonalization ensures that the attachment modes do not contain any rigid body contribution and that they only describe the static deformation of the structure. In order to obtain the orthogonalized attachment modes, we first need to pre-multiply by the projection matrix \mathbf{P} :

$$\boldsymbol{\psi}_a = \mathbf{P}^T \tilde{\boldsymbol{\psi}}_a = \mathbf{P}^T \mathbf{G}_c \mathbf{P} \mathbf{F}. \quad (\text{A.23})$$

The elastic flexibility matrix is found as:

$$\mathbf{G}_f = \mathbf{P}^T \mathbf{G}_c \mathbf{P}. \quad (\text{A.24})$$

A.5. Rigid body modes

The rigid body modes are modes that describe how a body is moving in space without deforming. This happens when a body is not fully constrained, i.e. there are no internal forces. This can be represented by the following relation:

$$\mathbf{K}\boldsymbol{\phi}_r = \mathbf{0}. \quad (\text{A.25})$$

However, this equation is not solvable directly, in fact, the rigid body modes are found as:

$$\boldsymbol{\phi}_r = \text{null}(\mathbf{K}) \quad (\text{A.26})$$

Each body in a two dimensional space has at most 3 rigid body modes: 2 translation modes and 1 rotational rigid body mode. For small stiffness matrices, the approach where the nullspace of \mathbf{K} is computed works well, however for more complex systems with bigger-sized stiffness matrices, the considered method is quite inefficient. In this work, since we are dealing with a two-dimensional system and since the number of elements is relatively low, this method in which the null space of \mathbf{K} is found works well enough.

B

Derivation of reduction bases

In this appendix, the derivations of the different reduction bases are presented.

B.1. Global reduction

One of the simplest reduction method is global reduction in which the system dynamics are described in terms of the vibration modes of the entire structure. In this case, the generalized displacement vector \mathbf{q} is projected on a suitable global reduction basis \mathbf{V} , represented as:

$$\mathbf{q} \approx \mathbf{V}_G \boldsymbol{\eta}_G. \quad (\text{B.1})$$

The reduction basis \mathbf{V}_G composed of vibration modes only is given as:

$$\mathbf{V}_G = [\phi_{G,1}, \phi_{G,2}, \dots, \phi_{G,m}], \quad (\text{B.2})$$

where $\mathbf{V}_G \in R^{n \times m}$, n is here the total number of degrees of freedom, m is the number of reduced degrees of freedom. With $m \ll n$. The global vibration modes ϕ_G are found by solving the following eigenvalue problem:

$$(\mathbf{K}_G - \omega_{G,i}^2 \mathbf{M}_G) \phi_{G,i} = \mathbf{0}. \quad (\text{B.3})$$

In order to account for geometric nonlinearity, the global reduction can be augmented with modal derivatives. This kind of reduction basis was effectively used and discussed in nonlinear analyses in [3, 16, 22]. The formulation of the reduction basis that contains k vibration modes and all their corresponding MDs is given as:

$$\mathbf{V}_G \approx [\boldsymbol{\phi}_G, \boldsymbol{\Theta}_G] = [\phi_{G,1}, \phi_{G,2}, \dots, \phi_k, \theta_{G,11}, \theta_{G,12}, \dots, \theta_{G,kk}]. \quad (\text{B.4})$$

The reduction basis \mathbf{V}_G normally only contains the dominant vibration modes. The main advantage of global reduction is that it does not require any substructuring during the offline computations or during the time integration process. Besides this, the system dynamics are described by a superposition of the vibration modes and corresponding MDs only. No other type of modes are required.

B.2. Guyan reduction

One of the simplest and oldest forms of modal order reduction is the Guyan reduction. The Guyan reduction starts with the equation that governs the system:

$$\mathbf{M} \ddot{\mathbf{q}} + \mathbf{K} \mathbf{q} = \mathbf{f}, \quad (\text{B.5})$$

where \mathbf{f} is a force vector. Under the condition that the forces only act on the boundary nodes, the system can be split in interior and boundary nodes as:

$$\begin{bmatrix} \mathbf{M}_{BB} & \mathbf{M}_{BI} \\ \mathbf{M}_{IB} & \mathbf{M}_{II} \end{bmatrix} \begin{bmatrix} \ddot{\mathbf{q}}_B \\ \ddot{\mathbf{q}}_I \end{bmatrix} + \begin{bmatrix} \mathbf{K}_{BB} & \mathbf{K}_{BI} \\ \mathbf{K}_{IB} & \mathbf{K}_{II} \end{bmatrix} \begin{bmatrix} \mathbf{q}_B \\ \mathbf{q}_I \end{bmatrix} = \begin{bmatrix} \mathbf{g}_B \\ \mathbf{0} \end{bmatrix}, \quad (\text{B.6})$$

or:

$$\mathbf{M}_{BB}\ddot{\mathbf{q}}_B + \mathbf{M}_{BI}\ddot{\mathbf{q}}_I + \mathbf{K}_{BB}\mathbf{q}_B + \mathbf{K}_{BI}\mathbf{q}_I = \mathbf{g}_B, \quad (\text{B.7})$$

$$\mathbf{M}_{IB}\ddot{\mathbf{q}}_B + \mathbf{M}_{II}\ddot{\mathbf{q}}_I + \mathbf{K}_{IB}\mathbf{q}_B + \mathbf{K}_{II}\mathbf{q}_I = \mathbf{0}. \quad (\text{B.8})$$

From rewriting the latter equation, it follows that the interior degrees of freedom can be calculated as follows:

$$\mathbf{q}_I = \mathbf{K}_{II}^{-1}(-\mathbf{M}_{IB}\ddot{\mathbf{q}}_B - \mathbf{M}_{II}\ddot{\mathbf{q}}_I - \mathbf{K}_{IB}\mathbf{q}_B) \quad (\text{B.9})$$

One could imagine that the condensed degrees of freedom \mathbf{q}_I can be split into two parts:

$$\mathbf{q}_I = \mathbf{q}_{i,stat} + \mathbf{q}_{i,dyn}. \quad (\text{B.10})$$

This means that in a static analysis, the interior degrees of freedom are calculated exactly as:

$$\mathbf{q}_I = -\mathbf{K}_{II}^{-1}(\mathbf{K}_{IB}\mathbf{q}_B) = \boldsymbol{\psi}_c \mathbf{q}_B. \quad (\text{B.11})$$

It is possible to show that under some conditions the dynamic part of \mathbf{q}_I is relatively small and may be neglected, it is possible to show that this holds when:

$$\omega^2 \ll \mu_1^2, \quad (\text{B.12})$$

where ω is the highest eigenfrequency of the structure that one wants to compute and μ is the lowest eigenfrequency in the case the boundary nodes of the structure are clamped. The Guyan reduction of interior degrees of freedom is now calculated as follows:

$$\begin{bmatrix} \mathbf{q}_B \\ \mathbf{q}_I \end{bmatrix} \approx \begin{bmatrix} \mathbf{I} \\ \boldsymbol{\psi}_c \end{bmatrix} \mathbf{q}_B. \quad (\text{B.13})$$

B.3. Craig-Bampton method

The Craig-Bampton reduction method can be seen as an extension of the Guyan's reduction method. Where the Guyan reduction is a good approximation for relatively slow dynamical systems, i.e. where the excitations are below the first eigenfrequency. In that case the dynamics can be approximated by static displacements, however it is not a good approximation for 'faster' systems where the excitation frequencies are higher than the first eigenfrequency. The Craig-Bampton method takes besides the constrained mode information also vibrational information into account, this results in a better and more accurate reduction method. The Craig-Bampton method uses the in Appendix A mentioned so-called internal vibration modes. In case of a truncated set of modes, the internal degrees of freedom can be approximated as follows:

$$\mathbf{q}_I \approx \boldsymbol{\psi}_c \mathbf{q}_B + \boldsymbol{\phi} \boldsymbol{\lambda} \quad (\text{B.14})$$

In case of a non-reduced boundary of the substructure, the reduction basis \mathbf{V}_{CB} for a structure can now be described as:

$$\begin{bmatrix} \mathbf{q}_B \\ \mathbf{q}_I \end{bmatrix} \approx \begin{bmatrix} \mathbf{I} & \mathbf{0} \\ \boldsymbol{\psi}_c & \boldsymbol{\phi} \end{bmatrix} \begin{bmatrix} \mathbf{q}_B \\ \boldsymbol{\lambda} \end{bmatrix} = \mathbf{V}_{CB} \boldsymbol{\eta}_{CB}, \quad (\text{B.15})$$

where $\boldsymbol{\eta}_{CB}$ is the reduced coordinate vector given as:

$$\boldsymbol{\eta}_{CB} = [\mathbf{q}_B, \boldsymbol{\lambda}]^T. \quad (\text{B.16})$$

In order to account for geometric nonlinearity, the Craig-Bampton reduction basis can be augmented with modal derivatives. In that case, the relation between the full set of displacements and the reduced set of displacements is given as:

$$\mathbf{q}_I \approx \boldsymbol{\psi}_c \mathbf{q}_B + \boldsymbol{\phi} \boldsymbol{\lambda} + \boldsymbol{\Theta} \boldsymbol{\zeta}. \quad (\text{B.17})$$

Now the projection equation with the reduction basis is given as:

$$\begin{bmatrix} \mathbf{q}_B \\ \mathbf{q}_I \end{bmatrix} \approx \begin{bmatrix} \mathbf{I} & \mathbf{0} & \mathbf{0} \\ \boldsymbol{\psi} & \boldsymbol{\phi} & \boldsymbol{\Theta} \end{bmatrix} \begin{bmatrix} \mathbf{q}_B \\ \boldsymbol{\lambda} \\ \boldsymbol{\zeta} \end{bmatrix} = \mathbf{V}_{CB} \boldsymbol{\eta}_{CB} \quad (\text{B.18})$$

where $\boldsymbol{\eta}_{CB}$ is the reduced coordinate vector given as:

$$\boldsymbol{\eta}_{CB} = [\mathbf{q}_B, \boldsymbol{\lambda}, \boldsymbol{\zeta}]^T \quad (\text{B.19})$$

Besides the modal derivatives following from the internal vibration modes, the reduction basis can be extended by the earlier mentioned constrained mode modal derivatives, now the internal degrees of freedom can be approximated by the following equation:

$$\mathbf{q}_I \approx \boldsymbol{\psi}_c \mathbf{q}_B + \boldsymbol{\phi} \boldsymbol{\lambda} + \boldsymbol{\Theta} \boldsymbol{\zeta} + \boldsymbol{\Gamma} \boldsymbol{\zeta}. \quad (\text{B.20})$$

This results in the following equation comprising the reduction basis:

$$\begin{bmatrix} \mathbf{q}_B \\ \mathbf{q}_I \end{bmatrix} \approx \begin{bmatrix} \mathbf{I} & \mathbf{0} & \mathbf{0} & \mathbf{0} \\ \boldsymbol{\psi} & \boldsymbol{\phi} & \boldsymbol{\Theta} & \boldsymbol{\Gamma} \end{bmatrix} \begin{bmatrix} \mathbf{q}_B \\ \boldsymbol{\lambda} \\ \boldsymbol{\zeta} \end{bmatrix} = \mathbf{V}_{CB} \boldsymbol{\eta}_{CB} \quad (\text{B.21})$$

where the reduced coordinate vector $\boldsymbol{\eta}_{CB}$ is thus given as:

$$\boldsymbol{\eta}_{CB} = [\mathbf{q}_B, \boldsymbol{\eta}, \boldsymbol{\zeta}, \boldsymbol{\varsigma}]^T. \quad (\text{B.22})$$

B.4. Rubin reduction

The Rubin reduction method is generally more complex than the Craig-Bampton reduction method. First of all, the components of the Rubin reduction basis require some more steps to compute (AMs, RBs). Instead of using internal vibration modes as in the Craig-Bampton reduction method, the Rubin reduction method uses free vibration modes, see Appendix A for the exact formulation of free vibration modes. Since Rubin reduction uses component modes that are related to a full set of DOFs, the modes approximate a full set of DOFs. In case of a truncated set of free vibration modes, the total degrees of freedom of the structure can be approximated by the following equation:

$$\mathbf{q} \approx \boldsymbol{\psi}_a \mathbf{g}_B + \boldsymbol{\phi}_r \boldsymbol{\xi} + \boldsymbol{\phi}_f \boldsymbol{\lambda}, \quad (\text{B.23})$$

where $\boldsymbol{\psi}_a$ are the attachment modes, $\boldsymbol{\phi}_r$ are the rigid body modes and $\boldsymbol{\phi}_f$ are the free vibration modes. However, for substructuring, it is desirable to have a formulation in which the boundary degrees of freedom are not reduced for assembling. Therefore, the latter equation needs to be rewritten in such a way that the boundary nodes are separated from the interior nodes. In order to achieve this, the latter equation is rewritten as:

$$\begin{bmatrix} \mathbf{q}_B \\ \mathbf{q}_I \end{bmatrix} \approx \begin{bmatrix} \boldsymbol{\psi}_{a,b} & \boldsymbol{\phi}_{r,b} & \boldsymbol{\phi}_{f,b} \\ \boldsymbol{\psi}_{a,i} & \boldsymbol{\phi}_{r,i} & \boldsymbol{\phi}_{f,i} \end{bmatrix} \begin{bmatrix} \mathbf{g}_B \\ \boldsymbol{\xi} \\ \boldsymbol{\lambda} \end{bmatrix} = \mathbf{V}_R \boldsymbol{\eta}_R. \quad (\text{B.24})$$

From this relation it follows that:

$$\mathbf{q}_B \approx \boldsymbol{\psi}_{a,b} \mathbf{g}_B + \boldsymbol{\phi}_{r,b} \boldsymbol{\xi} + \boldsymbol{\phi}_{f,b} \boldsymbol{\lambda}. \quad (\text{B.25})$$

Therefore it yields that:

$$\mathbf{g}_B \approx \boldsymbol{\psi}_{a,b}^{-1} (\mathbf{q}_B - \boldsymbol{\phi}_{r,b} \boldsymbol{\xi} - \boldsymbol{\phi}_{f,b} \boldsymbol{\lambda}). \quad (\text{B.26})$$

Substituting this equation in eq. B.25 gives:

$$\mathbf{q}_I \approx \boldsymbol{\psi}_{a,b} \boldsymbol{\psi}_{a,b}^{-1} (\mathbf{q}_B - \boldsymbol{\phi}_{r,b} \boldsymbol{\xi} - \boldsymbol{\phi}_{f,b} \boldsymbol{\lambda}) + \boldsymbol{\phi}_{r,i} \boldsymbol{\xi} + \boldsymbol{\phi}_{f,i} \boldsymbol{\lambda}. \quad (\text{B.27})$$

Rewriting and factorizing for \mathbf{q}_B , $\boldsymbol{\xi}$ and $\boldsymbol{\eta}$ results in:

$$\mathbf{q}_I \approx \boldsymbol{\psi}_{a,b} \boldsymbol{\psi}_{a,b}^{-1} \mathbf{q}_B + (\boldsymbol{\phi}_{r,i} - \boldsymbol{\psi}_{a,b} \boldsymbol{\psi}_{a,b}^{-1} \boldsymbol{\phi}_{r,b}) \boldsymbol{\xi} + (\boldsymbol{\phi}_{f,i} - \boldsymbol{\psi}_{a,b} \boldsymbol{\psi}_{a,b}^{-1} \boldsymbol{\phi}_{f,b}) \boldsymbol{\lambda}. \quad (\text{B.28})$$

This results in the final formulation of the Rubin reduction basis:

$$\begin{bmatrix} \mathbf{q}_B \\ \mathbf{q}_I \end{bmatrix} \approx \begin{bmatrix} \mathbf{I} & \mathbf{0} & \mathbf{0} \\ \boldsymbol{\psi}_{a,b} \boldsymbol{\psi}_{a,b}^{-1} & (\boldsymbol{\phi}_{r,i} - \boldsymbol{\psi}_{a,b} \boldsymbol{\psi}_{a,b}^{-1} \boldsymbol{\phi}_{r,b}) & (\boldsymbol{\phi}_{f,i} - \boldsymbol{\psi}_{a,b} \boldsymbol{\psi}_{a,b}^{-1} \boldsymbol{\phi}_{f,b}) \end{bmatrix} \begin{bmatrix} \mathbf{q}_B \\ \boldsymbol{\xi} \\ \boldsymbol{\lambda} \end{bmatrix} = \mathbf{V}_R \boldsymbol{\eta}_R. \quad (\text{B.29})$$

If we now consider a Rubin reduction basis that includes the modal derivatives, we obtain the following augmented reduction basis:

$$\begin{bmatrix} \mathbf{q}_B \\ \mathbf{q}_I \end{bmatrix} \approx \begin{bmatrix} \boldsymbol{\psi}_{a,b} & \boldsymbol{\phi}_{r,b} & \boldsymbol{\phi}_{f,b} & \boldsymbol{\theta}_b \\ \boldsymbol{\psi}_{a,i} & \boldsymbol{\phi}_{r,i} & \boldsymbol{\phi}_{f,i} & \boldsymbol{\theta}_I \end{bmatrix} \begin{bmatrix} \mathbf{q}_B \\ \boldsymbol{\xi} \\ \boldsymbol{\lambda} \\ \boldsymbol{\zeta} \end{bmatrix} = \mathbf{V}_R \boldsymbol{\eta}_R. \quad (\text{B.30})$$

Similar to what is done before, we can express \mathbf{g}_B as:

$$\mathbf{g}_B = \boldsymbol{\psi}_{a,b}^{-1} (\mathbf{q}_B - \boldsymbol{\phi}_{r,b} \boldsymbol{\xi} - \boldsymbol{\phi}_{f,b} \boldsymbol{\lambda} - \boldsymbol{\theta}_b \boldsymbol{\zeta}). \quad (\text{B.31})$$

This equation can be used to express \mathbf{q}_I as:

$$\mathbf{q}_I = \boldsymbol{\psi}_{a,i} \boldsymbol{\psi}_{a,b}^{-1} (\mathbf{q}_B - \boldsymbol{\phi}_{r,b} \boldsymbol{\xi} - \boldsymbol{\phi}_{f,b} \boldsymbol{\lambda} - \boldsymbol{\theta}_b \boldsymbol{\zeta}) + \boldsymbol{\phi}_{r,i} \boldsymbol{\xi} + \boldsymbol{\phi}_{f,i} \boldsymbol{\lambda} + \boldsymbol{\theta}_I \boldsymbol{\zeta}. \quad (\text{B.32})$$

Rearranging terms leads to:

$$\mathbf{q}_I = \boldsymbol{\psi}_{a,i} \boldsymbol{\psi}_{a,b}^{-1} \mathbf{q}_B + (\boldsymbol{\phi}_{r,i} - \boldsymbol{\psi}_{a,i} \boldsymbol{\psi}_{a,b}^{-1} \boldsymbol{\phi}_{r,b}) \boldsymbol{\xi} + (\boldsymbol{\phi}_{f,i} - \boldsymbol{\psi}_{a,i} \boldsymbol{\psi}_{a,b}^{-1} \boldsymbol{\phi}_{f,b}) \boldsymbol{\lambda} + (\boldsymbol{\theta}_I - \boldsymbol{\psi}_{a,i} \boldsymbol{\psi}_{a,b}^{-1} \boldsymbol{\theta}_b) \boldsymbol{\zeta}. \quad (\text{B.33})$$

Thus the reduced set of equations can now be written as:

$$\begin{bmatrix} \mathbf{q}_B \\ \mathbf{q}_I \end{bmatrix} \approx \begin{bmatrix} \mathbf{I} & \mathbf{0} & \mathbf{0} & \mathbf{0} \\ \boldsymbol{\psi}_{a,b} \boldsymbol{\psi}_{a,b}^{-1} & (\boldsymbol{\phi}_{r,i} - \boldsymbol{\psi}_{a,b} \boldsymbol{\psi}_{a,b}^{-1} \boldsymbol{\phi}_{r,b}) & (\boldsymbol{\phi}_{f,i} - \boldsymbol{\psi}_{a,b} \boldsymbol{\psi}_{a,b}^{-1} \boldsymbol{\phi}_{f,b}) & (\boldsymbol{\theta}_I - \boldsymbol{\psi}_{a,b} \boldsymbol{\psi}_{a,b}^{-1} \boldsymbol{\theta}_b) \end{bmatrix} \begin{bmatrix} \mathbf{q}_B \\ \boldsymbol{\xi} \\ \boldsymbol{\lambda} \\ \boldsymbol{\zeta} \end{bmatrix} = \mathbf{V}_R \boldsymbol{\eta}_R. \quad (\text{B.34})$$

Or equivalently:

$$\begin{bmatrix} \mathbf{q}_B \\ \mathbf{q}_I \end{bmatrix} \approx \begin{bmatrix} \mathbf{I} & \mathbf{0} & \mathbf{0} & \mathbf{0} \\ \mathbf{A} & \mathbf{B} & \mathbf{C} & \mathbf{D} \end{bmatrix} \begin{bmatrix} \mathbf{q}_B \\ \boldsymbol{\xi} \\ \boldsymbol{\lambda} \\ \boldsymbol{\zeta} \end{bmatrix} = \mathbf{V}_R \boldsymbol{\eta}_R, \quad (\text{B.35})$$

where $\boldsymbol{\xi}$, $\boldsymbol{\lambda}$, and $\boldsymbol{\eta}$ are vectors that contain the amplitudes of the modes that are contained in \mathbf{A} , \mathbf{B} , \mathbf{C} , and \mathbf{D} respectively. \mathbf{A} , \mathbf{B} , \mathbf{C} , and \mathbf{D} are given as:

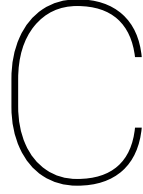
$$\mathbf{A} = \boldsymbol{\psi}_{a,b} \boldsymbol{\psi}_{a,b}^{-1}, \quad (\text{B.36})$$

$$\mathbf{B} = (\boldsymbol{\phi}_{r,i} - \boldsymbol{\psi}_{a,b} \boldsymbol{\psi}_{a,b}^{-1} \boldsymbol{\phi}_{r,b}), \quad (\text{B.37})$$

$$\mathbf{C} = (\boldsymbol{\phi}_{f,i} - \boldsymbol{\psi}_{a,b} \boldsymbol{\psi}_{a,b}^{-1} \boldsymbol{\phi}_{f,b}), \quad (\text{B.38})$$

and:

$$\mathbf{D} = (\boldsymbol{\theta}_i - \boldsymbol{\psi}_{a,b} \boldsymbol{\psi}_{a,b}^{-1} \boldsymbol{\theta}_b). \quad (\text{B.39})$$



Principles of parametric resonance

It is well known that a time-periodic force acting on a simple beam structure can create various dynamic effects [20]. These effects are depending on different parameters, for example the direction of the force, the excitation frequency and the direction of motion of the structure. In the case that a force is acting in the axial direction of the beam system, stiffness and damping terms in the equations of motion may become time-dependent. This kind of excitation is known as parametric excitation [20]. Parametric resonance may appear if the excitation frequency ω is close to resonance frequencies of the system or close to a so-called parametric combination resonance [20]. Let's first consider a 2-DOF beam dynamical system in which the variables u (DoF in axial direction) and w (DoF in transverse direction) are given as:

$$M_u \ddot{u} + K_u u + f_2^u(w) = g(t), \quad (\text{C.1})$$

and:

$$M_w \dot{w} + K_w w + f_2^w(u, w) + f_3^w(w) = 0. \quad (\text{C.2})$$

Or in matrix notation:

$$\begin{bmatrix} M_u & 0 \\ 0 & M_w \end{bmatrix} \begin{bmatrix} \ddot{u} \\ \dot{w} \end{bmatrix} + \begin{bmatrix} K_u & 0 \\ 0 & K_w \end{bmatrix} \begin{bmatrix} u \\ w \end{bmatrix} + \begin{bmatrix} f_2^u(w) \\ f_2^w(u, w) \end{bmatrix} + \begin{bmatrix} 0 \\ f_3^w(w) \end{bmatrix} = \begin{bmatrix} g(t) \\ 0 \end{bmatrix}. \quad (\text{C.3})$$

Let's now make the system as simple as possible and consider a 2 DoF system, in that case we can use scalar quantities as coefficients in the formulations of the internal force vectors. In that case the terms f_2^u , f_2^w and f_3^w are simply:

$$f_2^u = a \cdot w^2, \quad (\text{C.4})$$

$$f_2^w = b \cdot u \cdot w, \quad (\text{C.5})$$

and:

$$f_3^w = c \cdot w^3. \quad (\text{C.6})$$

The time-dependent forcing term $g(t)$ is simply given as:

$$g(t) = A \sin(\omega t). \quad (\text{C.7})$$

We can rewrite eq 5.1 as:

$$u = K_u^{-1}(g(t) - M_u \ddot{u} - f_2^u(w)). \quad (\text{C.8})$$

Here u in parametric resonance will become time-dependent as $u(t)$. Normally the inertia term $M_u \ddot{u}$ is very small compared to the forcing term $g(t)$. Besides that, in the case that we assume

small amplitudes of the system, i.e. w is relatively small, the second order non-linear force vector f_2^u is relatively small as well. Therefore we can write an approximated expression for $u(t)$ for small amplitudes of the beam:

$$u(t) \approx K_u^{-1} g(t). \quad (\text{C.9})$$

Now we can substitute the approximated expression of $u(t)$ in equation 5.2 which yields:

$$M_w \ddot{w} + K_w w + f_2^w(K_u^{-1} g(t), w) + f_3^w(u, w) = 0, \quad (\text{C.10})$$

which we can rewrite as:

$$M_w \ddot{w} + (K_w + b \cdot K_u^{-1} g(t)) w + f_3^w(u, w) = 0. \quad (\text{C.11})$$

From the derivations it follows that the stiffness term $b \cdot K_u^{-1} g(t)$ is now time-dependent and can be written as:

$$b \cdot K_u^{-1} g(t) = \hat{K}_w(t). \quad (\text{C.12})$$

The time dependent linear stiffness matrix in w -direction is now found:

$$\bar{K}_w(t) = K_w + \hat{K}_w(t). \quad (\text{C.13})$$

This derivation clearly shows that the stiffness in w -direction of the 2D beam model has become time dependent, or actually dependent of the periodic axial excitation $g(t)$.

D

Derivation of modal derivatives

Conventional reduction bases as mentioned before give very good approximations for linear dynamic systems. Reduction bases composed of vibration modes seem to be perfectly able to describe the response in such a dynamic system. However, vibration modes are normally not sufficient to feature the dynamic coupling effects. This normally means that geometrically non-linear effects are not taken into account, therefore non-linear applications are not well approximated. Only a model in which the displacements remain small, the solution will be approximately the same as the linearized solution. If the displacements become larger, the displacements of the structure will not be able to follow the linearized solution anymore due to departure from the linear behaviour. Modal derivatives can be used to overcome this problem such that geometric nonlinearity is taken into account. Modal derivatives are based on a Taylor expansion. Let's consider the following case in which we assume a nonlinear mapping Λ between the full solution $\mathbf{q} \in R^n$ and a vector of reduced linear modal coordinates $\boldsymbol{\eta} \in R^m$:

$$\mathbf{q} - \mathbf{q}_{eq} = \Lambda(\boldsymbol{\eta}), \quad (\text{D.1})$$

where \mathbf{q}_{eq} is the equilibrium configuration, and $m < n$. We now can Taylor expand Eq. D.1 in the following way:

$$\mathbf{q} - \mathbf{q}_{eq} = \left. \frac{\partial \Lambda}{\partial \eta_i} \right|_{eq} \eta_i + \frac{1}{2} \left. \frac{\partial^2 \Lambda}{\partial \eta_i \partial \eta_j} \right|_{eq} \eta_i \eta_j + \dots. \quad (\text{D.2})$$

Here Einstein's summation convention for repeated indices is used. The first order derivative in Eq. D.2 can be written as:

$$\left. \frac{\partial \Lambda}{\partial \eta_i} \right|_{eq} = \phi_i, \quad (\text{D.3})$$

where ϕ_i is simply an eigenvector of the problem:

$$(\mathbf{K} - \omega_i^2 \mathbf{M}) \phi_i = \mathbf{0}. \quad (\text{D.4})$$

Which corresponds to the linear normal mode (vibration mode) of the system. The second order term of eq. D.2 is presented as:

$$\left. \frac{\partial^2 \Lambda}{\partial \eta_i \partial \eta_j} \right|_{eq} = \left. \frac{\partial \phi_i}{\partial \eta_j} \right|_{eq}. \quad (\text{D.5})$$

This term represents the directional derivative of the vibration mode at the equilibrium. The terms can be calculated by differentiation of the eigenvalue problem, this results in:

$$\left(\left. \frac{\partial \mathbf{K}^{NL}}{\partial \eta_j} \right|_{eq} - \frac{\partial \omega_i^2}{\partial \eta_j} \mathbf{M} \right) \phi_i + (\mathbf{K} - \omega_i^2 \mathbf{M}) \frac{\partial \phi_i}{\partial \eta_j} = \mathbf{0}. \quad (\text{D.6})$$

The term $\frac{\partial \phi_i}{\partial \eta_j}$ is the modal derivative, noted as θ_{ij} . This set of equations cannot be solved directly since the term $(\mathbf{K} - \omega_i^2 \mathbf{M}) \frac{\partial \phi_i}{\partial \eta_j}$ is singular [16]. Several methods exist in order to circumvent this problem, for instance Nelson's method [39] or by using pseudo inverses [16]. Imposing a normalization condition for the eigenmodes is another way to deal with the singularity. The normalization conditions adds additional equations such that the set of equations can be extended and solved. Let's consider the widely used mass normalization, given as:

$$\phi_i^T \mathbf{M} \phi_i = 1, \quad \forall i \in [1, 2, \dots, m]. \quad (\text{D.7})$$

Differentiation of the latter equation results in:

$$\phi_i^T \mathbf{M} \frac{\partial \phi_i}{\partial \eta_j} + \phi_i^T \mathbf{M}^T \frac{\partial \phi_i}{\partial \eta_j} = 0, \quad \forall i, j \in [1, 2, \dots, m]. \quad (\text{D.8})$$

Utilizing the symmetry of the mass matrix and subsequent evaluation at equilibrium position results in the relation:

$$\phi_i^T \mathbf{M} \frac{\partial \phi_i}{\partial \eta_j} = 0, \quad \forall i, j \in [1, 2, \dots, m], \quad (\text{D.9})$$

or:

$$\phi^T \mathbf{M} \theta_{ij} = \mathbf{0}, \quad \forall i, j \in [1, 2, \dots, m]. \quad (\text{D.10})$$

Now a system of equations which can be used in order to calculate the modal derivatives is given as:

$$\begin{bmatrix} \mathbf{K} - \omega^2 \mathbf{M} & -\mathbf{M} \phi_i \\ -(\mathbf{M} \phi_i)^T & 0 \end{bmatrix} \begin{bmatrix} \theta_{ij} \\ \frac{\partial \omega_i^2}{\partial \eta_j} \end{bmatrix} = \begin{bmatrix} -\frac{\partial \mathbf{K}^{NL}}{\partial \eta_j} \Big|_{eq} \phi_i \\ 0 \end{bmatrix}. \quad (\text{D.11})$$

The set of equations described above will result in an exact calculation of the modal derivatives θ_{ij} . However, we may assume that the term $\frac{\partial \omega_i^2}{\partial \eta_j}$ equals zero since the frequency is not dependent on the modal amplitude. Furthermore, we could leave the inertia term since the inertia term has no influence on the shape of the modal derivative. It only changes the magnitude of the modal derivatives. Therefore we can simplify the set of equations. Now the modal derivatives can be obtained in the following way:

$$\frac{\partial \mathbf{K}^{NL}}{\partial \eta_j} \Big|_{eq} \phi_i = \mathbf{K} \frac{\partial \phi_i}{\partial \eta_j}. \quad (\text{D.12})$$

The modal derivative is now calculated as:

$$\theta_{ij} = \frac{\partial \phi_i}{\partial \eta_j} = \mathbf{K}^{-1} \frac{\partial \mathbf{K}^{NL}}{\partial \eta_j} \Big|_{eq} \phi_i \quad (\text{D.13})$$

These types of modal derivatives are called the static modal derivatives since they are related to the static equilibrium state by ignoring the inertia terms. It turns out that the static modal derivatives will result in quite accurate approximation of a nonlinear dynamic system as well. It should be noted that the modal derivatives are symmetric as such that $\theta_{ij} = \theta_{ji}$. The physical meaning of modal derivatives are in fact that they represent the sensitivity of a vibration mode ϕ_i corresponding to a displacement given in the direction of the vibration mode ϕ_j .

D.1. Illustration of the modal derivatives

In this section, the static modal derivatives related to the first 4 internal vibration modes of a beam system are presented. The 4 relevant internal vibration modes are shown in Fig.D.1. The corresponding modal derivatives are presented in Fig.D.2.

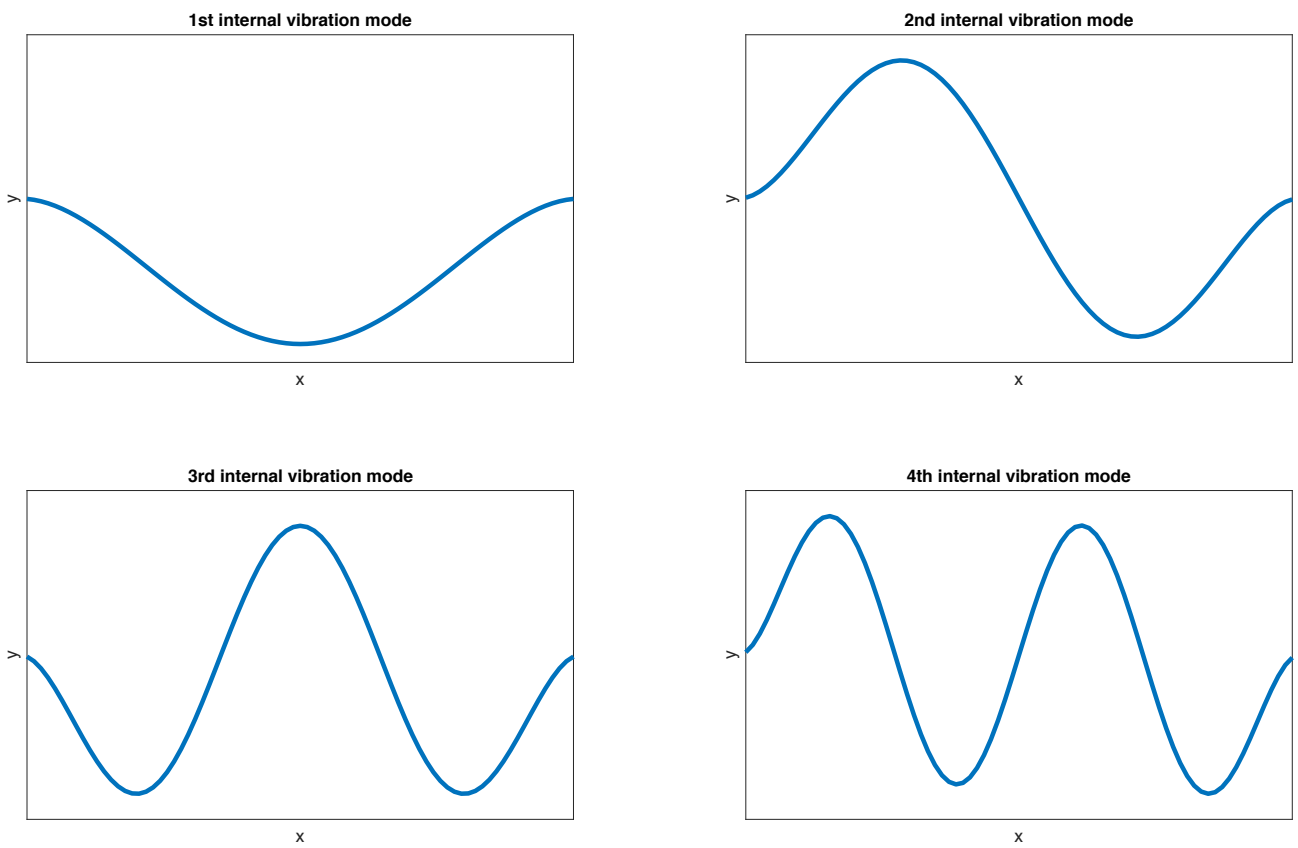


Figure D.1: Representation of the first 4 internal vibration modes of a beam system.

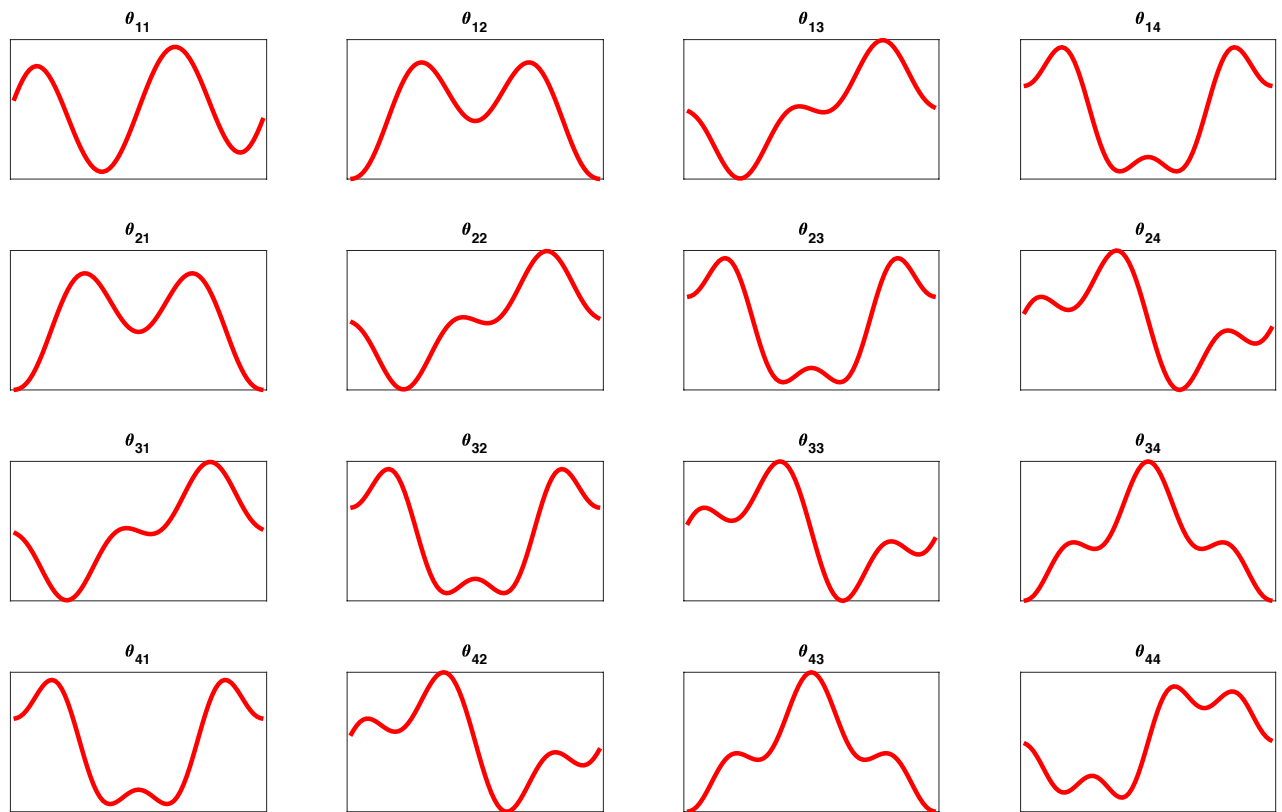
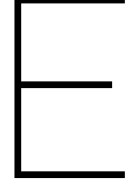


Figure D.2: Representation of the modal derivatives corresponding to the 4 internal vibration modes of a beam system. Only the in-plane contributions are considered and plotted in y-direction for clarity.



Derivation of constraint modal derivatives

A special type of modal derivatives is the Constraint Modal Derivatives (CMDs). we can compute the constrained modal derivative as:

$$\Gamma_{ij} = -\mathbf{K}^{-1} \Big|_{eq} \frac{\partial \mathbf{K}}{\partial q_{B,j}} \Big|_{eq} \psi_i \quad (\text{E.1})$$

Let us now assume an element contribution of the static displacement Ψ , denoted as:

$$\Psi^e = \sum_{i=1}^r \psi_i^e q_{B,i} = \boldsymbol{\psi}^e \mathbf{q}_B. \quad (\text{E.2})$$

Now we can partition ψ_i^e in contributions in u (*axial direction*): $\psi_i^{e,u}$ and in w (*transverse direction*): $\psi_i^{e,w}$. Substituting these contributions in formulations of the nonlinear stiffness matrix \mathbf{K} results in:

$$\mathbf{K}_{UU} \Big|_{\psi_i q_{B,i}} = JEA \int_{-1}^1 \mathbf{b}_u \mathbf{b}_u^T d\zeta, \quad (\text{E.3})$$

$$\mathbf{K}_{UW} \Big|_{\psi_i q_{B,i}} = JEA \int_{-1}^1 (\mathbf{b}_w^T \psi_i^{e,w} q_{B,i}) \mathbf{b}_u \mathbf{b}_w^T d\zeta, \quad (\text{E.4})$$

$$\mathbf{K}_{WU} \Big|_{\psi_i q_{B,i}} = \mathbf{K}_{UW} \Big|_{\psi_i q_{B,i}}^T, \quad (\text{E.5})$$

$$\mathbf{K}_{WW} \Big|_{\psi_i q_{B,i}} = J \int_{-1}^1 (EI \mathbf{c} \mathbf{c}^T + EA (\mathbf{b}_w^T \psi_i^{e,w} q_{B,i})^2 \mathbf{b}_w \mathbf{b}_w^T + N \mathbf{b}_w \mathbf{b}_w^T) d\zeta, \quad (\text{E.6})$$

with:

$$N = EA (\mathbf{b}_u^T \psi_i^{e,u} q_{B,i} + \frac{1}{2} (\mathbf{b}_w^T \psi_i^{e,w} q_{B,i})^2). \quad (\text{E.7})$$

Differentiating with respect to $q_{B,i}$ and evaluating at $q_{B,i} = 0$ gives the directional derivative $\frac{\mathbf{K}^e}{q_{B,i}}$:

$$\frac{\mathbf{K}^e}{q_{B,i}} = \begin{bmatrix} \mathbf{0} & JEA \int_{-1}^1 (\mathbf{b}_w^T \psi_i^{e,w}) \mathbf{b}_u \mathbf{b}_w^T d\zeta \\ (JEA \int_{-1}^1 (\mathbf{b}_w^T \psi_i^{e,w}) \mathbf{b}_u \mathbf{b}_w^T d\zeta)^T & JEA \int_{-1}^1 (\mathbf{b}_u^T \psi_i^{e,u}) \mathbf{b}_w \mathbf{b}_w^T d\zeta \end{bmatrix}. \quad (\text{E.8})$$

Multiplication with ψ_i^e yields:

$$\frac{\mathbf{K}^e}{q_{B,i}} \psi_i^e = \begin{bmatrix} \mathbf{0} & JEA \int_{-1}^1 (\mathbf{b}_w^T \psi_i^{e,w}) \mathbf{b}_u \mathbf{b}_w^T d\zeta \\ (JEA \int_{-1}^1 (\mathbf{b}_w^T \psi_i^{e,w}) \mathbf{b}_u \mathbf{b}_w^T d\zeta)^T & JEA \int_{-1}^1 (\mathbf{b}_u^T \psi_i^{e,u}) \mathbf{b}_w \mathbf{b}_w^T d\zeta \end{bmatrix} \begin{bmatrix} \psi_j^{e,u} \\ \psi_j^{e,w} \end{bmatrix}. \quad (\text{E.9})$$

Once the elemental contributions are computed, the total system is formed through standard finite element assembly:

$$\frac{\mathbf{K}}{q_{B,i}} \psi_j = \text{assembly} \left(\frac{\mathbf{K}^e}{q_{B,i}} \psi_j^e \right). \quad (\text{E.10})$$

Now the constraint modal derivative of the structure is found through multiplication by the inverse of the stiffness matrix evaluated at equilibrium:

$$\Gamma_{ij} = \mathbf{K}^{-1} \frac{\mathbf{K}}{q_{B,i}} \Big|_{eq} \psi_j. \quad (\text{E.11})$$

E.1. Illustration of constraint modal derivatives

In this section, an illustration of the constraint modal derivatives is given. Let's first consider the 6 relevant constraint modes for a beam system, the constraint modes are represented in Fig.E.1. The 5 corresponding constraint modal derivatives are presented in Fig. E.2.

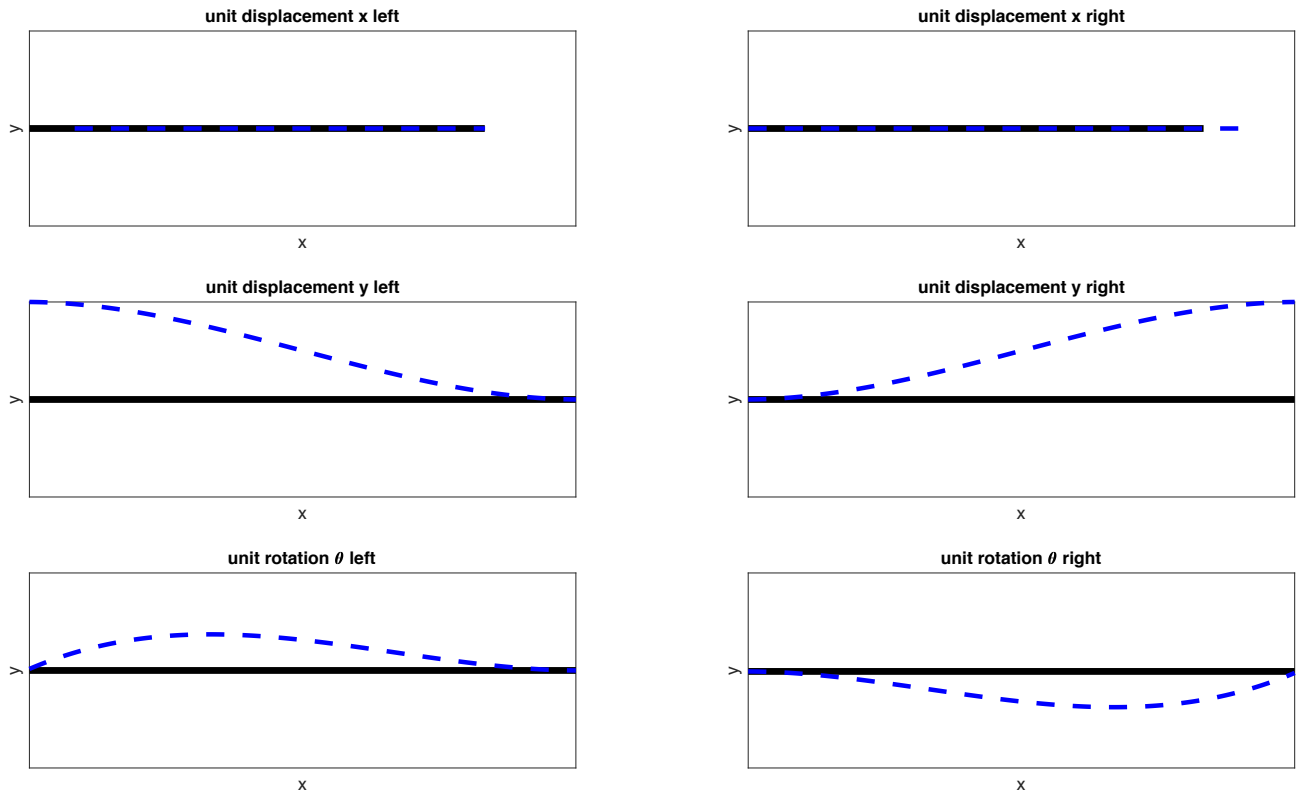


Figure E.1: Representation of the 6 constraint modes for a beam structure. The black line indicates the undeformed beam system, the blue line indicates shape of the constraint modes, where the displacement of a boundary DoF is set to unity.

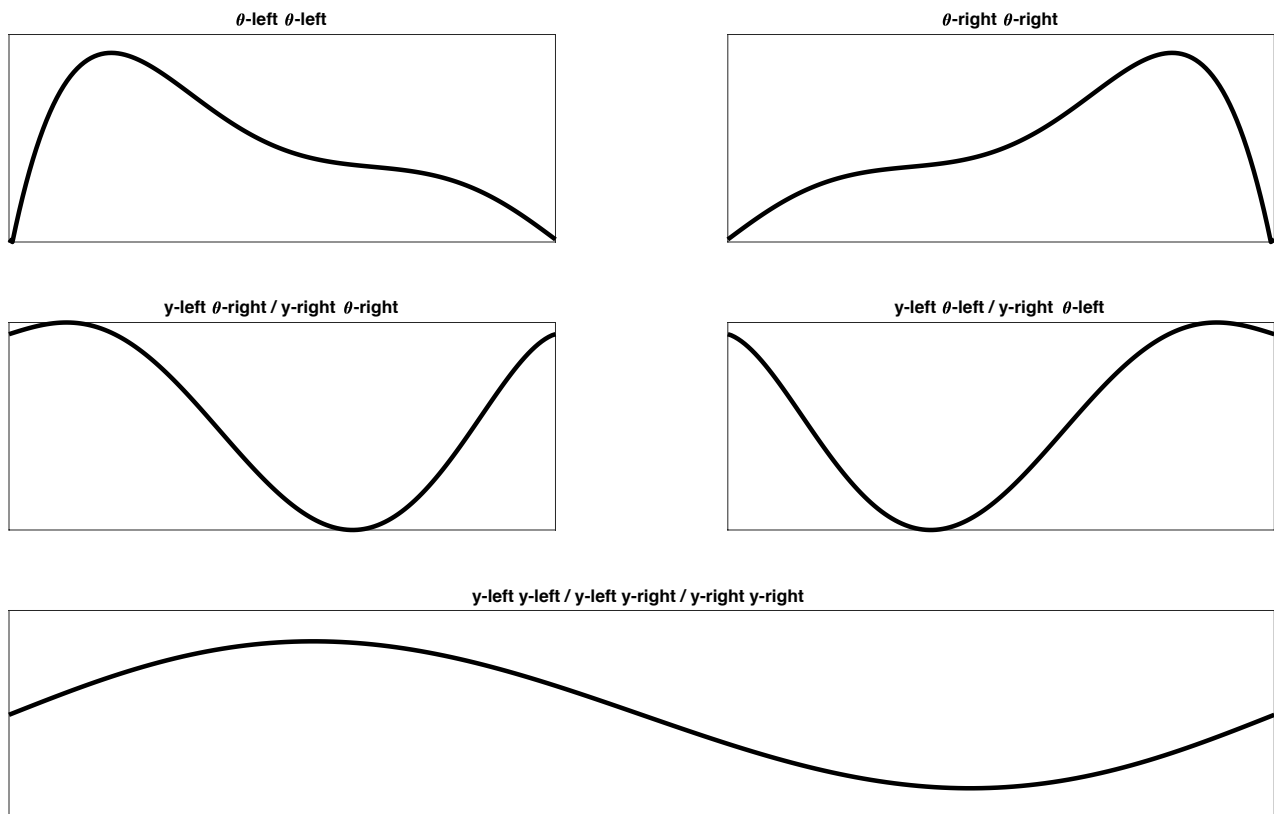
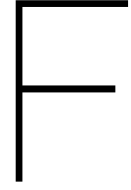


Figure E.2: Representation of the 5 linear independent constraint modal derivatives of a beam system. CMDs exhibit in-plane displacements only. The CMDs are plotted on the y-axis for clarity. Above the plots of the CMDs, the pairs of two constraint modes that lead to the specific CMD is indicated.



Derivation of the tensors

This appendix describes how the tensors of the tensor formulations are computed.

F.1. Computing the tensors on element level

In order to find the reduced nonlinear tensors of a certain structure, the first step is to find the formulations of the tensors on element level: ${}^2\mathbf{Q}^e \in R^{6 \times 6}$, ${}^3\mathbf{Q}^e \in R^{6 \times 6 \times 6}$ and ${}^4\mathbf{Q}^e \in R^{6 \times 6 \times 6 \times 6}$. The element tensors are the building blocks of both the full-sized tensors and the reduced tensors. First the vector that describes the displacements of an element is formulated as:

$$\mathbf{q}^e = \mathbf{p} = [u_1, w_1, \theta_1, u_2, w_2, \theta_2]^T \quad (\text{E.1})$$

Where u_i are the axial displacements, w_i are the transverse displacements and θ_i are the rotations, the subscripts refer to the ends of the beam element. Now 3 vectors are introduced that contain the differentials of the interpolation functions $\mathbf{b}_u, \mathbf{b}_w$ and \mathbf{c} . These 3 vectors are given as:

$$\mathbf{\Gamma} = \begin{bmatrix} b_u(1) \\ 0 \\ 0 \\ b_u(2) \\ 0 \\ 0 \end{bmatrix} = \frac{1}{l} \begin{bmatrix} 1 \\ 0 \\ 0 \\ -1 \\ 0 \\ 0 \end{bmatrix} \quad (\text{E.2})$$

$$\mathbf{\Omega} = \begin{bmatrix} 0 \\ b_w(1) \\ b_w(2) \\ 0 \\ b_w(3) \\ b_w(4) \end{bmatrix} = \frac{1}{4l} \begin{bmatrix} 0 \\ 6(\zeta^2 - 1) \\ l(3\zeta^2 - 2\zeta - 1) \\ 0 \\ 6(1 - \zeta^2) \\ l(3\zeta^2 + 2\zeta - 1) \end{bmatrix} \quad (\text{E.3})$$

$$\mathbf{\Pi} = \begin{bmatrix} 0 \\ c(1) \\ c(2) \\ 0 \\ c(3) \\ c(4) \end{bmatrix} = \frac{l}{l^2} \begin{bmatrix} 0 \\ 6\zeta \\ l(3\zeta - 1) \\ 0 \\ -6\zeta \\ l(3\zeta + 1) \end{bmatrix} \quad (\text{E.4})$$

Using Γ, Ω and Π we can write the element nonlinear force vector as

$$\mathbf{f}^{NL} = \begin{bmatrix} U(1) \\ W(1) \\ W(2) \\ U(2) \\ W(3) \\ W(4) \end{bmatrix} = J \int (EA(\Gamma^T \mathbf{p} + \frac{1}{2}(\Omega^T \mathbf{p})^2)\Gamma) d\zeta + J \int (EA(\Gamma^T \mathbf{p} + \frac{1}{2}(\Omega^T \mathbf{p})^2)(\Omega^T \mathbf{p})\Omega + EI\Pi^T \mathbf{p}\Pi) d\zeta \quad (\text{E5})$$

Now we can decompose this integral in different contributions depending on the order of \mathbf{p} . Also a distinction between the contribution for u and w is made. The formulation of \mathbf{f}^{NL} can now be written as:

$$\mathbf{f}^{NL} = \mathbf{f}^{(u,1)} + \mathbf{f}^{(u,2)} + \mathbf{f}^{(w,1)} + \mathbf{f}^{(w,2)} + \mathbf{f}^{(w,3)}, \quad (\text{E6})$$

where it follows that the terms are calculated as:

$$\mathbf{f}^{(u,1)} = JEA \int (\Gamma^T \mathbf{p})\Gamma d\zeta = JEA \int \lambda_1 d\zeta, \quad (\text{E7})$$

$$\mathbf{f}^{(u,2)} = \frac{1}{2}JEA \int (\Omega^T \mathbf{p})^2 \Gamma d\zeta = \frac{1}{2}JEA \int \lambda_2 d\zeta, \quad (\text{E8})$$

$$\mathbf{f}^{(w,1)} = JEI \int \Pi^T \mathbf{p}\Pi d\zeta = JEI \int \lambda_5 d\zeta, \quad (\text{E9})$$

$$\mathbf{f}^{(w,2)} = \frac{1}{2}JEA \int (\Omega^T \mathbf{p})^3 \Omega d\zeta = \frac{1}{2}JEA \int \lambda_4 d\zeta, \quad (\text{E10})$$

$$\mathbf{f}^{(w,3)} = JEA \int (\Gamma^T \mathbf{p})(\Omega^T \mathbf{p})\Omega d\zeta = JEA \int \lambda_3 d\zeta. \quad (\text{E11})$$

Therefore we can write:

$$\mathbf{f}^{NL} = JEA \int \lambda_1 d\zeta + \frac{1}{2}JEA \int \lambda_2 d\zeta + JEA \int \lambda_3 d\zeta + \frac{1}{2}JEA \int \lambda_4 d\zeta + JEI \int \lambda_5 d\zeta \quad (\text{E12})$$

In order to be able to write the formulation of \mathbf{f}_{NL} in a tensor form, the terms $\lambda_1, \lambda_2, \lambda_3, \lambda_4$ and λ_5 need to be rewritten in the following forms:

$$\lambda_1 = {}^2_1\Lambda \cdot \mathbf{p}, \quad (\text{E13})$$

$$\lambda_2 = {}^3_2\Lambda : (\mathbf{p} \otimes \mathbf{p}), \quad (\text{E14})$$

$$\lambda_3 = {}^3_3\Lambda : (\mathbf{p} \otimes \mathbf{p}), \quad (\text{E15})$$

$$\lambda_4 = {}^4_4\Lambda : (\mathbf{p} \otimes \mathbf{p} \otimes \mathbf{p}), \quad (\text{E16})$$

$$\lambda_5 = {}^2_5\Lambda \cdot \mathbf{p}. \quad (\text{E17})$$

Now the element tensors ${}^2\mathbf{Q}^e$, ${}^3\mathbf{Q}^e$ and ${}^4\mathbf{Q}^e$ can be calculated as:

$${}^2\mathbf{Q}^e = JEA \int_{-1}^1 {}^2_1\Lambda d\zeta + JEI \int_{-1}^1 {}^2_5\Lambda d\zeta, \quad (\text{E18})$$

$${}^3\mathbf{Q}^e = \frac{1}{2}JEA \int_{-1}^1 {}^3_2\Lambda d\zeta + JEA \int_{-1}^1 {}^3_3\Lambda d\zeta \quad (\text{E19})$$

$${}^4\mathbf{Q}^e = \frac{1}{2} JEA \int_{-1}^1 {}^4\Lambda d\zeta. \quad (\text{E20})$$

Now the tensors ${}^2\mathbf{Q}$, ${}^3\mathbf{Q}$ and ${}^4\mathbf{Q}$ are found via standard finite element assembly, simply denoted as:

$${}^x\mathbf{Q} = \text{assembly}({}^x\mathbf{Q}_i^e) \quad (\text{E21})$$

Where x indicates the order of the tensor.

F.2. Rotation of the element tensor

During the assembly of the system tensors, some of the element tensors need be rotated from a local coordinate system to a global coordinate system, this is done as follows:

$${}^2\mathbf{Q}_{global}^e = ((\mathbf{R}_e^T \cdot_{(11)} ({}^2\mathbf{Q}_{local}^e)) \cdot_{(21)} \mathbf{R}_e), \quad (\text{E22})$$

$${}^3\mathbf{Q}_{global}^e = (((\mathbf{R}_e^T \cdot_{(11)} ({}^3\mathbf{Q}_{local}^e)) \cdot_{(21)} \mathbf{R}_e) \cdot_{(21)} \mathbf{R}_e), \quad (\text{E23})$$

$${}^4\mathbf{Q}_{global}^e = (((((\mathbf{R}_e^T \cdot_{(11)} ({}^4\mathbf{Q}_{local}^e)) \cdot_{(21)} \mathbf{R}_e) \cdot_{(21)} \mathbf{R}_e) \cdot_{(21)} \mathbf{R}_e) \cdot_{(21)} \mathbf{R}_e). \quad (\text{E24})$$

Here, the matrix $\mathbf{R}_e \in R^{6 \times 6}$ is the rotation matrix given as:

$$\begin{bmatrix} \cos(\alpha) & \sin(\alpha) & 0 & 0 & 0 & 0 \\ -\sin(\alpha) & \cos(\alpha) & 0 & 0 & 0 & 0 \\ 0 & 0 & 1 & 0 & 0 & 0 \\ 0 & 0 & 0 & \cos(\alpha) & \sin(\alpha) & 0 \\ 0 & 0 & 0 & -\sin(\alpha) & \cos(\alpha) & 0 \\ 0 & 0 & 0 & 0 & 0 & 1 \end{bmatrix} \quad (\text{E25})$$

Where α is the rotation angle. The subscript $(\bullet) \cdot_{(nm)} (\bullet)$ indicates that the n -th dimension of the first tensor is contracted with the m -th dimension of the second tensor.

F.3. Computation of the reduced-order tensors

The relation between the full structure tensors as found in eq. E.21 and the reduced structure tensors is given as:

$${}^2\tilde{\mathbf{Q}}_{(s)} = ((\mathbf{V}_{(s)}^T \cdot_{(11)} ({}^2\mathbf{Q}_{(s)})) \cdot_{(21)} \mathbf{V}_{(s)}), \quad (\text{E26})$$

$${}^3\tilde{\mathbf{Q}}_{(s)} = (((\mathbf{V}_{(s)}^T \cdot_{(11)} ({}^3\mathbf{Q}_{(s)})) \cdot_{(21)} \mathbf{V}_{(s)}) \cdot_{(21)} \mathbf{V}_{(s)}), \quad (\text{E27})$$

$${}^4\tilde{\mathbf{Q}}_{(s)} = (((((\mathbf{V}_{(s)}^T \cdot_{(11)} ({}^4\mathbf{Q}_{(s)})) \cdot_{(21)} \mathbf{V}_{(s)}) \cdot_{(21)} \mathbf{V}_{(s)}) \cdot_{(21)} \mathbf{V}_{(s)}) \cdot_{(21)} \mathbf{V}_{(s)}), \quad (\text{E28})$$

where $\mathbf{V}_{(s)} \in Rn \times m$ is the substructure reduction basis. Note that Eq.21 and Eqs.26-28 do not reflect the way how the reduced tensors are computed, since the size of the high-order unreduced tensors will rapidly become huge as the number of DoFs increases. A way to circumvent this problem is the assembly of the reduced order tensors on element level. For example, the third order reduced tensor can be computed as:

$${}^4\tilde{\mathbf{Q}} = \sum_{i=1}^{n_e} (((((\mathbf{V}_e^T \cdot_{(11)} ({}^4\mathbf{Q}_{(s)})) \cdot_{(21)} \mathbf{V}_e) \cdot_{(21)} \mathbf{V}_e) \cdot_{(21)} \mathbf{V}_e) \cdot_{(21)} \mathbf{V}_e), \quad (\text{E29})$$

where \mathbf{V}_e is the part of the reduction basis that is associated to the element e .

F.4. Matlab implementations

This section describes how the relevant tensor formulations are implemented in matlab. Using the tensor toolbox [30], the matlab code that computes Eq.F.24 is written as:

$$2Qelglobal = ttt(ttt(R, 2Qellocal, 1, 1), R, 2, 1), \quad (E30)$$

$$3Qelglobal = ttt(ttt(ttt(R, 3Qellocal, 1, 1), R, 2, 1), R, 2, 1), \quad (E31)$$

$$4Qelglobal = ttt(ttt(ttt(ttt(R, 4Qellocal, 1, 1), R, 2, 1), R, 2, 1), R, 2, 1). \quad (E32)$$

Using the tensor toolbox, the reduced-order tensors are in Matlab computed as:

$$2Qreds = ttt(ttt(V, 2Qs, 1, 1), V, 2, 1), \quad (E33)$$

$$3Qreds = ttt(ttt(ttt(V, 3Qs, 1, 1), V, 2, 1), V, 2, 1), \quad (E34)$$

,and

$$4Qreds = ttt(ttt(ttt(ttt(V, 4Qs, 1, 1), V, 2, 1), V, 2, 1), V, 2, 1). \quad (E35)$$

Bibliography

- [1] Wu, L., Tiso, P., Tatsis, K., Chatzi, E., & van Keulen, F. (2019). A modal derivatives enhanced Rubin substructuring method for geometrically nonlinear multibody systems. *Multibody System Dynamics*, 45(1), 57-85. <https://doi.org/10.1007/s11044-018-09644-2>
- [2] Wenneker, E, Tiso, P: A substructuring method for geometrically nonlinear structures. In: *Dynamics of Coupled Structures*, vol. 1, pp. 157–165. Springer, Berlin (2014)
- [3] Rutzmoser, J.B., Rixen, D.J., Tiso, P, Jain, S.: Generalization of quadratic manifolds for reduced order modeling of nonlinear structural dynamics. *Comput. Struct.* 192(Supplement C), 196–209 (2017)
- [4] Weeger, O., Wever, U., Simeon, B.: On the use of modal derivatives for nonlinear model order reduction. *Int. J. Numer. Methods Eng.* (2016)
- [5] Wu, L., Tiso, P: Nonlinear model order reduction for flexible multibody dynamics: a modal derivatives approach. *Multibody Syst. Dyn.* 36(4), 405–425 (2016)
- [6] Qalandar, R.K., Strachan, B.S., Gibson, B., Sharma, M., Ma, A., Shaw, W.S., Turner, L.K.: Frequency division using a micromechanical resonance cascade. *Appl. Phys. Lett.* 105, 244103 (2014)
- [7] D. de Klerk, D. J. Rixen, and S. N. Voormeeren. “General framework for dynamic substructuring: history, review and classification of techniques”. In: *AIAA journal* 46.5 (2008), pp. 1169–1181.
- [8] P. Tiso. “Optimal second order reduction basis selection for nonlinear transient analysis”. In: *Modal Analysis Topics*, Volume 3. Springer, 2011, pp. 27–39.
- [9] P. Van Der Valk. “Model Reduction & Interface Modeling in Dynamic Substructuring”. MA thesis. Delft University of Technology, 2010.
- [10] S. Voormeeren. “Dynamic Substructuring Methodologies for Integrated Dynamic Analysis of Wind Turbines”. PhD thesis. Delft University of Technology, 2012.
- [11] R. Guyan. “Reduction of stiffness and mass matrices”. In: *AIAA journal* 3.2 (1965), p. 380.
- [12] R. R. Craig and M. C. C. Bampton. “Coupling of substructures for dynamic analysis”. In: *AIAA journal* 6.7 (1968), pp. 1313–1319.
- [13] S. R. Idelsohn and A. Cardona. “A reduction method for nonlinear structural dynamic analysis”. In: *Computer Methods in Applied Mechanics and Engineering* 49.3 (June 1985), pp. 253–279.
- [14] S. Rubin. “Improved component-mode representation for structural dynamic analysis”. In: *AIAA journal* 13.8 (1974).
- [15] Strachan BS, Shaw SW, Kogan O. “Subharmonic resonance cascades in a class of coupled resonators”. In: *Journal of Computational and Nonlinear Dynamics* v8 n4 (2013 12 02).
- [16] C.S.M. Sombroek, P. Tiso, L. Renson, G. Kerschen, Numerical computation of nonlinear normal modes in a modal derivative subspace, *Comput. Struct.* 195 (2018) 34-46,

- [17] Lifshitz, R., Cross, M.: Response of parametrically driven nonlinear coupled oscillators with application to micromechanical and nanomechanical resonator arrays. *Phys. Rev. B* 67(13), 134302 (2003)
- [18] C. Farhat and M. Géradin. "On the general solution by a direct method of a large-scale singular system of linear equations: application to the analysis of floating structures". In: *International Journal for Numerical Methods in Engineering* 41.4 (1998), pp. 675–696. issn: 1097-0207.
- [19] Tiso P, Rixen DJ. Reduction methods for MEMS nonlinear dynamic analysis. New York, NY: Springer New York; 2011. <https://doi.org/10.1007/978-1-4419-9719-7-6>.
- [20] Dohnal F, Ecker H. and Springer H. Enhanced damping of a cantilever beam by axial parametric excitation. *Archives of Applied Mechanics*, 2008, 78, No. 12, 935–947
- [21] Shklarski, Gil, and Sivan Toledo. "Computing the Null Space of Finite Element Problems." *Computer Methods in Applied Mechanics and Engineering* 198, no. 37-40 (2009): 3084–3095.
- [22] Jain, Shobhit, Paolo Tiso, Johannes B Rutzmoser, and Daniel J Rixen. "A Quadratic Manifold for Model Order Reduction of Nonlinear Structural Dynamics." *Computers and Structures* 188 (2017): 80–94.
- [23] Wu, Jong-Shyong. *Analytical and Numerical Methods for Vibration Analyses*, John Wiley and Sons, Incorporated, 2014.
- [24] D. Lee, T.-S. Ahn, H.-S. Kim, A metric on the similarity between two frequency response functions, *J. Sound Vib.* 436 (2018) 32–45
- [25] Theodosiou, C., Sikelis, K., Natsiavas, S.: Periodic steady state response of large scale mechanical models with local nonlinearities. *Int. J. Solids Struct.* 46, 3565–3576 (2009).
- [26] R.H. MacNeal. A Hybrid Method of Component Mode Synthesis. *Computers and Structures*, 1(4):581–601, 1971.
- [27] Kraker, de, A, and van, D.H Campen. 1996. "Rubin's Cms Reduction Method for General State-Space Models." *Computers and Structures* 58 (3): 597–606.
- [28] M.A. Crisfield, *Non-Linear Finite Element Analysis of Solids and Structures, Advanced Topics*, vol. 2, Wiley, New York, 1997.
- [29] Jain, S., Breunung, T. and Haller, G. *Nonlinear Dyn* (2019) 97: 313. <https://doi-org.tudelft.idm.oclc.org/10.1007/s11071-019-04971-1>
- [30] B. W. Bader, T. G. Kolda, et al., *Matlab tensor toolbox version 2.6*, Available online (2015).
- [31] Z.-Q. Qu. *Model Order Reduction Techniques: With Applications in Finite Element Analysis*. Springer, 2004. isbn: 9781852338077.
- [32] W.H.A. Schilders, H.A. van der Vorst, J. Rommes. *Model Order Reduction: Theory, Research Aspects and Applications*. Springer. 2008. ISBN 978-3-540-78840-9
- [33] Geuzaine, C, B Meys, F Henrotte, P Dular, and W Legros. 1999. "A Galerkin Projection Method for Mixed Finite Elements." *Ieee Transactions on Magnetics Mag* 35 (3): 1438–41.
- [34] Apiwattanalungarn, P, Shaw, S.W. & Pierre, C. *Nonlinear Dyn* (2005) 41: 17. <https://doi-org.tudelft.idm.oclc.org/10.1007/s11071-005-2791-2>

-
- [35] W.C. Hurty. Dynamic Analysis of Structural Systems using Component Modes. *AIAA Journal*, 3(4):678–685, 1965.
- [36] R.R. Craig and C.J. Chang. A review of substructure coupling methods for dynamic analysis. *NASA. Langley Res. Center Advan. in Eng. Sci.*, 2(CR-2781):393–408, 1976.
- [37] Wu.L. Model order reduction and substructuring methods for nonlinear structural dynamics. PhD thesis. Delft University of Technology, 2018.
- [38] C. Farhat, P. Avery, T. Chapman, and J. Cortial, Dimensional reduction of nonlinear finite element dynamic models with finite rotations and energy-based mesh sampling and weighting for computational efficiency, *International Journal for Numerical Methods in Engineering* 98, 625 (2014).
- [39] Nelson RB. Simplified calculation of eigenvector derivatives. *AIAA J* 1976;14 (9):1201–5
- [40] D.J. Nefske, S.H. Sung, Correlation of a coarse-mesh finite element model using structural system identification and a frequency response assurance criterion, in: *Proceedings of the 14th International Modal Analysis Conference (IMAC XIV)*, 1996, pp. 597e602.
- [41] P. Tiso, Finite element based reduction methods for static and dynamic analysis of thin-walled structures, Ph.D. thesis, Delft University of Technology (2006).
- [42] Shin, Kihong. “An Alternative Approach to Measure Similarity between Two Deterministic Transient Signals.” *Journal of Sound and Vibration* 371 (2016): 434–445.
- [43] Nayfeh, T. A., Asrar, W., and Nayfeh, A. H., 1992, “Three-Mode Interactions in Harmonically Excited Systems With Quadratic Nonlinearities,” *Nonlinear Dyn.*, 3(5), pp. 385–410.
- [44] R.R. Craig and A.J.Kurdila. *Fundamentals of Structural Dynamics*. Wiley, 2006. ISBN: 9780471430445